Technical Note

CEL

TN no. N-1468

title: FLANGED ACRYLIC PLASTIC HEMISPHERICAL SHELLS FOR UNDERSEA SYSTEMS - Static and Cyclic Fatigue Life Under Hydrostatic Loading

author: J. D. Stachiw and R. Sletten

date: January 1977

sponsor: NAVAL FACILITIES ENGINEERING COMMAND

program nos: YF54.593.008.01.004

CIVIL ENGINEERING LABORATORY
NAVAL CONSTRUCTION BATTALION CENTER
Port Hueneme, California 93043

J. D. Stachiw is a technical consultant, Ocean Technology Department, Naval Undersea Research and Development Center, San Diego, California.

R. Sletten is a marine engineer, Division of Marine Technology, Det norske Veritas, Oslo, Norway, on temporary assignment at the Civil Engineering Laboratory, May 1974 to March 1975 and September to November 1975.

Unclassified

SECURITY CLASSIFICATION OF THIS PAGE (When Data Entered)

REPORT DOCUMENTATION PAGE	READ INSTRUCTIONS BEFORE COMPLETING FORM
1. REPORT NUMBER: TN-1468	2. GOVT ACCESSION NO.: DN244039
3. RECIPIENT'S CATALOG NUMBER	
4. TITLE (and Subtitle): FLANGED ACRYLIC PLASTIC HEMISPHERICAL SHELLS FOR UNDERSEA SYSTEMS - Static and Cyclic Fatigue Life Under Hydrostatic Loading	5. TYPE OF REPORT & PERIOD COVERED: Final; Jul 1973 - Jun 1975
	6. PERFORMING ORG. REPORT NUMBER
7. AUTHOR(s): J. D. Stachiw, R. Sletten	8. CONTRACT OR GRANT NUMBER(s)
9. PERFORMING ORGANIZATION NAME AND ADDRESS: CIVIL ENGINEERING LABORATORY, Naval Construction Battalion Center, Port Hueneme, California 93043	10. PROGRAM ELEMENT, PROJECT, TASK AREA & WORK UNIT NUMBERS: 62755N; YF54.593.008.01.004
11. CONTROLLING OFFICE NAME AND ADDRESS: Naval Facilities Engineering Command, Alexandria, Virginia 22332	12. REPORT DATE: January 1977 13. NUMBER OF PAGES: 104
14. MONITORING AGENCY NAME & ADDRESS (if different from Controlling Office)	15. SECURITY CLASS. (of this report): Unclassified 15a. DECLASSIFICATION DOWNGRADING SCHEDULE
16. DISTRIBUTION STATEMENT (of this Report): Approved for public release; distribution unlimited.	
17. DISTRIBUTION STATEMENT (of the abstract entered in Block 20, if different from Report)	
18. SUPPLEMENTARY NOTES	
19. KEY WORDS (Continue on reverse side if necessary and identify by block number): Windows, deep ocean, acrylic plastic, spherical shell, hydrostatic pressure tests.	

20. ABSTRACT (Continue on reverse side if necessary and identify by block number):

Twenty-four acrylic plastic windows in the shape of hemispherical domes with equatorial flanges have been thermoformed from flat sheets and tested under short-term, long-term, and cyclic pressure loading at 65°F to 75°F (18.5° to 24.1°C) ambient temperature. Two kinds of flanges were studied: Type I, a flat lip with a rounded heel and instep, and Type VI, a conical lip with a rounded heel. The 14,500-psi, short-term critical pressure for hemispherical windows with $t/R_i = 0.364$ was found to be independent of the equatorial

→ next page

DD FORM 1 JAN 73 1473 EDITION OF 1 NOV 65 IS OBSOLETE

continued

Unclassified

SECURITY CLASSIFICATION OF THIS PAGE (When Data Entered)

Unclassified

SECURITY CLASSIFICATION OF THIS PAGE(When Data Entered)

20. Continued

cont →

flange configuration. Both the static and cyclic fatigue lives of the windows were also found to be independent of equatorial flange configuration. In either case, the maximum acceptable working pressure for 65° to 75°F temperature range was found to be 1,000 psi. Only by elimination of the O-ring groove in the bearing surface of the window flange and the use of a thin neoprene bearing gasket between the acrylic flange and the steel seat is it possible to extend the working pressure for 65° to 75°F (18.5° to 24.1°C) temperature range to 2,000 psi. Operating the flanged windows at pressures in excess of the safe working pressures shown above will generate fatigue cracks in the bearing surface of the flange in less than 1,000 pressure cycles; at 5,000-psi pressure the cyclic fatigue life decreases to less than 100 cycles.

Library card

Civil Engineering Laboratory
FLANGED ACRYLIC PLASTIC HEMISPHERICAL SHELLS FOR UNDERSEA SYSTEMS – Static and Cyclic Fatigue Life Under Hydrostatic Loading (final), by J. D. Stachiw and R. Sletten
TN-1468 104 pp illus January 1977 Unclassified

1. Acrylic windows 2. Deep ocean structures I. YF54.593.008.01.004

Twenty-four acrylic plastic windows in the shape of hemispherical domes with equatorial flanges have been thermoformed from flat sheets and tested under short-term, long-term, and cyclic pressure loading at 65° to 75°F (18.5° to 24.1°C) ambient temperature. Two kinds of flanges were studied: Type I, a flat lip with a rounded heel and instep, and Type VI, a conical lip with a rounded heel. The 14,500-psi, short-term critical pressure for hemispherical windows with t/R_i = 0.364 was found to be independent of the equatorial flange configuration. Both the static and cyclic fatigue lives of the windows were also found to be independent of equatorial flange configuration. In either case, the maximum acceptable working pressure for 65° to 75°F temperature range was found to be 1,000 psi. Only by elimination of the O-ring groove in the bearing surface of the window flange and the use of a thin neopren. bearing gasket between the acrylic flange and the steel seat is it possible to extend the working pressure for 65° to 75°F (18.5° to 24.1°C) temperature range to 2,000 psi. Exceeding the safe working pressures will generate fatigue cracks in the flange bearing surface <1,000 pressure cycles; at 5,000-psi, the cyclic fatigue life decreases to <100 cycles.

Unclassified

SECURITY CLASSIFICATION OF THIS PAGE(When Data Entered)

CONTENTS

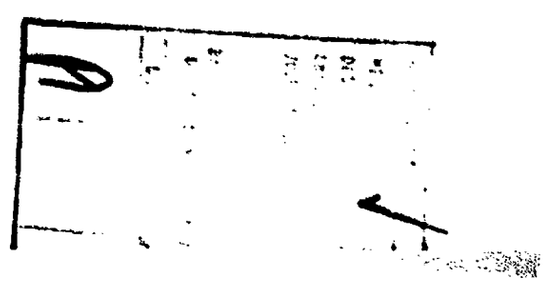

CONTENTS

INTRODUCTION

Since its introduction into the hydrospace field by Professor Auguste Piccard, acrylic plastic has become the acknowledged standard material for windows in submersibles, diving bells, and hyperbaric chambers. Several shapes have been developed over the years for the acrylic windows.

The most common shape is the plane conical frustum. Its behavior under hydrostatic loading has been extensively researched and its design criteria well-established [1-5]. A somewhat less common shape is a plane circular disc [6,7]. Its application has been confined to pressures under 1,000 psi; as for greater pressures, the retaining flanges become too bulky.

The spherical shell sector, whose included spherical angle can vary from 30 to 180 degrees, has been used only recently for undersea systems. Considerable effort has been devoted to understanding the characteristics of this window because the spherical surfaces endow such windows with increased field of vision and resistance to hydrostatic pressure [8,9]. In parallel with the research into structural and optical properties of spherical shell sector windows, investigations have been conducted into the problems associated with economical fabrication of large diameter windows for the whole depth range [10,11,12].

Because spherical shell sector windows are not as easy to retain in their flanges as plane conical frustum or plane disc windows, consideration has been given to equipping the spherical shell sector windows with integral flanges [13,14]. Such flanges, however, generally introduce bending moments and stress concentrations into the otherwise uniformly stressed spherical window. To assess the effects of flanges on the stress distribution in spherical windows an experimental study was undertaken; the results of that study form the body of this report.

BACKGROUND

Equatorial flanges on spherical shell sector windows are sometimes the byproduct of the fabrication process, while at other times they are the planned result of engineering design. The fabrication processes which produce equatorial flanges on acrylic hemispherical shells are thermoforming techniques utilizing either compressed air or mechanical plungers (Figure 1). In either case, an equatorial flange is produced whose thickness is equal to that of the acrylic sheet utilized in thermoforming.

After completion of the thermoforming process, the flanges can be removed by machining so that the end product is a flangeless hemisphere whose structural response has been studied both analytically and experimentally in the past. The removal of the flange by machining is, however, an expensive operation that increases the cost of the end product approximately 100%. The thermoforming fabrication techniques for acrylic hemispherical shells would be more economically competitive if an equatorial flange could be tolerated from the structural viewpoint.

Furthermore, an equatorial flange on the acrylic hemisphere can often be used in securing the window to its seat in the viewport. This is of particular importance if the window is exposed during a typical operational cycle not only to external but also to internal pressure. Also, the flange can serve as a convenient location for the pressure seal. Since exploratory studies conducted in the past [13 and 14] have shown that an equatorial flange does not decrease significantly the short-term strength of acrylic plastic hemispherical shells, it appeared worthwhile to investigate further the concept of flanged hemispherical windows.

The flanged hemispherical shell windows tested in the first exploratory study utilized flanges with a sharp right-angle heel [14]. The sharp heel was chosen at that time as it was shown by another study [13] that a well-rounded heel on the flange may generate excessive bending moments in the shell accompanied by a high positive flexural stress component on the interior and a high negative flexural stress component on the exterior surfaces in the immediate vicinity of the flange-shell interface. It was felt that further studies on flanged acrylic hemispherical shells should include a curvature at the heel and the instep of the flange to simulate better the appearance of typical flanged hemispheres produced by thermoforming processes.

STUDY PARAMETERS

The objective of the study was to establish the safe operational pressure for typical flanged hemispherical shells of acrylic plastic utilized in pressure vessels for human occupancy.

The approach chosen was to fabricate and test representative flanged acrylic plastic hemispherical shells under short-term, long-term, and cyclic pressure loadings until signs of failure appeared.

The scope of the study was limited to a single thickness over inside diameter (t/D_i) ratio and two flange configurations (Figures 2 and 3). The t/D_i ratio chosen was 0.182, equal to a t/R_i ratio of 0.364. This ratio was considered to be adequate for working pressures in the 1,000- to 2,000-psi range based on the short-term collapse data from a previous study on flangeless acrylic plastic hemispherical shells.

TEST SPECIMENS

The flanged test specimens of acrylic plastic hemisphere were fabricated by thermoforming 3-inch-thick Plexiglas G stock. The thermoforming process consisted of forcing an appropriately shaped metallic plunger into the acrylic stock supported by a metal ring on four legs (Figures 4 and 5). The wall thickness of the extrusion was found to be more uniform than in hemispheres thermoformed by free blowing with compressed air [13]. The hemispherical extrusion was subsequently machined on the outside and inside to give the shell appropriate thickness, in and around the flange particularly.

Since the thermoforming process produced flanges that could be economically modified to another shape, if so desired, the test specimens were equipped with either a Type I or a Type VI flange (Figures 2 and 3). Twenty-four flanged windows were fabricated; 10 were equipped with Type I and 14 with Type VI flanges. Each window was identified by a capital letter.

The Plexiglass G material utilized in the thermoforming process met all the minimum physical requirements specified for man-rated windows by the Navy and the American Society of Mechanical Engineers [15].

TEST SETUP

Flanges

The flanged windows were tested on thick circular discs machined from low carbon steel (Figure 6). The steel test flanges were equipped with a central opening through which strain gage wires could be passed from inside the window. Holes around the circumference of the steel test flange were used for attaching the test flange to the vessel end closure adaptor plate and for securing the window to the flange. A smooth surface was provided on the steel test flange to minimize sliding friction between the contracting window and the test flange.

Pressure Vessels

For the testing of flanged windows both the 18- and 9.5-inch-diameter pressure vessels were utilized. The window was secured with a retainer ring or rubber bands to a steel test flange which, in turn, was attached to a pressure vessel closure adaptor that screwed directly into the vessel end closure. Since the steel test flange, vessel closure adaptor, and vessel end closure were equipped with a central opening, electric strain gage wires and a mechanical dial indicator rod could pass from the window interior to the vessel exterior.

Some of the vessels were provided with insulated jackets containing heating and cooling coils. In these vessels the temperature could be maintained within narrow limits. In other vessels the temperature of

the pressurized water could be maintained only within a wide range as the uninsulated vessels would rapidly follow the diurnal temperature variations inside the uninsulated laboratory building. As a result, the ambient test temperature in these vessels during the pressure testing of windows over a period of 24 months varied from a low of 65°F to a high of 75°F.

Instrumentation

The instrumentation for the pressure vessel consisted of a Bourdon type pressure gage and a remote reading thermometer. The pressure gage could be read within 50-psi intervals and the thermometer within 1°F.

The instrumentation for the acrylic plastic window undergoing hydrostatic testing consisted of rectangular 1/8 inch long* electrical resistance strain gage rosettes located on the interior face of the windows and a mechanical dial indicator measuring the radial displacement of the window's apex within 0.001 inch. The strain gages were attached to the acrylic at specific locations (Figure 7) with M-Bond 200 cement and subsequently waterproofed with Dow Corning 3140 room temperature vulcanizing silicone rubber coating.

The strains were recorded by a 100-channel B & F automatic data logger with magnetic tape data storage and digital paper tape printout. This recording unit was capable of recording at a rate of either 1 or 10 channels per second. As a rule, the 10-channel/second recording rate was utilized during pressurization and the 1-channel/second rate during sustained loading of window specimens.

Test Procedure

The bearing surface of the window flange was coated with silicone grease, a 1/8-inch-diameter O-ring was placed into the groove in the window flange, and the whole assembly was carefully placed on the steel test flange. Strain gage wires were fed through the opening in the steel test flange to the outside of the vessel end closure, and the dial indicator rod was centered on the window's low-pressure face.

To secure the window to the steel test flange, either steel retaining rings or elastic bands were employed. The steel rings were primarily utilized in the 18-inch-diameter pressure vessel (Figure 8) while the elastic bands were used to secure the windows to the steel test flange in the 9.5-inch diameter pressure vessel (Figure 9). In both cases, the radial restraint imposed on the window flange was minimal, only sufficient to compress the O-ring for proper sealing.

After the window was secured to the steel test flange, the interior of the pressure vessel was pressurized with tap water at a 650-psi/minute rate utilizing a positive displacement air-driven pump.

---

*Micro-Measurements gages type EP-08-125RA-120.

TEST PROGRAM

The experimental test program was designed to establish the maximum safe working pressures for the two types of flanged windows. On the basis of experimental data, the two types of windows could be compared to each other and to windows of the same geometry without a flange. The maximum safe working pressure was to be established by subjecting the windows of Type I and VI to a series of tests that would:

(1) *Determine short-term critical-pressure (STCP)* by pressurizing windows at a standard rate of 650 psi/minute until failure occurred.

(2) *Determine long-term critical pressure* by maintaining a constant sustained pressure loading until failure occurred.

(3) *Determine cyclic fatigue life* by subjecting the windows to cyclic pressure loading until failure occurred. The pressure cycles employed in the test program consisted of (a) pressurizing the window at 650 psi/minute to a specified pressure, (b) holding that pressure for 7 hours, (c) depressurizing to zero pressure at a rate of 650 psi/minute, and finally (d) relaxing at zero pressure for at least 17 hours before the next cycle was started. This cycle is termed for the purposes of this report the "standard load cycle."

Since there were more tests planned than the available number of windows, some windows had to be used in more than one test. Two windows were modified after testing to establish the effect of structural modification to the flange. In one case the rounded heel of the flange on Type I window E was replaced with a square heel to become Ⓕ while in the other case, the flange was removed completely, converting the Type I window I into a true hemisphere Ⓘ. All of the tests to which the windows were subjected have been summarized in Tables 1 through 5.

TEST OBSERVATIONS

Short-Term Critical Pressure Tests

Pressure. Five windows were subjected to continuous pressurization at the standard rate of 650 psi/minute until they failed (Table 1) (windows Y and Z had been tested previously). Window Y had endured long-term hydrostatic testing at 2,000-psi pressure without any visual damage. Window Z had been pressure-cycled twice to 8,000 psi with a rubber gasket and had suffered some crazing and a few slight cracks in the seating surface. The two Type I windows tested had an average short term critical pressure of 14,310 psi while the three Type VI windows had an average critical pressure of 14,700 psi.

Modes of Failure. All the windows that failed did so catastrophically after cracking sounds had been heard for a short time. Extensive fragmentation took place in all these cases.

Table 1. Short-Term Critical Pressure Tests

Window	Flange Type	Test Temperature (°F)	Location of Strain Gages (Figure 7)	Displacement	Short-Term Critical Pressure (psi)	Principal Results
A	I	a	-	yes	14,000	Catastrophic failure
B	I	a	-	-	14,620	Catastrophic failure
C	I	a	A, C, E	-	-	Test stopped at 12,500 psi and depressurized to zero
S	VI	a	A, C, E	-	14,530	Catastrophic failure
Y[b]	VI	71	-	-	14,325	Catastrophic failure; bottom plug blowout of pressure vessel at the same time the window failed
Z[c]	VI	70		-	15,223	Catastrophic failure

[a] Room temperature not specifically recorded.
[b] Window was previously tested at 2,000 psi (see Table 3).
[c] Window was previously tested at 8,000 psi with a gasket (see Table 4).

Table 2. Long-Term Critical Pressure Tests

Window	Flange Type	Average Test Pressure (psi)	Test Temperature (°F)	Location of Strain Gages (Figure 7)	Principal Results
D	I	9,670	a	A, C, E	Catastrophic failure after 22 hours
J	I	10,000	75	A, C, E, G, I	Catastrophic failure after 3 hours
H	I	7,675	45-75	A, C, E	Catastrophic failure after 153 hours
O	VI	9,700	a	A, C, E[b]	Catastrophic failure after 1+ hours
P	VI	≈ 10,000	a	A, E[b]	Catastrophic failure after 6 hours
V	VI	≈ 11,800	a	A, C, E[c]	Catastrophic failure after 42 hours
T	VI	≈ 9,850	a	A, C, E[c]	Catastrophic failure after 100 hours
R[d]	VI	≈ 12,000	71-75		Catastrophic failure after 0.5 hour

[a] Room temperature not specifically recorded.
[b] Gages functioned properly.
[c] Gages failed prematurely.
[d] Window was previously tested at 4,000 psi for 262 hours (see Table 3).

Table 3. Long Term Tests Without Implosion

Window	Flange Type	Average Test Pressure (psi)	Test Temperature (°F)	Location of Strain Gages (Figure 7)	Displacement	Duration of Loading (hours)	Principal Results
E	I	4,000	*a*	A, C, E	–	240	Some circumferential cracks in the bearing surface on the flange
I	I	2,000	75-76	A, B, C, D, E, F, G, H, I	–	269	No cracks or crazing detectable by visual inspection
Q	VI	7,000	*a*	A, C, E	–	139	Extensive crazing and large circumferential cracks in seat; one crack penetrating to outside
R	VI	4,000	*a*	A, C, E	–	262	Some crazing and shallow cracks in seat
U	VI	8,000	*a*	–	–	312	Window flange sheared off; numerous cracks and extensive crazing of seating surface; seat conical
Y	VI	2,000	71-73	A, B, C, D, E, F, G, H, I	–	119	No cracks or crazing detectable by visual inspection
Y	VI	2,000	72	A, B, C, D, E, F, G, H, I	–	7	No cracks or crazing detectable by visual inspection
W	VI	2,000	71-73	–	yes	95	No cracks or crazing detectable by visual inspection

[a] Room temperature not specifically recorded.
[b] Rubber gasket used instead of O-ring; window previously tested to 2,000 psi without gasket.

Deformation Under Short-Term Loading. At the standard rate of pressurization of 650 psi/minute, the compressive strain recorded by the strain gages increased in direct proportion to the pressure up to about 4,000 psi (Figure 10). Above this pressure the strain began to increase more rapidly, thus indicating the nonlinearity of stress versus strain.

The strain produced in the window in the linear range varied according to direction and location of the strain gages. At the apex, the strain was approximately the same in all directions with little change in magnitude from one point to another (Figures 11, 12, and 13). Moving away from the polar area, the circumferential strain increased by an average of 22% for the Type I windows and by an average of 14% for the Type VI windows (Figure 11), and at the same time, the meridional strains fell off sharply to small values (Figure 12).

Table 4. Cyclic Tests

Window	Flange Type	Test Pressure (psi)	Test Temperature (°F)	Location of Strain Gages (Figure 7)	Number of Pressure Cycles	Principal Results
I[a]	I	2,000	70-75	A, B, C, D, E, F, G, H, I	58	Cracking in window-bearing surface developed between cycle No. 33 and last cycle
J	I	10,000	75	A, C, E, G, I	1	Window failed catastrophically after about 3 hours of first pressure cycle
K	I	8,000	69-72	E	1	Window failed during first cycle by cracking along flange, causing leakage when pressure was released
M	I	6,000	66-73	A, C, E	22	Window developed cracks during second cycle; leaked after twenty-second cycle
BB	VI	[illegible]	68-72	[illegible]	2	Small cracks and crazing of bearing surface after first cycle; window leaked after second cycle
Z[b]	VI	8,000	70-72	A, C, E	2	Some crazing and three very shallow cracks in bearing surface after second cycle
AA	VI	6,000	66-73	–	22	Crack along O-ring groove after third cycle; cracks and crazing in bearing surface after fifth cycle
X	VI	5,000	68-73	E	40	Crazing of bearing surface developed between second and sixth cycles; cracks in bearing surface developed between twenty-second and twenty-seventh cycles

[a]This window was previously tested under sustained loading at 2,000 psi (see Table 3).
[b]A window was pressurized to failure under short-term loading (see Table 1).

The circumferential strain varied only moderately from test to test, the maximum deviation from the average of any test being only about 6% for the Type I windows and about 10% for the Type VI windows (Figure 11). For the strain in the meridional direction, there was a similar spread in the data for the polar area. Closer to the edge, however, the meridional strain varied markedly from test to test and at gage

Table 5. Cyclic Tests of Modified Windows

Window	Modification	Test	Test Temperature (°F)	Location of Strain Gages (Figure 7)	Principal Results
(E)[a]	O-ring groove and rounded heel removed by machining. Disc glued on to restore original dimensions, but with a sharp heel on the flange	11 pressure cycles at 2,000 psi	68-72	A, C, E	Some change in strain distribution compared to windows with rounded heel; 10 cycles performed with neoprene bearing gasket and 1 cycle without
(E)[a]	O-ring groove and rounded seat corner removed by machining. Disc glued on to restore original dimensions but with a sharp heel on the flange	1 cycle at 8,000 psi	70-74	A, C, E	Window bearing surface almost unharmed. Window cracked radially
(I)[b]	Flange and cylindrical part removed by machining	7 cycles at 2,000 psi	68-72	A, C, E	The strains are more uniform all over the interior surface of the window
(I)[b]	Flange and cylindrical part removed by machining	2 cycles at 8,000 psi	70-75	A, C, E	No cracks observed on the bearing surface or anywhere else on the window

[a] Window was tested for 240 hours at 4,000 psi prior to modification (see Table 3).
[b] Window was tested for 269 hours at 2,000 psi prior to modification (see Table 3).

A (Figure 12) the results were almost erratic, particularly for the Type VI windows. The cause of this large spread has not been investigated.

At hydrostatic pressures in excess of 4,000 psi, the nonuniform character of the strain over the window surface was exaggerated (Figure 14), and the strains were higher than predicted by linear extrapolation of the strains at low pressure. Thus, at 10,000-psi external pressure, the nonlinear part was between one-third and one-half of the linear strain, depending on location (Figure 15).

Displacement of Apex. In one case, the displacement of the windows at the apex towards the center of the sphere was measured. The specimen was a Type VI window (window W). After an initial phase where the window seated itself, the displacement was linear with pressure up to the test pressure of 2,000 psi. The displacement per unit change of pressure divided by the internal radius of the spherical part of the window was 3.5×10^{-6}/psi (Figure 16).

Long-Term Tests

Tests Resulting in Implosion. Five Type VI windows and three Type I windows were pressurized at the standard rate of 650 psi/minute up to the test pressure. The test pressure was maintained constant until failure occurred.

The life of the windows loaded this way varied inversely with the test pressure. The relationship between the life and the test pressure was nonlinear with a very rapid fall off in life above approximately 8,000 psi (Figure 17). The spread in the data was very large compared to the spread in the magnitude of short-term critical pressures, indicating that long-term test parameters, like temperature, were not maintained within a sufficiently narrow range to preclude large spread in test data.

In all cases of failure under long-term loading, the failure was catastrophic, resulting in heavy fragmentation of the windows (Figures 18 through 26). Typically, the force of implosion blew a hole in the window dome producing grain size fragments of the blown-out material. The rest of the dome stayed relatively intact, although it was always fractured radially into several pieces (Figure 21). In addition to the radial fractures, a large number of in-plane fractures occurred. The number of in-plane fractures increased toward the interior surface of the window. The outer 1/4 inch or so of the wall was usually not laminated (Figure 24).

After implosion, the flanges were found to be separated from the main body of the windows. In Type I windows, the separation was all around the flange (Figures 18 and 19), while in the Type VI windows the separation was partial (Figures 20 and 21). The flange separated from the dome generally before implosion occurred, as demonstrated by window U whose long-term loading was terminated prior to implosion (Figures 22 and 23).

The window flange bearing surfaces fractured during the tests in the circumferential direction (Figure 25). The heel (inside edge) of the flange was permanently deformed, resulting in the formation of a sharp edge that contrasted sharply with the original well-rounded-heel geometry (Figure 25). The deformed fragments also showed that the thickness of the wall above the flange permanently increased by about 25% of the original thickness (window J). A similar increase was observed in the width of the flange measured between the inside edge of the heel and the O-ring groove. The height of the flange, however, was unchanged (Figure 25). These observations were further confirmed by a study of the fragments of window P (Figure 26).

Tests Terminated Prior to Implosion. Two Type I and five Type VI windows were subjected to long-term tests of varying length and at different pressures (Table 3).

At 2,000 psi, no visible damage was caused during the 269 hours of loading on window I at 75°F. The window strains relaxed completely after the test (Figure 27).

At 4,000 psi, some crazing and shallow cracks were observed in the seat of window R when inspected after 262 hours (Figure 28). Also, this window relaxed completely after the test. All strain gage readings were within 100 μin./in. of the reading before the test after a relaxation time of about 100 hours. The bearing surface on the flange, however, had some permanent deformation, producing a slight conical shaped surface similar to that shown in Figure 22.

At 7,000 psi, window Q suffered extensive crazing and several large cracks at the seat during the 439-hour test (Figures 29 and 30). In this window, the strain in the polar area averaged 0.056/in./in. at the end of the creep period. But even so, after about 100 hours of relaxation, the strain in this area was within 0.001 in./in. of the reading before the test. Significant permanent deformation was observed in the bearing surface of the flange, transforming it from a plane to a conical surface.

At 8,000 psi, window U lasted 312 hours without imploding; the window was, however, severely damaged. The flange had separated and the bearing surface was deformed into a conical surface which had several large cracks in it (Figures 22 and 23).

In those tests where the pressure was kept constant for a long period of time, the strain on the interior surface did not become tensile at the end of the relaxation period.

Deformation Under Long-Term Loading. At 10,000 psi (70% of STCP) of external pressure, the strain increased very rapidly after pressurization was completed. The increase was largest in the window areas that already had the largest strains. Thus, the unevennesses of the window deformation already apparent after pressurization became more pronounced with time (Figure 31). As evident from the end result, the rate of deformation at 10,000 psi was so high that after a few hours the window became so plastically deformed that it could no longer sustain the load (window J).

At 8,000 psi (56% of STCP) and lower pressures, the strains still increased rapidly immediately after the end of pressurization. The strain rate slowed down sufficiently, however, after the first 2 to 3 hours to give the window extended life. At 7,000 psi (49% of STCP), window Q did not fail catastrophically during the 139 hours the pressure was maintained. At 8,000 psi, the unevenness of the window deformation became greater with time (Figure 32), just as for the window tested at 10,000 psi (Figure 31). At lower pressures, this tendency became less pronounced and at 2,000 psi was hardly noticeable (Figure 33).

At moderate strain levels, the deformation of the windows appeared to be quite symmetrical. This was evident from the measurements on windows I, Y, and J, which had strain gages on both sides (Figure 13, 31, and 33). In these cases, all three gages of the rectangular strain gage rosette at the apex indicated essentially the same strain values. As the strains increased in magnitude, however, the differences in the readings of the three gages at the apex often became greater.

This occurrence may be the result of the window starting to lose its sphericity. In the case of window J (tested at 10,000 psi) the distribution of circumferential strain appeared to be symmetrical at the end of pressurization. During the first hour under pressure, however, the strain increased much faster on one side than on the other indicating that the window was losing its spherical shape (Figure 31).

Taking into account the scatter in data, no significant difference was observed in the time-dependent deformation of the two types of windows (Figure 34). In both cases, the location on the window that had the highest strains at the end of pressurization also had the highest strain throughout the creep period. In both cases, the strain distribution became more uneven as time went on (Figures 32 and 35).

The strain in the window after any given duration of sustained load was found to be a nonlinear function of the load. Thus, after 1 hour at 4,000 psi, the strain at the apex of the window was approximately 2.1 times the strain after 1 hour at 2,000 psi. After 1 hour at 10,000 psi, the strain at the apex was 10 times the strain after 1 hour at 2,000 psi (Figure 36). This clearly demonstrates that acrylic material becomes more compliant as temperature or stress is increased. If the additional strain due to creep alone is plotted, the nonlinear behavior becomes even more apparent (Figure 37).

As noted before, long-term loading at pressures high enough to cause catastrophic failure, also caused permanent tensile radial strain in the dome. By measuring the thickness of fragments of the dome of the imploded windows, the average permanent radial strain was found to vary from about 25% (0.25 in./in.) above the flange to about 12.5% halfway between the flange and the apex (windows J and H) (Figure 38).

Cyclic Pressure Tests

Fatigue Life. It was immediately realized after initiation of cyclic pressure testing that the fatigue life of the windows would be lower than expected.

At 10,000 psi, which is approximately 70% of STCP, the test specimen (window J) did not complete the first cycle. The window failed catastrophically after about 3 hours.

At 8,000 psi (56% STCP) the Type I (window K) cracked during the first cycle to the extent that when the pressure approached zero at the end of the cycle, water filled up the low pressure cavity. The Type VI window that was tested at 8,000 psi (window BB) developed similar cracks and leakage during its second cycle.

At 6,000 psi (42% of STCP) the Type I window (window M) cracked catastrophically during its twenty-second load cycle. The Type VI window (window AA) tested at the same pressure was still intact after 22 load cycles, but had deep cracks in the seat area.

At 5,000 psi (35% of STCP) crazing of the seat was apparent when the Type VI window (window X) was inspected after the sixth pressure cycle. Cracks developed in the seat between cycle 22 and 27, but no leaks occurred before the test was terminated after the fortieth cycle.

At 2,000 psi (14% of STCP) the Type I window (window I) did not show any change after 33 pressure cycles. When the window was inspected again after the fifty-eighth cycle, however, a deep crack was found in the flange starting from the O-ring groove.

Modes of Failure. In all cases, cracks initiating from the bearing surface on the flange were the cause of failure. In some cases (windows AA, Figures 39, 40, and 41; and I, Figure 42), the first sign of fatigue was a crack originating from the O-ring groove. The cracks had a characteristic half-moon shape when viewed from the side and appeared to be approximately parallel to the low-pressure face of the window as shown in Figure 43.

In all the other cases, the cracks originated at the bearing surface of the flange between the heel and the O-ring groove and were always preceded by crazing. The crazing, as well as the subsequent cracks, had the same orientation as the cracks originating from the O-ring groove (Figures 39 to 46). The cracks not originating in the O-ring groove had the characteristic mushroom shape instead (Figures 39, 40, 41, 47, and 48).

Cracking of the interior face occurred in two Type I windows (windows M and Ⓔ). In window M, the failure occurred after 22 standard load cycles to 6,000 psi and consisted of three fractures running in the meridional direction originating on the bearing surface of the window. One of the cracks ran like a meridian across the apex from one side of the window to another, while two other cracks stopped at the apex (Figure 49). The cracks penetrated between 25 and 50% of the wall thickness. On the inside face of the window, the width of the cracks varied from close to zero at the apex to about 0.040 inch at the flange. The entire inside surface was markedly crazed after the test but less than on the bearing surface (Figure 50).

Window Ⓔ failure occurred after one cycle at 8,000 psi. The window had previously been subjected to 11 standard load cycles at 2,000 psi and a long-term test at 4,000 psi for 259 hours. After the long-term test, but before the cyclic tests, the seat of the window was machined down to remove the rounded inside edge of the heel and the O-ring groove. An annular disc was bonded in its place to restore the original height of the flange. When the pressure was down to about 500 psi during depressurization from 8,000 psi at the standard rate, three or four loud cracks were heard and the window's interior filled with water.

Inspection of the window Ⓔ revealed that spalling had taken place on the square edge of the heel, that crazing and a number of shallow half moon cracks had formed in the bearing surface of the flange, and that the interior face of the window had three large cracks as shown in Figures 51, 52, and 53.

Low-pressure leaks developed in four cases. In two of these (windows BB and K, both tested at 8,000 psi) the leak was due to the circumferential cracks propagating through the flange to the exterior face of the windows (Figure 54 and 55). In the third case (window N, tested at 6,000 psi), the usual circumferential cracks occurred after the second cycle, but the window did not develop a leak until it cracked on

the interior face after 22 load cycles as noted above (Figure 49). In the fourth case (window (E) tested at 8,000 psi), a leak occurred after the first cycle.

Deformation. Deformation of the windows was measured with electrical strain gages located on the low-pressure face (Figure 7). In three tests (windows I, M, and X), where such measurements were performed, it was found that tensile strains were building up on the internal face at the end of each relaxation period; i.e., the strain datum value prior to each load cycle was increasing in the positive sense. The tensile strains had a distribution over the face of the window similar to the distribution of maximum compressive strains at the end of each load cycle (Figures 56 and 57). In the case of window M, this buildup of tension on the inside surface caused the failure of the window — apparent from the radial cracks that developed during the twenty-second load cycle (Figure 49). After several days of relaxation, the cracks in window M were actually widening as time went on indicating that the interior face was contracting.

The rate of buildup of the tensile strains on the window's interior face increased dramatically with magnitude of pressure loading during a typical pressure cycle. During pressure cycling to 2,000 psi (window I) the increase in tensile strain during the relaxation period averaged about 45 μin./in./load cycles performed (Figure 58). During pressure cycling to 5,000 psi (window X) the same level of tensile strain was reached in 3 cycles that it previously took 40 cycles to reach during the cycling to 2,000 psi. Also, at 5,000 psi, the increase in tensile strain per cycle was no longer linear and increasing rapidly (Figure 59). At 6,000 psi, the tensile strain built up even more rapidly (Figure 60). The data were somewhat scattered, but it was apparent that the buildup rate was more than twice that observed during the pressure cycling to 5,000 psi.

The specimen tested at 5,000 psi (window X) had only one strain gage rosette (at the apex) so that no information was obtained about the buildup of tensile strain at other locations. Window M, which was tested at 6,000 psi, however, had rosettes also at locations A and C in addition to one at the pole. This test confirmed the results from the test on window I at 2,000 psi, i.e., that the strain builds up even faster closer to the window flange than at the apex. The data from pressure cycling to 5,000 psi (window M) show appreciable scatter from cycle to cycle. It is not known why this occurred but a contributing cause may have been that in some cases the pressure vessel was closed off during the relaxation period instead of being connected to the constant header tank. If the vessel was closed off, the expansion of the window would cause some buildup of pressure in the vessel which would tend to counteract the relaxation. Unfortunately, no record was kept of the times that this was done.

For window I the cycling at 2,000 psi did not lead to changes in the maximum strain produced during each separate load cycle; i.e., the strain recorded at the end of the creep period minus the recording just prior to pressurization was very close to the same for all cycles (Figure 56 and 57).

The same behavior was observed also for window M cycled at 6,000 psi (Figure 60) and window X cycled at 5,000 psi. The total change of strain at the pole of window M was about 0.030 in./in. with a random variation of less than 2% up and down. The total change of strain at the pole of window X was about 0.024 in./in. and, again, the variation was less than ±2%.

Modifications of Seating Arrangement

After most of the test program was completed but during the initial stages of the cyclic tests, it became apparent that the cyclic life of the Type I and Type VI windows would be substantially less than anticipated. Compared to conical frustum windows with the same STCP, the cyclic fatigue life of Type I and Type VI windows was significantly less. Cyclic fatigue primarily consisted of circumferential cracks in the bearing surface of the flange and secondarily of radial cracks in the low-pressure face of the window. To improve the fatigue life of the bearing surface on the flange, it was decided to try the following modifications:

(1) Remove O-ring and use a thin neoprene bearing gasket to seal and absorb shear strain.

(2) Remove O-ring groove and replace the rounded heel of the flange with a square heel.

(3) Remove flange and cylindrical part of window.

Only a very limited number of tests were performed on each modification.

Effect of Neoprene Bearing Gasket. To reduce the shearing force on the acrylic plastic in contact with the steel surface, a soft neoprene gasket of 0.020-inch thickness was bonded to the bearing surface on the window flange. The gasket consisted of nylon cloth coated with neoprene. The O-ring used previously for sealing was removed from the groove in the window flange, and the gasket was placed over the whole bearing surface on the flange. Before assembly, silicone grease was applied to the steel bulkhead as in the earlier tests.

Two tests were carried out with this arrangement. The first was Type I window Z, subjected to two standard pressure cycles at 8,000 psi. The effect was very marked. The acrylic plastic bearing surface protected by the neoprene gasket was only slightly damaged. The damage consisted of minor crazing of the bearing surface, reflecting the pattern of the weave in the gasket plus three very shallow cracks (Figures 61 and 62). In contrast, the two windows tested at 8,000 psi without the gasket (windows K and BB) suffered through-the-thickness cracks after two cycles. The crazing and small cracks in the seat of window Z almost disappeared after the window had relaxed for 14 days after the test (Figure 63) in atmospheric environment.

On the other hand, the deformation of the window having the neoprene gasket was not significantly changed compared to the deformation of windows seated directly on steel. In the linear range (up to approxi-

mately 4,000 psi) the strains recorded were all within the range of earlier tests. (Compare Figure 64 to Figure 12.) This also applied to the strains recorded at pressures above 4,000 psi and during the creep periods. (Compare Figure 64 to Figure 34.)

The gasket was cut during the vessel cycling to 8,000 psi. Two cuts were found in the circumferential direction at the inside corner of the window seat. The cuts were about 3 inches long and located diametrically opposite each other (Figure 65).

The second window tested with the neoprene gasket was Type VI (window Y). This window had previously been tested for 119 hours at 2,000 psi (Table 3). A neoprene gasket was cut radially at four locations about halfway through to enable its being slipped over the window without having to disconnect the strain gage wires. This time the neoprene gasket was not bonded to the window flange, but was coated with silicone grease on both sides. The window was tested at 2,000 psi for 7 hours, and strains were recorded both during the pressurization and the creep period. As in window Z, the strains in the window were not significantly changed by the presence of the gasket (Figure 66).

Effect of Rounded Flange Heel. Window E was machined down about 1/4 inch to remove the rounded heel and the O-ring groove. An annular acrylic plastic disc was bonded in its place to restore the original height to the flange, as shown in Figure 67. Finally, the window was annealed at 170°F for 24 hours.

The modified window (E) was subjected to 10 standard pressure cycles at 2,000 psi while mounted on the neoprene gasket and one standard load cycle at 2,000 psi without the gasket sealing but with silicone grease. Finally, window (E) was tested at room temperature for 7 hours at 8,000 psi, again with no gasket. The intentions of the tests were to determine whether or not the modifications had changed (1) strain distribution on the interior face of the window, (2) buildup of tensile strain on the interior face of the window after relaxation, and (3) the tendency for the bearing surface to crack under high loading.

The change in strain distribution without a gasket as measured after 7 hours at 2,000 psi was quite marked near the heel of the window while the strain at the apex was changed very little (Figure 68). As expected, the distribution of meridional strain became more uniform.

The 10 cycles with a gasket seal produced a steady buildup of tensile strain in the interior face of the dome (Figure 69). The rate of buildup was similar to that measured earlier in Type I window I tested at 2,000 psi without gasket (Figure 58).

In the final test consisting of one standard cycle at 8,000 psi, no gasket was used. The window performed normally until the pressure reached about 500 psi during depressurization at the end of the load period. At that time several load cracks were heard. On inspection afterwards, it was seen that:

(1) the seat was in good condition with only moderate crazing and some small circumferential half-moon cracks less than 1/16 inch deep. No spalling had taken place on the sharp flange heel (Figure 70).

(2) The window had cracked radially in the meridional direction on the inside of the dome (Figure 51).

It may be concluded that a square inside seat edge improves the life of the window seat, while the effect on the tendency for the dome to crack is probably small or absent.

Effect of Flange Removal. Window I was machined down so that the entire flange was removed as shown in Figures 71 and 72.

The modified (I) window was then cycled four times to 2,000 psi. The first and the fourth cycle consisted of 23 hours under pressure followed by at least 17 hours of relaxation. In the second and third cycles, the pressure was held for 7 hours. At the end of the 23-hour load period of the fourth loading, the pressure was raised to 8,000 psi and held at that level for 6-1/2 hours. After 17 hours of relaxation, window (I) was finally pressurized once more to 8,000 psi for 7 hours. At 2,000 psi, the window deformed uniformly over most of the dome. At the edge, the meridional strain increased somewhat compared to the level at the apex. The circumferential strain at the edge was slightly lower than at the apex (Figure 73). This distribution is quite different from the distribution in typical Type I flanged window.

After the two cycles to 8,000 psi, window (I) was removed from the vessel for inspection. The findings were: (1) the seat was still in good condition — no cracks and only very slight crazing (Figures 74 and 75), and (2) the plane seat was permanently deformed (Figure 76) to form a conical surface similar to that observed in flanged windows (Figure 22).

The test was too short to give firm data on any buildup of tensile strain on the interior face.

DISCUSSION OF FINDINGS

Short-Term Critical Pressure (STCP)

Findings.

(1) The average STCP of Type I windows at 70°F was 14,310 psi while the average STCP of Type VI windows at 70°F was 14,700 psi. The difference between the two values is statistically insignificant, and the average of all short-term window tests (that is, 14,500 psi) is considered to be the STCP for both types of windows.

(2) The failure of the windows on reaching the STCP was catastrophic. The window failed by plastic instability of an area on the window located between the flange and the apex. The implosion caused complete fragmentation of the window. The formation of the flat spots on the windows (typical of plastic instability failure) was reflected in the strain distribution on the interior face of the windows. Whereas the strain distribution was symmetric about the apex at lower hydrostatic loadings, the distribution became unsymmetric prior to catastrophic failure.

(3) The flange of the windows sheared from the dome before or during catastrophic failure at STCP.

Discussion. Short-term critical pressure tests of hemispherical windows were reported previously for flangeless (Reference 8) and flanged (Reference 14) configurations. Compared to the predicted STCP based on previously published data for flangeless hemispherical windows, the STCP of the present windows is about 5% lower. A reduction of the STCP of flanged windows when compared to flangeless windows in the higher t/R_i range has been previously reported (Reference 14). This indicates that, for $t/R_i \geq 0.25$, flanged windows may have a lower STCP than similar windows without a flange (Figure 77). Since the comparison is based on tests carried out at different times on windows of different manufacture, firm conclusions on this point cannot be drawn. The reason for the seemingly lower STCP of flanged windows as compared to flangeless windows is probably the increase in meridional edge bending moment caused by the rounded heel of the equatorial flange.

It has been shown previously that thick-wall spherical windows fail catastrophically by plastic instability of the dome (References 8 and 14). The windows with thinner walls fail by elastic buckling, and the transition between the two modes of failure is found to be at t/R_i ratios of approximately 0.09. The present tests confirm that at $t/R_i = 0.364$, the failure is caused by plastic instability of the dome.

It can also be shown theoretically that a thick-wall spherical window attains complete plasticity through its wall thickness before it fails. Using Lame's equations for thick-wall hollow spheres subjected to external hydrostatic pressure, it is seen that as the external pressure increases, the material at the inner face of the sphere reaches its yield point first. If the pressure is raised further, yielding extends deeper and deeper into the wall until finally, yielding reaches the outer surface.

By making two simplifying assumptions, the external pressure at which the whole wall becomes plastic can be estimated. The assumptions are: (1) the distribution of radial stress is not affected by the yielding of the material (i.e., it can be calculated based on elastic theory); and (2) once the yield point is reached, the material will not support higher stresses, but continues to support the same stress independent of further increase in strain.

Using these assumptions, the Lamé's equation can be applied to predict conservatively the pressure P_c at which complete plasticity is reached during short term pressurization. The formula becomes:

$$\frac{P_c}{\sigma_y} = \frac{(1 + \alpha)(1 - \alpha^3)}{3\alpha^2}$$

where $\alpha = 1/(1 + t/R_i)$

σ_y = yield stress of material in uniaxial compression under short term loading

t = wall thickness of sphere

R_i = internal radius of sphere

The equation has been plotted for a yield stress of 18,000 psi, typical of Plexiglass G acrylic plastic used in the fabrication of flanged windows (Figure 77). It can be seen that the result is nearly a straight line falling below all the experimental points for $t/R_i > 0.1$.

For experimental points with $t/R_i \leq 0.1$, the complete plasticity curve lies above the experimental points indicating that elastic instability and not plasticity is the cause of failure in these cases. It can be stated therefore, that for hemispherical windows with a $t/R_i > 0.15$ the P_c as calculated by the above equation (using the appropriate σ_y value for the ambient temperature) gives a conservative estimate of the STCP of these windows.

Long-Term Critical Pressure

Findings.

(1) No significant difference was found between the long-term life of the Type I and Type VI windows (Figure 17).

(2) Above 8,000 psi of external pressure loading (55% of STCP) the life of the windows decreased rapidly with increasing pressure, approaching only a few hours at 10,000 psi.

(3) The maximum external pressure loading at which the windows still retain the 10^6 minutes minimum static fatigue life required of man-rated windows (Reference 15) was extrapolated to be approximately 5,800 psi.

(4) The failure of the windows subjected to long-term loading was catastrophic in all cases with extensive fragmentation.

(5) Prior to failure, extensive plastic deformation had taken place in the windows increasing the wall thickness by about 25% immediately above the flange and decreasing the interior diameter at the flange by about 10% (windows R and J, Figures 25, 26, and 78).

Discussion. It is evident from the large spread in the results that at pressures above about 65% of the STCP, the windows become increasingly sensitive to variations in factors affecting their load-carrying capacity.

Tests were not conducted to investigate this point further. However, since a similar spread in results was not observed for the STCP, the spread in long-term critical pressures is probably tied to long-term variables in the tests. One such variable was sustained external pressure loading. Because of a relatively large ratio of window displacement to pressure vessel volume, there were problems in maintaining a constant test pressure during the high-pressure tests. Typically, the pressure would be restored each hour during the daytime but not at night. To compensate for this, an estimated average pressure was worked out for each test, but this procedure had obvious deficiencies.

Another long-term test variable was the ambient temperature, which changed somewhat from test to test. Although the difference was generally less than $5^{o}F$, the effect on the creep properties of the material was significant. Published data from other studies indicates that a $5^{o}F$ variation in ambient temperature can change the fatigue life of an acrylic structure by a factor of at least 10 and possibly 15 (Reference 16).

The fact that the window walls increased in thickness by as much as 25% during the long-term critical pressure tests, further substantiates the postulate made before that the window wall is completely plasticized before failure takes place (Figure 26).

Cyclic Fatigue Life

Original Design Findings.

(1) Both types of windows exhibited signs of fatigue at hydrostatic pressures at less than 15% of their short-term critical pressure. The failures, defined here as leakage through cracks, occurred in less than 100 cycles of the standard load cycles at 30% of their short-term critical pressure.

(2) The first sign of fatigue was circumferential crazing marks on an annular bearing area between the O-ring groove and the heel of the flange (Figure 62), except for one case where a crack started from the O-ring groove before any crazing had developed.

(3) If cycling continued after appearance of crazing on the window seat, the crazing increased until eventually actual cracks were formed. The cracks always ran in the circumferential direction, sometimes in the O-ring groove but more often in the bearing surface between the heel of the flange and the O-ring. The cracks typically had a mushroom shape (Figures 39, 46, and 41).

(4) Under moderate cyclic loading of up to 5,000 psi external pressure, both crazing and cracks in the seat grew slowly once they had formed and did not render the window incapable of sealing in less than 30 load cycles. At cyclic loading of 6,000 psi, cracks grew noticeably faster with each cycle; but even so, the window sustained 20 cycles without leaking.

(5) At severe cyclic loading of 8,000 psi, the rate of crack propagation was greatly increased. Only two cycles were needed at this pressure for the cracks to propagate through the flange to the outside and hence cause a low-pressure leak (Figures 54 and 55).

(6) Cracks were found in the bearing surfaces of windows that imploded during the first standard cycle (Figure 25). The cracks must therefore have formed while the windows were under sustained pressure and not during relaxation periods.

(7) Cycling of the windows caused a step-wise buildup of tensile strain on the interior face of the spherical dome during relaxation after each load period. The magnitude of tensile strain recorded during relaxation periods between individual pressure cycles was found to be a nonlinear function of pressure and number of load cycles sustained. In both cases, the magnitude of tensile strain increased faster than the maximum pressure, or the number of load cycles. The tensile strain also built up faster in the areas where the compressive strains were the highest during the loading period (Figures 58, 59, and 60).

(8) In one case the buildup of tensile strain was the cause of severe cracking of the window's concave surface. The cracking occurred as the pressure was approaching zero during depressurization after 22 standard load cycles at 6,000 psi with the magnitude of tensile strain estimated at about 0.050 in./in. (Figures 49 and 50).

(9) Fatigue cracking did not cause catastrophic failure of any window during cyclic load testing. In the worst case, the windows leaked after the pressure had been relieved. (This seems reasonable because cracking at the seat is not a part of the STCP failure mode of the window.)

Original Design Discussion. In view of the above findings, the fatigue life of a window must be taken as either the number of cycles taken to produce the first crack or the number of cycles taken to produce a leak. The criteria chosen may depend on the application of the windows. For man-rated applications, the first criterion should be used; for example, the fatigue life of a window used in a man-rated chamber is the number of cycles sustained by the window when the first crack appears anywhere in the window (Figures 79 and 80).

Due to the scatter in the data and the limited number of cyclic tests performed, it is not possible to establish a firm fatigue life for the windows. The recommended course of action at the present time is to inspect the windows after each pressurization *in excess of 1,000 psi* and replace any window immediately that shows signs of fatigue.

Modified Design Findings. Improved fatigue life was obtained by each of the following modifications:

(1) Use of 0.020-inch-thick neoprene gasket between the window and the steel flange.

(2) Removal of the O-ring groove and replacing the rounded heel of the flange with a square heel.

(3) Removal of the flange to make the window a true hemispherical dome.

The limited number of tests available did not allow determination of quantitative improvement obtainable by each, or by a combination of these modifications.

Modified Design Discussion. The original Type I and Type VI design is not suitable for cyclic loading except at pressures below 1,000 psi at 75°F. If the original designs were to be used, Type VI would probably give the longest life.

If the flanges are to be retained, it is required that for cyclic loading above 1,000 psi both the O-ring groove and the rounded heel of the flange be removed and that a thin, soft, nylon-fiber-reinforced neoprene gasket be installed underneath the window's bearing surface to absorb the shear strain at the steel/window interface. To find what the improved cyclic fatigue life is if these modifications are incorporated into Type I and Type VI windows, a series of new tests would have to be carried out. These tests should be designed not only to check the effect on the bearing surface of the window, but also the buildup of strain on the interior surface of the window at the apex, as it is postulated that this will be the limiting factor of the cyclic fatigue life in the modified design. By incorporating the above-mentioned modifications an adequate fatigue life (1,000 cycles without leakage) is predicted for operational pressures to 2,000 psi.

Removal of the flange improves the cyclic fatigue life significantly both for the bearing surface and the interior face at the apex. Although the improvement in cyclic fatigue life has not been quantitatively established for flangeless windows it is conservatively estimated to be in excess of 2,500 psi at 75°F.

As stated above, the fatigue life of the windows is limited by cracking of the bearing surface on the flange and the interior face of the dome. Both conditions have been observed by earlier investigators [8,10].

The cracking of the bearing surface on the flange is undoubtedly tied to the differential motion taking place at the window/steel interface during the sustained pressure phase. The natural remedy for this problem is, therefore, to enable the window to slide with the least possible resistance. Hence, the neoprene gasket was tried. It is possible that even better results could be obtained using other materials, such as polycarbonate which has been successfully incorporated in the NEMO Mod 2,000 [17]. The polycarbonate insert not only is capable of absorbing the shear strain to a much larger degree than the acrylic, but should it crack, only the insert needs to be changed and not the whole window. Whatever material is used for the insert, it has to be either sufficiently stiff or sufficiently thin to prevent its being pushed into the window cavity by external hydrostatic pressure.

The problem of cracking on the interior face of the window due to buildup of tensile strain is more difficult to explain and to remedy. Probably, this phenomenon is a result of the loading conditions, the geometry of the window and the physical properties of acrylic plastic. If the dome had been made from steel, the stress (effective von Mise's) at the inner face would have been about 2.5 times higher than the stress at the outer face. If the dome was overpressurized, the steel at the inner face would yield. During depressurization, the plastically deformed interior face would therefore not be able to expand as much as required by the material at larger radii that had been deformed only elastically. Releasing the pressure, therefore, generates tensile stresses in the interior face of the dome.

In the acrylic plastic dome the mechanism, although similar, is complicated by the time, temperature, and stress-dependent properties of the material. Because of the viscoelastic property of acrylic elastic tensile stress may be generated on the inner face of the window during depressurization even though the hydrostatic loading was not of sufficient magnitude to deform the material on the inner face permanently. Thus, in the acrylic plastic, a sudden release of pressure is likely to cause higher tensile stresses on the inner face than a slow release, as the rate of relaxation for the inner face is slower than for the outer face that is subjected to a viscoelastic strain of lesser magnitude. Also, the duration of the sustained loading, the length of the relaxation, and ambient temperature influence the magnitude of tensile stresses during relaxation.

Deformations

Original Design Findings.

(1) The interior surface of the windows at the apex deformed elastically up to at least 0.020 in./in. of compressive strain. Relaxation from this strain level was about 99% complete in 10 hours after release of pressure.

(2) Polar strains (interior surface at the apex) of 0.0020 in./in. magnitude were attained at about 6,250 psi of external pressure during short-term loading (650 psi/minute rate). During long-term loading, this strain level was reached in less than 1 hour at 5,000 psi, while at 4,000 psi the same strain level was reached only after 262 hours. At sustained hydrostatic loading of 2,000 psi, this strain level would definitely not be reached in less than 10,000 hours.

(3) Permanent deformation of the material at the bearing surface of the window's flange occurred even when no permanent deformation took place elsewhere. In all cases of permanent deformation in the flange, the deformation was such as to change the bearing surface from a plane surface into a slightly conical surface having an imaginary apex inside the window cavity. The onset of permanent deformation of this type was observed in the window loaded at 2,000 psi of hydro-

static pressure for 269 hours at 75°F. The deformation was very slight, being hardly measurable. On the other hand, in a window subjected to hydrostatic loading of 8,000 psi for 312 hours, the bearing surface of the window was deformed approximately 4 degrees (Figure 22).

(4) In the elastic strain region, the internal window surface of the windows at the apex deformed uniformly with the same strains in all directions. Comparing the measured strain in this area with the theoretical value for the interior face of a thick-wall hollow sphere (Lame's equation with $\mu = 0.4$ and $E = 400{,}000$ psi), the measured value was found to be about 18% smaller than the theoretical (Figure 81). This indicates that the effect of restraint imposed by the flange is almost damped out in this area. The equatorial area of the window also deformed uniformly in the circumferential direction. In the meridional direction on the other hand, the strain changed substantially, reflecting the effect of flange restraint. Moving from the apex towards the edge, the meridional strains decreased; at the same time, the circumferential strains increased. This behavior is probably due to the outward bending movement at the edge caused by the rounded heel of the flange. The deformed shape of the window is postulated to be as shown in Figure 82.

(5) Under extreme loading, the deformation of the window inevitably would also become nonuniform at the apex and in the circumferential direction elsewhere. This was substantiated by the formation of flat spots; and, unless the pressure was reduced, the window failed catastrophically. If the pressure was maintained, the windows would implode when the compressive strain on the interior surface at the apex reached a magnitude of 0.080 to 0.10 in./in. The strains at the flat spot were often even higher, possibly more than double, as indicated by the data from one test (Figure 31).

Modified Design Findings.

(1) The introduction of a thin neoprene gasket between the window and the steel led to a slight increase of strain on the dome of the window (Figure 66).

(2) The replacement of the rounded heel with a square heel in window (E) led to a much more even distribution of meridional strains on the inside of the window. The meridional and the circumferential strains also became more equal, particularly near the heel of the flange (Figure 68).

(3) The total removal of the whole flange led to a remarkable change in the deformation of the window. Window (C) now a true hemisphere with no wall-thickness variation, deformed quite evenly from the apex to the equator (Figure 83). The ratio of the highest to the lowest compressive strain measured on the interior face of the window was now 1.3 (compared to 1.8 for the window with rectangular heel on the flange and 12 for the original geometry with well-rounded heel).

SUMMARY OF FINDINGS

The maximum safe working pressure of a hemispherical window with equatorial flange is, as has been experimentally determined previously for other window shapes, a function of short-term critical pressure,[a] long-term critical pressure, and cyclic fatigue. For flanged hemispheres with a $t/R_i = 0.364$, the short-term critical pressure at 75°F has been found to be 14,500 psi; long term critical pressure,[b] 6,000 psi; and cyclic fatigue life,[c] 1,000 psi. No significant difference was found in the performance of windows with Type I or Type VI flanges.

The primary effects of cyclic fatigue is in the form of circumferential cracks that develop on the bearing surface of the flange at approximately 1,000-psi cyclic pressure loading level. If stress discontinuities in the form of O-ring grooves on the bearing surface are eliminated and the effect of shear loading on the bearing surface ameliorated by use of neoprene bearing gaskets, the effects of cyclic fatigue on the bearing surface can be eliminated at cyclic pressure loadings $\leq$4,000 psi.

Raising the cyclic fatigue life threshold on the bearing surface from 1,000 psi to 4,000 psi pressure does not, however, raise the overall cyclic fatigue life of the flanged window to 4,000 psi since now the secondary effects of cyclic fatigue on other areas of the window become the factor controlling the overall cyclic fatigue life.

The secondary effects of cyclic fatigue in the form of meridional cracks become apparent on the concave face of the window at pressure loadings $\geq$2,000 psi. These cracks are caused by tensile strains found on the concave face of the window during relaxation phases of pressure cycles. The magnitude of tensile strains in flanged windows are a function of t/R_i ratio and the magnitude of compressive creep during the loading phases of pressure cycles. Since the t/R_i ratio is a geometrical and the magnitude of creep a physical constant, little can be done to decrease their effect on the generation of tensile strains on the concave face of the window during relaxation phases of pressure cycles. Thus, the secondary effects of cycling fatigue in the form of meridional cracks on the concave face of the window become at 2,000-psi loading level the limiting factor on the fatigue life of the flanged hemispherical window.

---

[a] Short term critical pressure = pressure at which catastrophic failure of window occurs when pressurized at 650 psi/minute rate.

[b] Long term critical pressure = sustained pressure at which catastrophic failure of window occurs after uninterrupted sustained loading of 10^6-minute duration.

[c] Cyclic fatigue life = cyclically applied pressure (7 hours sustained loading followed by 17 hours of relaxation at 0 psi) that will initiate cracks in the window after 1,000 pressure cycles.

The ratio of 1:0.414:0.138 (14,500 psi:6,000 psi:2,000 psi) between short-term critical pressure, long-term critical pressure and cyclic fatigue pressure established experimentally in this study for flanged hemispherical windows with $t/R_i = 0.364$ seated on neoprene gaskets is also applicable conservatively to similar windows with $t/R_i < 0.364$. For flanged hemispherical windows with $t/R_i > 0.364$ the above ratio probably applies also, but not on the conservative side.

CONCLUSIONS

Flanges on acrylic plastic windows of hemispherical shape do not affect significantly their short-term critical pressure; however, they seriously decrease their static and cyclic fatigue life. When such windows with $t/R_i = 0.364$ are mounted on thin neoprene bearing gaskets, they can be subjected safely in the 65-75°F temperature range to a maximum working pressure of 2,000 psi, which is approximately equal to one-seventh of the window's short-term critical pressure.

RECOMMENDATIONS

To maximize the cyclic and static fatigue life of flanged hemispherical windows, the following precautions must be taken in their design, fabrication, and installation.

Design

Since the cyclic fatigue life of a flanged window is primarily determined by the appearance of cracks on the bearing surface of the flange, special attention must be paid to the design of the flange. To decrease the magnitude of bending movements in the flange, the instep of the flange must have a generous radius while the heel must approach the shape of a square edge. No discontinuities like O-ring grooves can be tolerated on the bearing surface of the flange as they tend to act as crack initiators. The maximum working pressures at which acrylic hemispherical windows with Type I or Type VI flanges can probably be safely operated are shown in Table 6.

Fabrication

Appearance of cracks in the bearing surface of the flange can be delayed significantly by following up the machining process with polishing. After polishing, the whole window must be annealed, preferably at 175°F for 22 hours.

Table 6. Maximum Recommended Working Pressures for Hemispherical Windows With Type I and Type VI Equatorial Flanges

Temperature Ranges (^{o}F)	Maximum Working Pressures[a]
≤50	0.167 x short-term critical pressure
≤75	0.143 x short-term critical pressure
≤100	0.111 x short-term critical pressure
≤125	0.091 x short-term critical pressure
≤150	0.059 x short-term critical pressure

[a]Short-term critical pressure is established by pressurizing the window at 650 psi/minute rate and 75^{o}F ambient environment until explosive implosion of the window takes place.

Installation

The surface of the steel seat in the pressure vessel must have at least a 63 rms, and preferably 32 rms finish. A thin neoprene-coated nylon gasket (Fairprene 5722A or equal) must be bonded with polyvinyl resin glue (Pliobond or equal) to the bearing surface of the window flange. The steel seat must be liberally coated with silicone grease (Dow Corning No. 4) prior to placement of the gasketed window. Although the bearing gasket serves adequately as a seal, an O-ring is placed around the circumference of the flange to act as a secondary seal (Figure 84). A retaining ring placed around the flange is dimensioned to compress simultaneously both the window flange and the O-ring seal. The bolts holding down the retaining ring must be of adequate size and tensile strength to retain the window against accidental internal pressurization of the hemispherical window to 0.05 times short-term critical pressure.

REFERENCES

1. Naval Civil Engineering Laboratory. Technical Report R-512: Windows for external or internal hydrostatic pressure vessels; part I: Conical acrylic windows under short-term pressure application, by J. D. Stachiw and K. O. Gray. Port Hueneme, CA, 1967 (AD656882)

2.————. Technical Report R-645: Windows for external or internal hydrostatic pressure vessels; part IV: Conical acrylic windows under long-term pressure applications at 20,000 psi, by J. D. Stachiw, Port Hueneme, CA, Oct 1969 (AD697272)

3._____. Technical Report R-708: Windows for external or internal hydrostatic pressure vessels; part V: Conical acrylic windows under long-term pressure application of 10,000 psi, by J. D. Stachiw and W. A. Moody. Port Hueneme, CA, Jan 1970 (AD718812)

4._____. Technical Report R-747: Windows for external or internal hydrostatic pressure vessels; part VI: Conical acrylic windows under long-term pressure application of 5,000 psi, by J. D. Stachiw and K. O. Gray. Port Hueneme, CA, Jun 1971 (AD736594)

5._____. Technical Report R-773: Windows for external or internal hydrostatic pressure vessels; part VII: Effect of temperature and flange configurations on critical pressure of 90-degree conical acrylic windows under short-term loading by J. D. Stachiw and J. R. McKay. Port Hueneme, CA, Aug 1972.

6._____. Technical Report R-527: Windows for external or internal hydrostatic pressure vessels; Part II: Flat acrylic windows under short-term pressure application, by J. D. Stachiw, G. M. Dunn, and K. O. Gray. Port Hueneme, CA, May 1967 (AD652343)

7._____. Technical Note N-1127: Flat disc acrylic plastic windows for man-rated hyperbaric chambers at the USN Experimental Diving Unit, by J. D. Stachiw. Port Hueneme, CA, Nov 1970 (AD716751)

8._____. Technical Report R-631: Windows for external or internal hydrostatic pressure vessels; part III: Critical pressure of acrylic spherical shell windows under short-term pressure application by J. D. Stachiw and F. W. Brier. Port Hueneme, CA, Jun 1969 (AD689789)

9. Naval Undersea Center. NUC TP 486: Acrylic plastic spherical shell windows under point impact loading, by J. D. Stachiw and O. Burnside. San Diego, CA, Jul 1975.

10._____. NUC TP 410: Development of a precision casting process for acrylic plastic spherical shell windows applicable to high pressure service, by J. D. Stachiw. San Diego, CA, May 1974.

11._____. NUC TP 383: Cast acrylic dome for undersea applications, by J. D. Stachiw. San Diego, CA, Jan 1974.

12._____. NUC TP 493: Improved fabrication process for spherical acrylic plastic submersible hulls, by J. D. Stachiw. San Diego, CA, Dec 1975.

13._____. NUC TP 315: Acrylic plastic hemispherical shells for NUC undersea elevator, by J. D. Stachiw. San Diego, CA, Jan 1974.

14._____. NUC TP 355: Flanged acrylic plastic hemispherical shells for undersea systems, by J. D. Stachiw. San Diego, CA, Aug 1973 (AD 769213)

15.————. NUC TP 378: Recommended practices for the design, fabrication, prooftesting and inspection of windows in man-rated hyperbaric chambers, by J. D. Stachiw. San Diego, CA, Dec 1973 (AD773737).

16. J. J. Lohr, et al. "Accelerated Testing of the Mechanical and Thermal Integrity of Polymeric Materials, in Proceedings of 8th Structural Dynamics and Materials Conference, AIAA/ASME. Palm Springs, CA, Mar 1967.

17. Naval Undersea Center. NUC TP 451: NEMO Model 2000 acrylic plastic spherical hull for manned submersible operation, by J. D. Stachiw. San Diego, CA, Dec 1974.

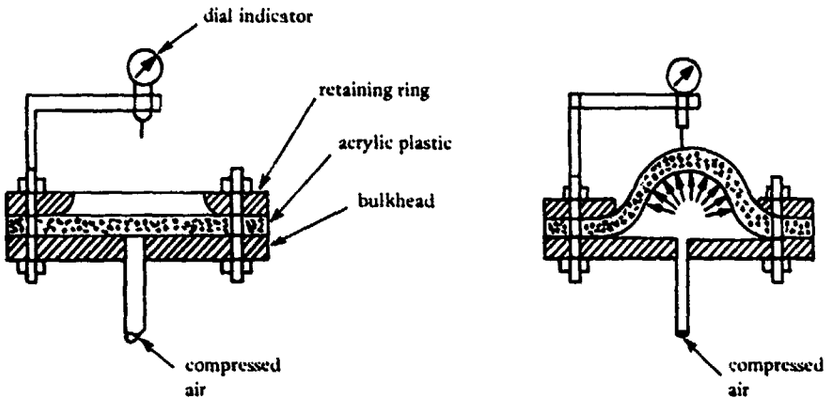

Free Forming With Compressed Gas

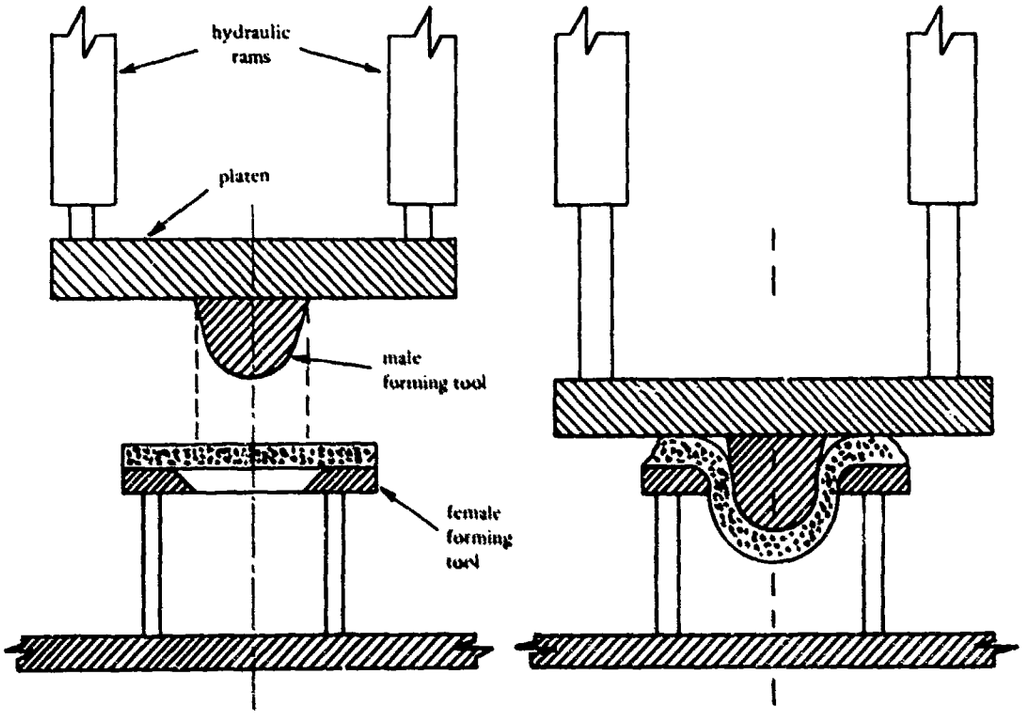

Extrusion Forming With Dies

Figure 1. Typical techniques for thermoforming flanged hemispherical windows of acrylic plastic.

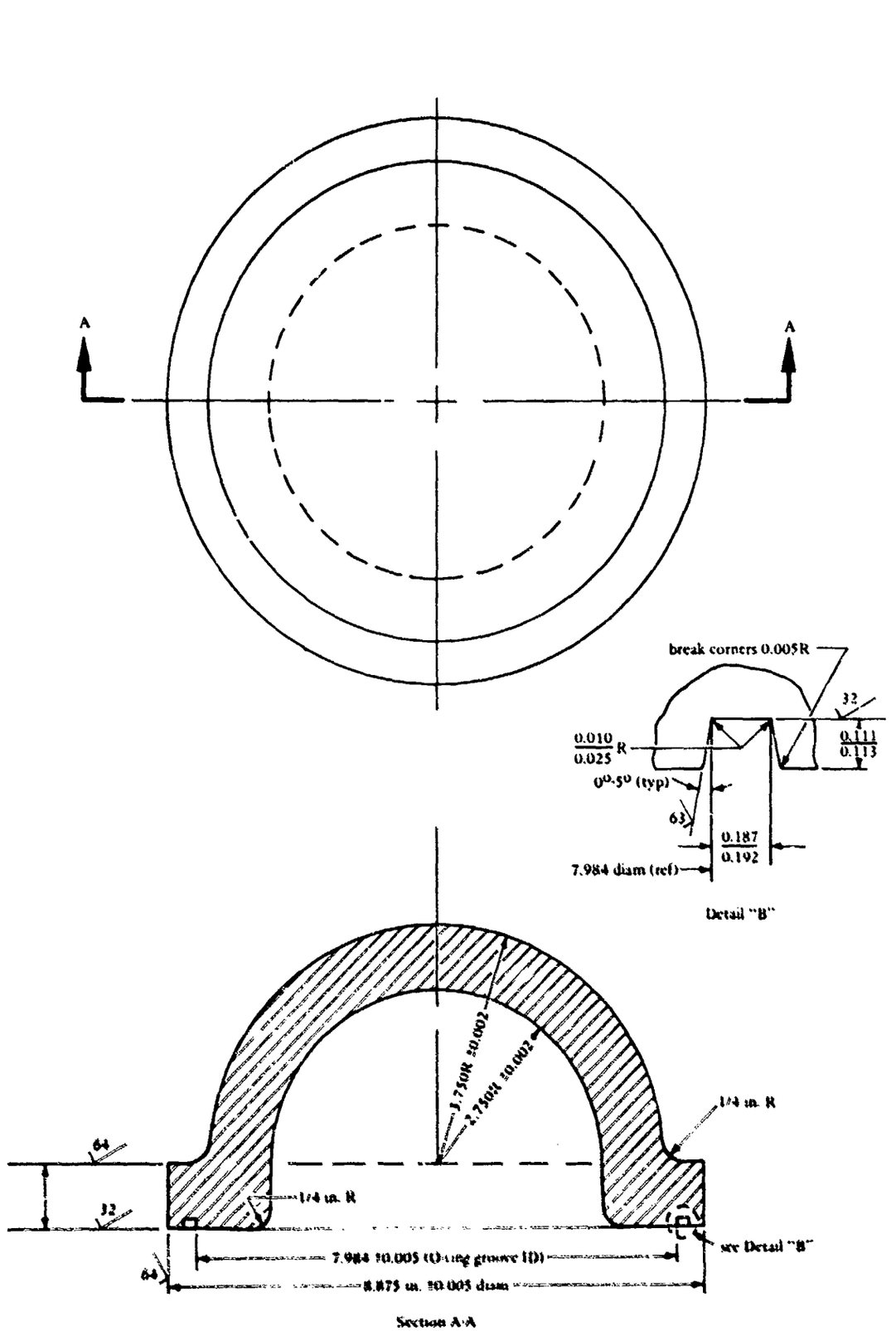

Figure 2. Type I flanged hemispheres used as test specimens in the experimental test program.

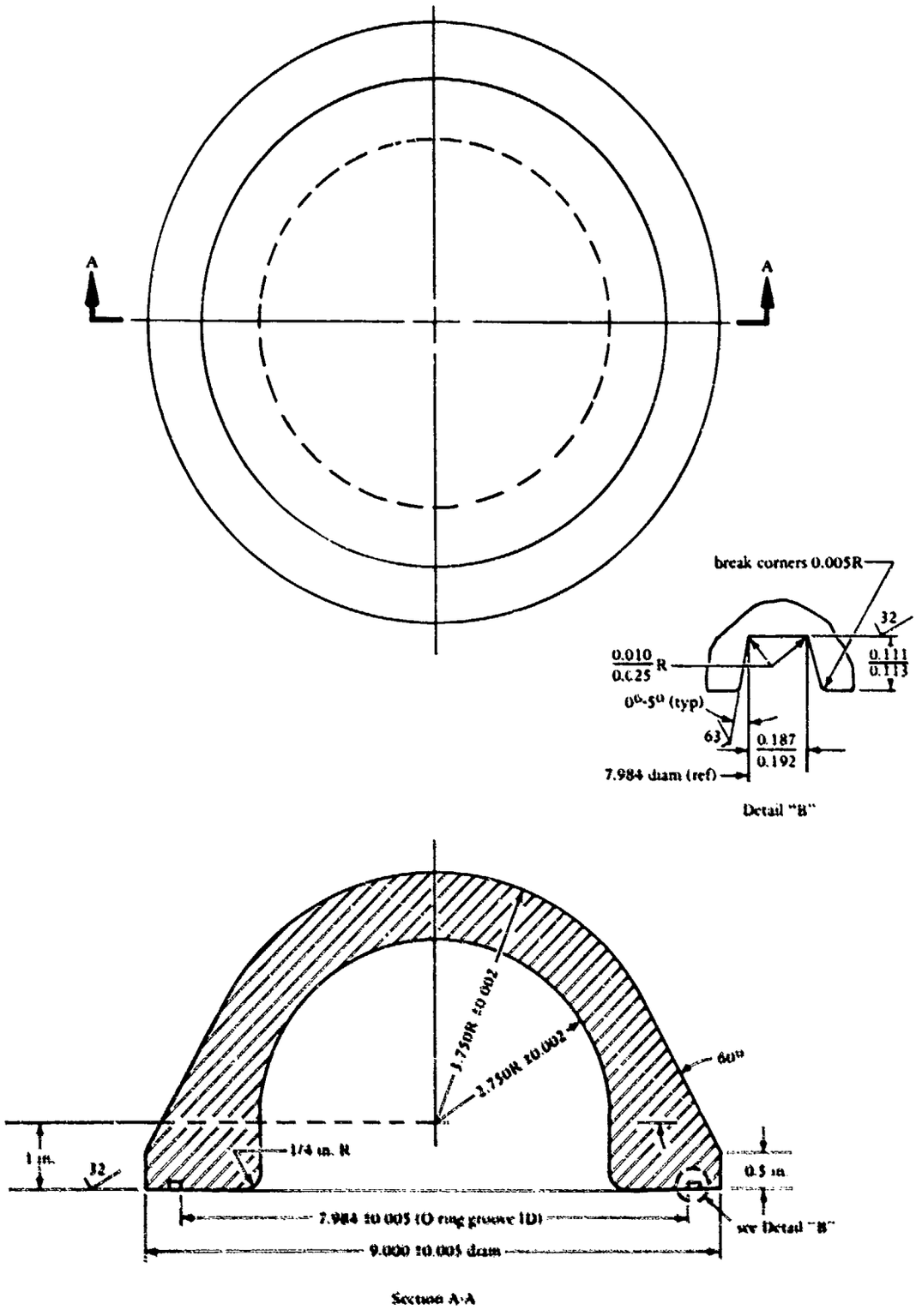

Figure 3. Type VI flanged hemispheres used as test specimens in the experimental test program.

(a) Placing the blank between dies.

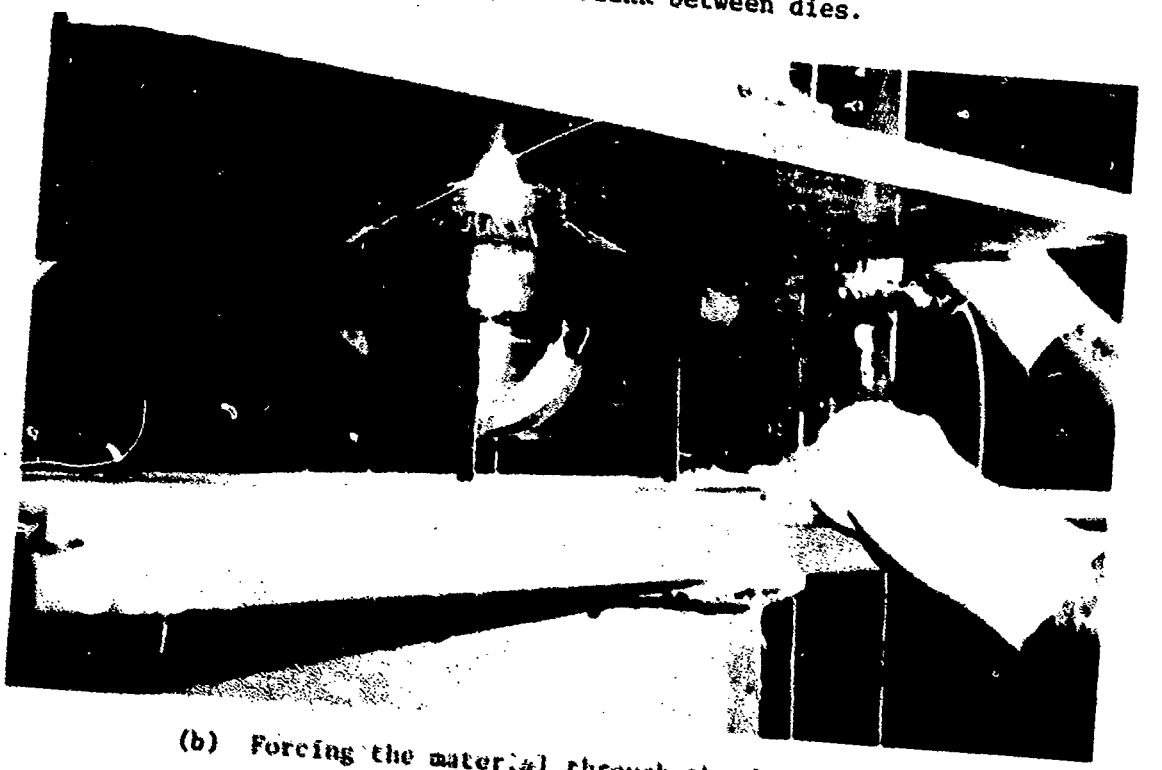

(b) Forcing the material through the female die.

Figure 4. Thermoforming of flanged hemispheres for the experimental test program.

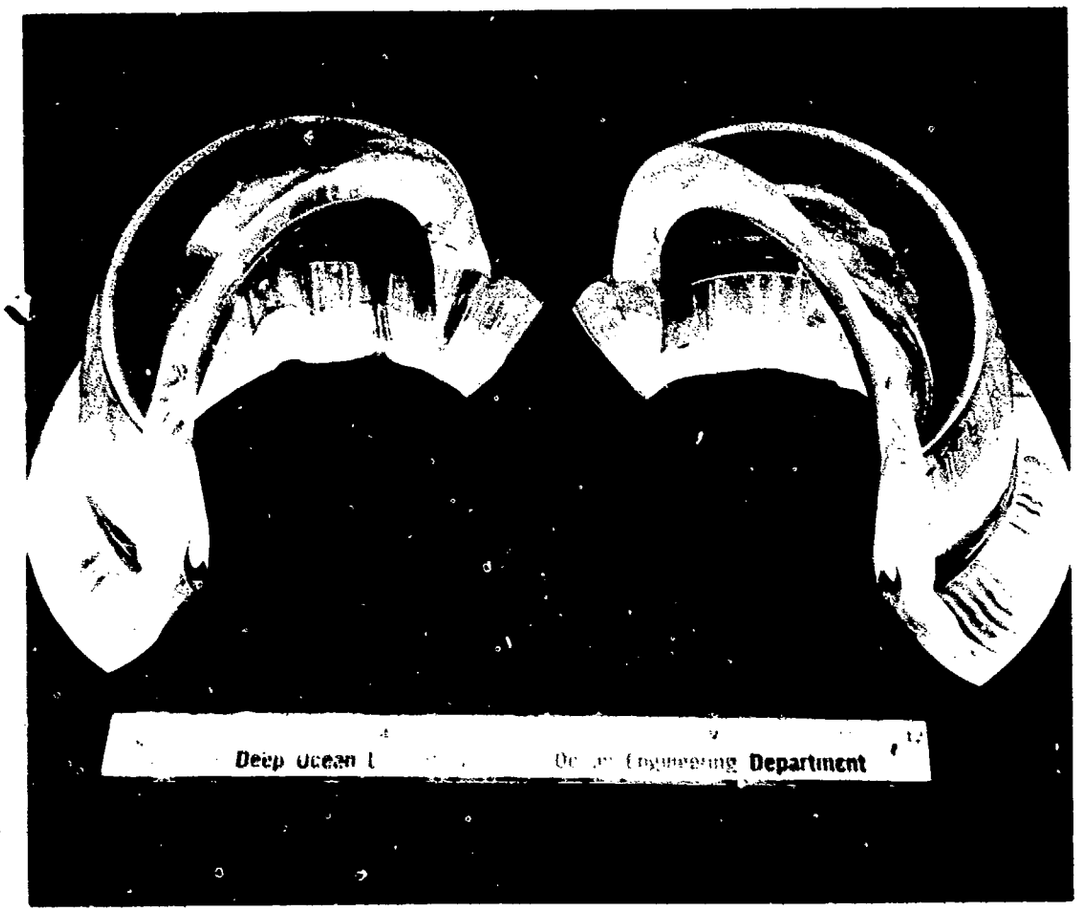

Figure 5. Typical cross section of thermoformed windows prior to machining.

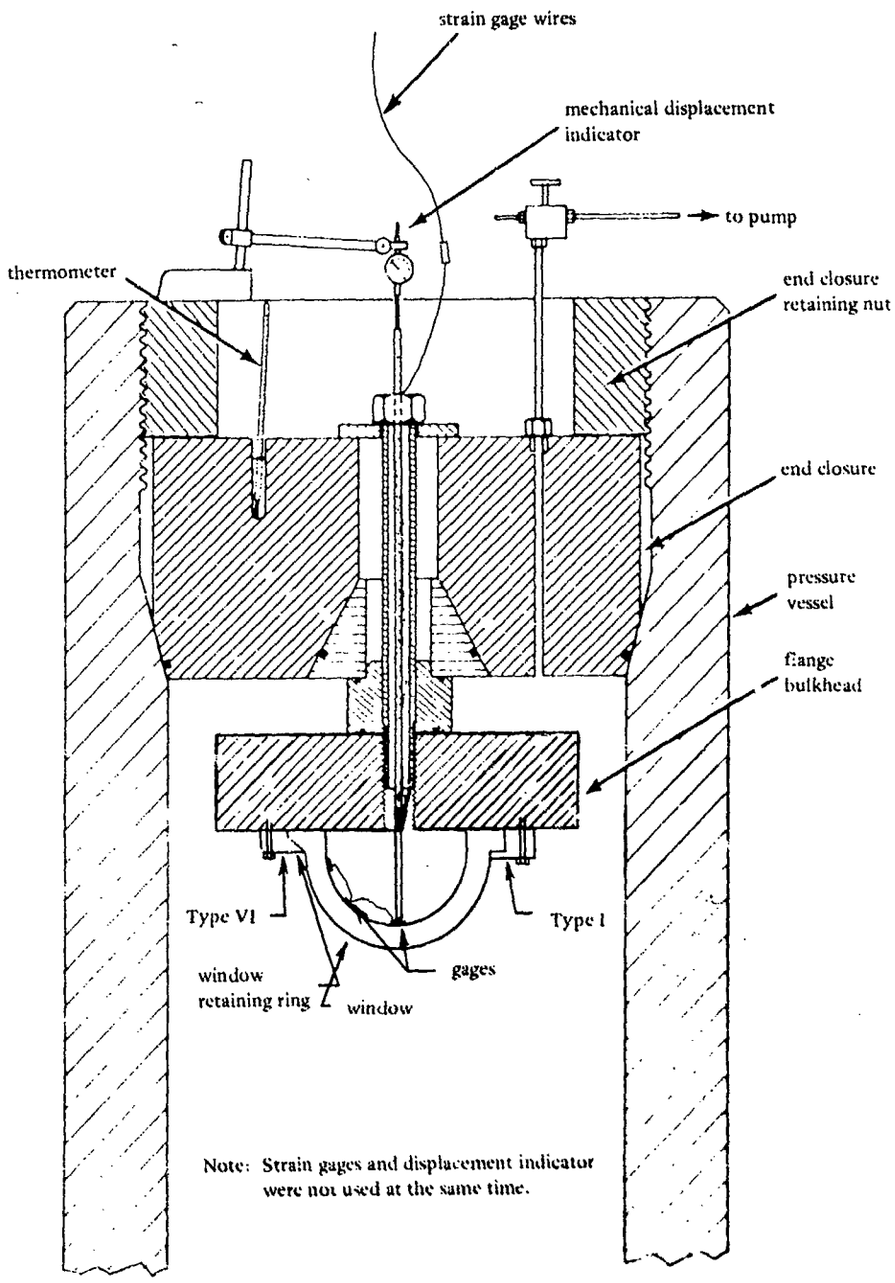

Figure 6. Test arrangement for Type I and Type VI windows in the 18-inch-diameter pressure vessel of CEL's Deep Ocean Simulation Facility.

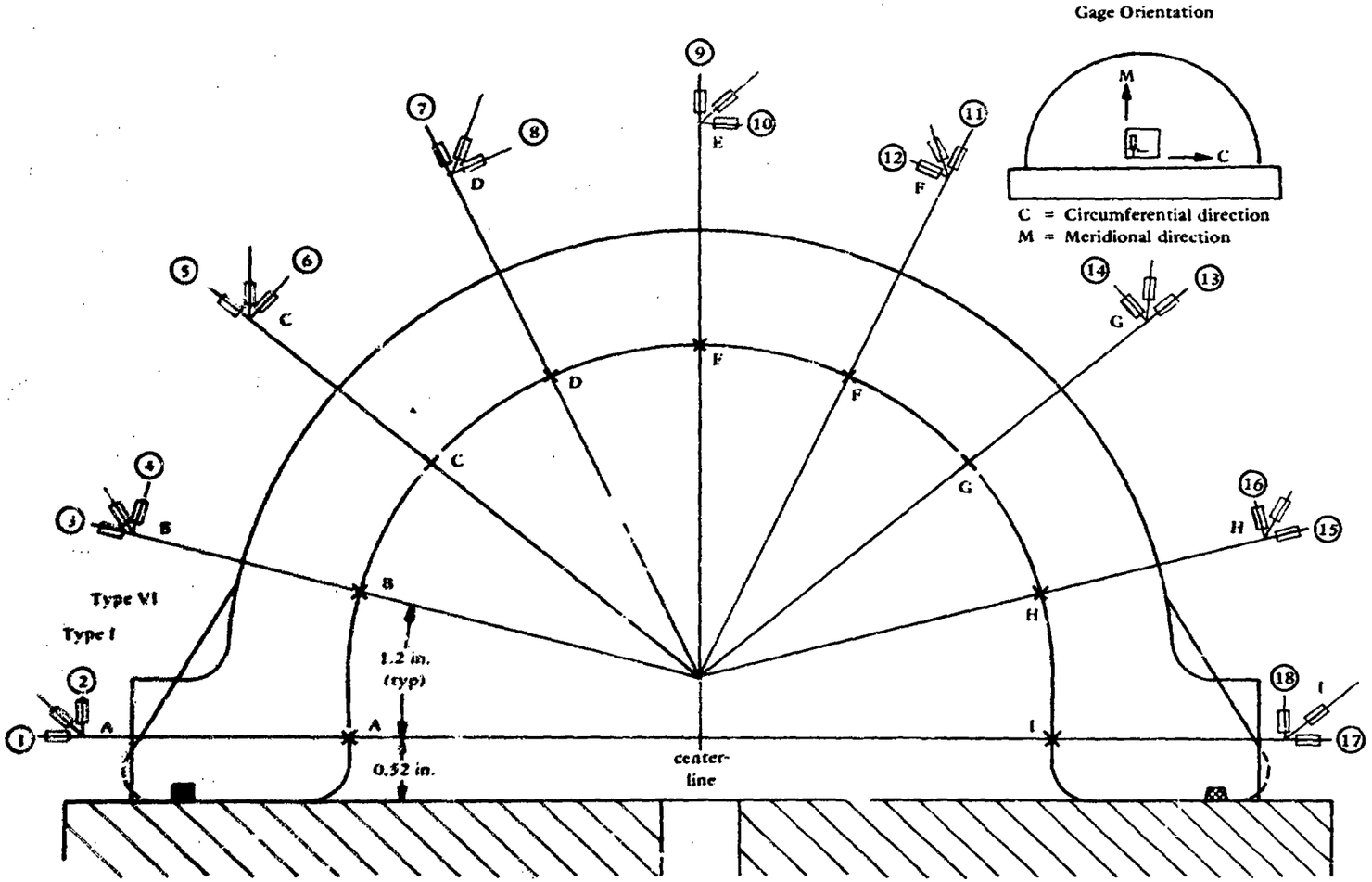

Figure 7. Location of electric resistance strain gages on the interior face of the flanged hemispheres.

Figure 8. Retaining ring for Type VI window testing in 18-inch-diameter pressure vessel; window V after 42 hours at 11,800-psi sustained hydrostatic loading.

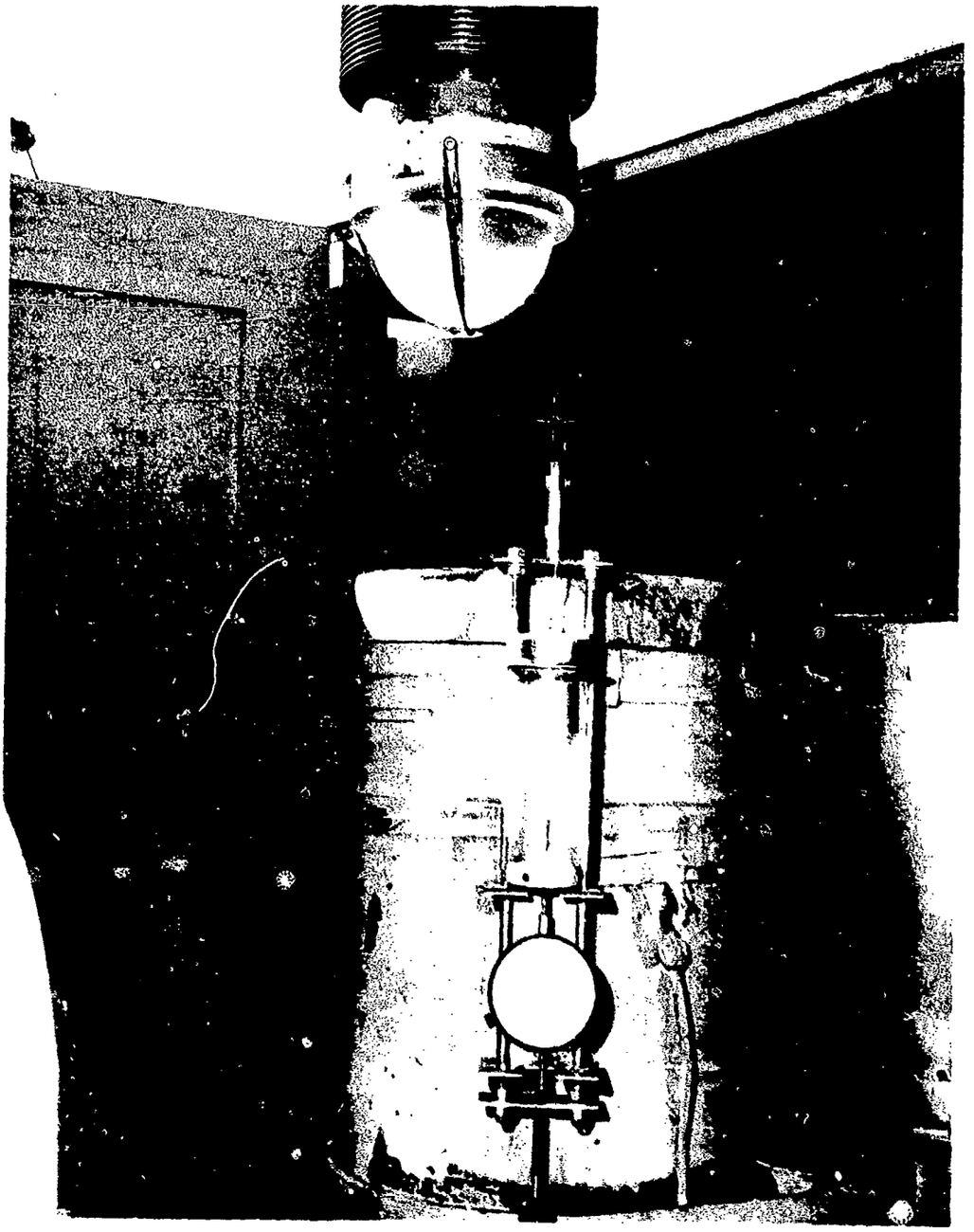

Figure 9. Retaining rubber bands for testing of windows in 9.5-inch-diameter pressure vessel.

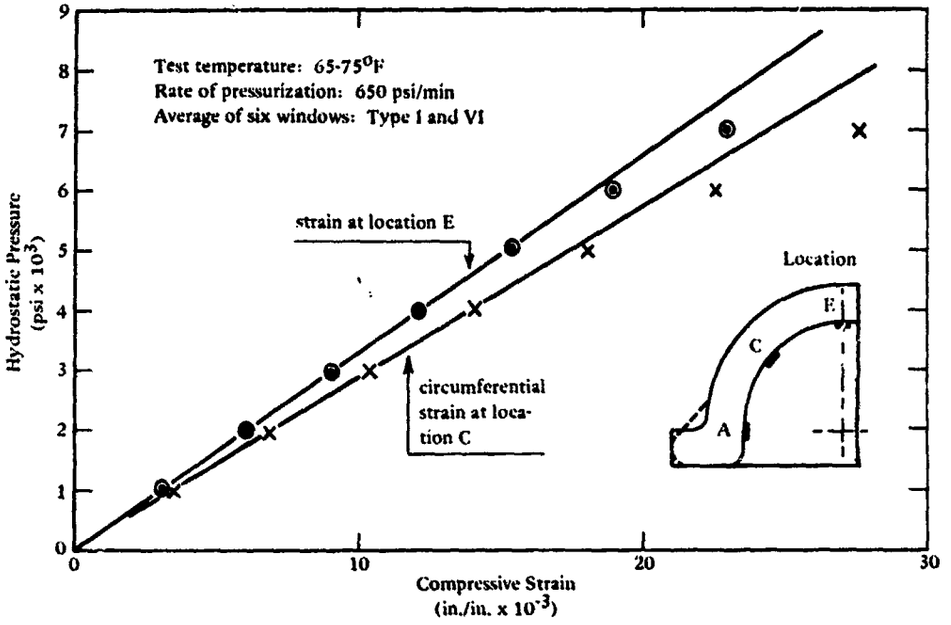

Figure 10. Linearity of strains in flanged windows during short-term pressurization in the 0 to 4,000 psi range.

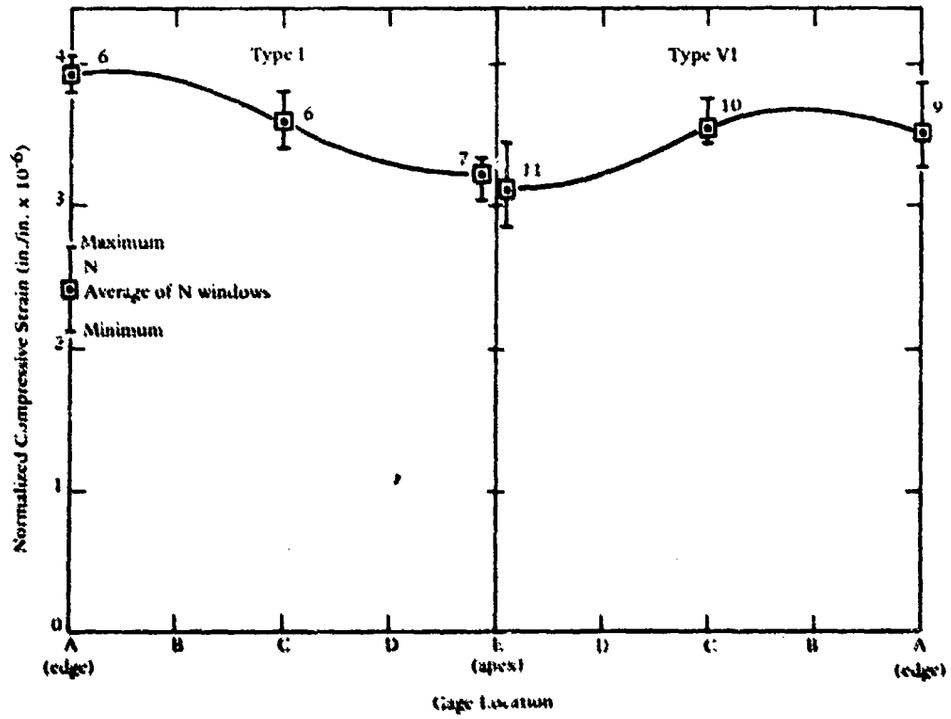

Figure 11. Distribution of circumferential strains on the interior face of Type I and Type VI windows during short-term pressurization in the 0 to 4,000 psi range; the strain plotted has been normalized to show magnitude of strain per unit of pressure in linear range.

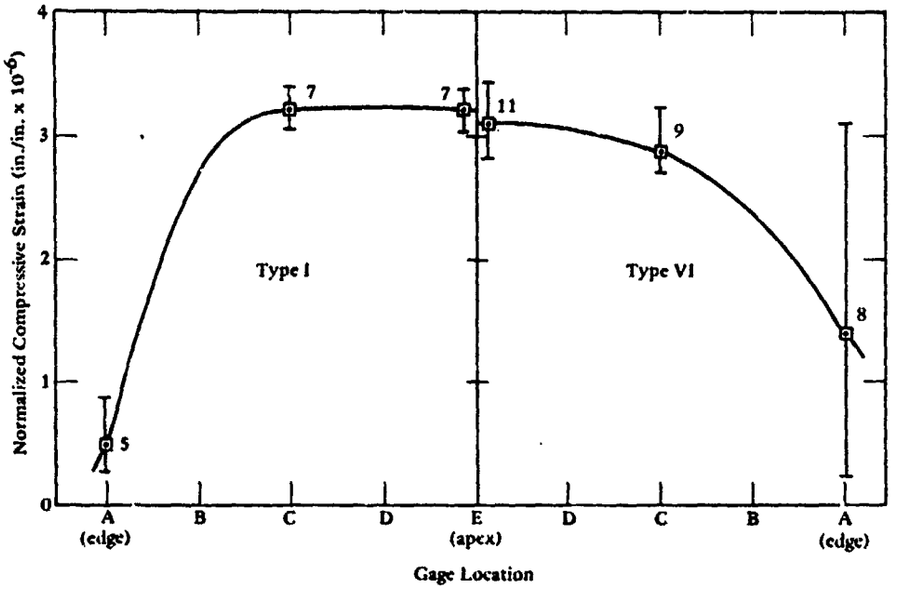

Figure 12. Distribution of meridional strains on the interior face of Type I and Type VI windows during short-term pressurization in the 0 to 4,000 psi range; the strain plotted has been normalized to show magnitude of strain per unit pressure in linear range.

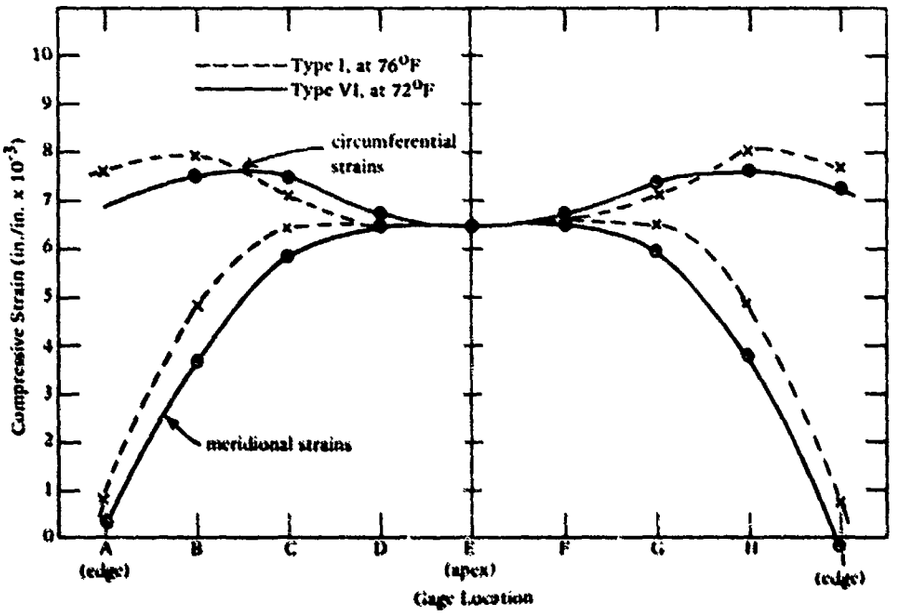

Figure 13. Distribution of strains on the interior face of Type I and Type VI windows at the conclusion of short-term pressurization to 2,000 psi.

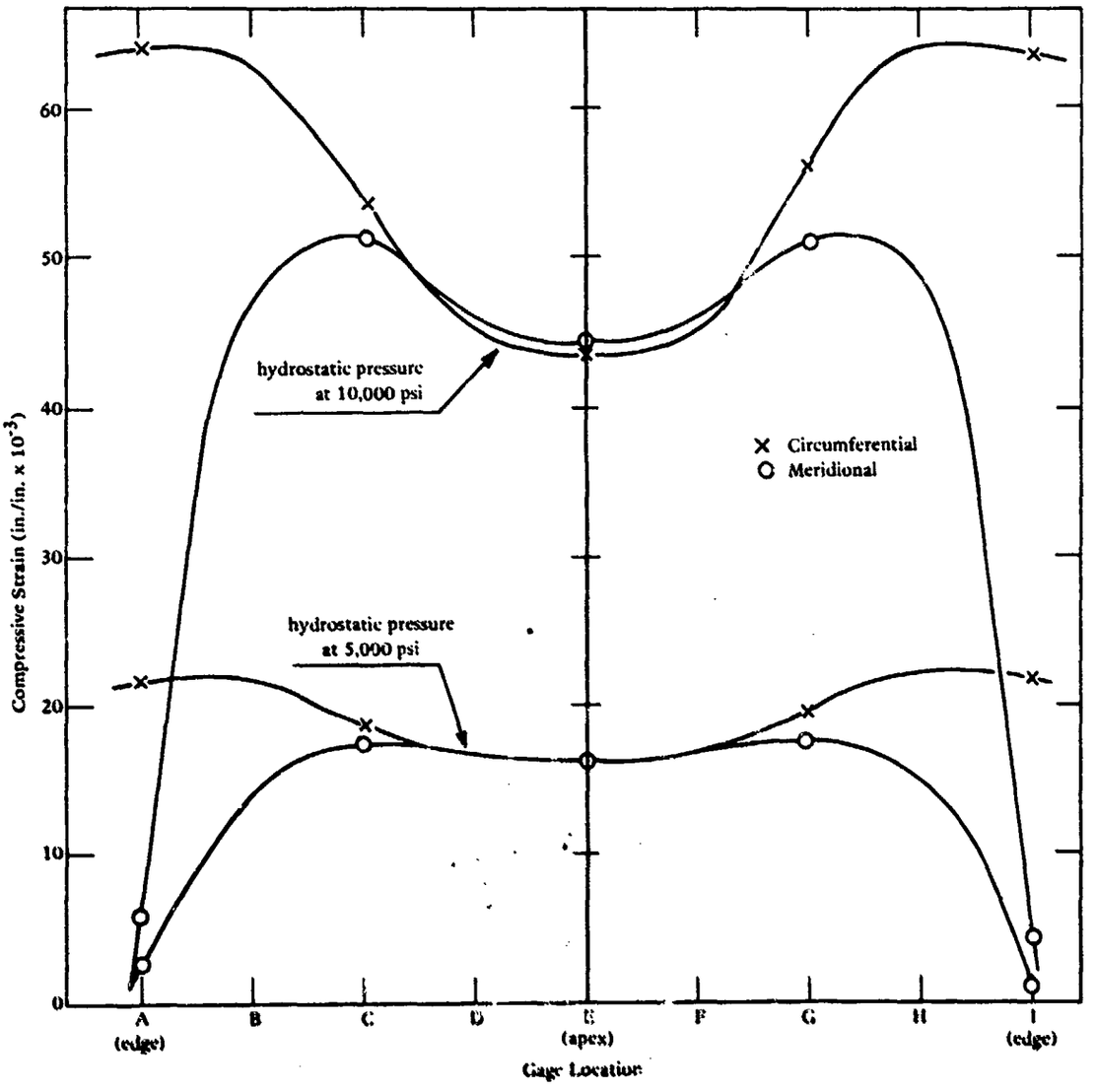

Figure 14. Distribution of strains on the interior face of Type I window J at 5,000 and 10,000 psi pressure levels during short-term pressurization; note the nonlinearity in strain increases at different locations.

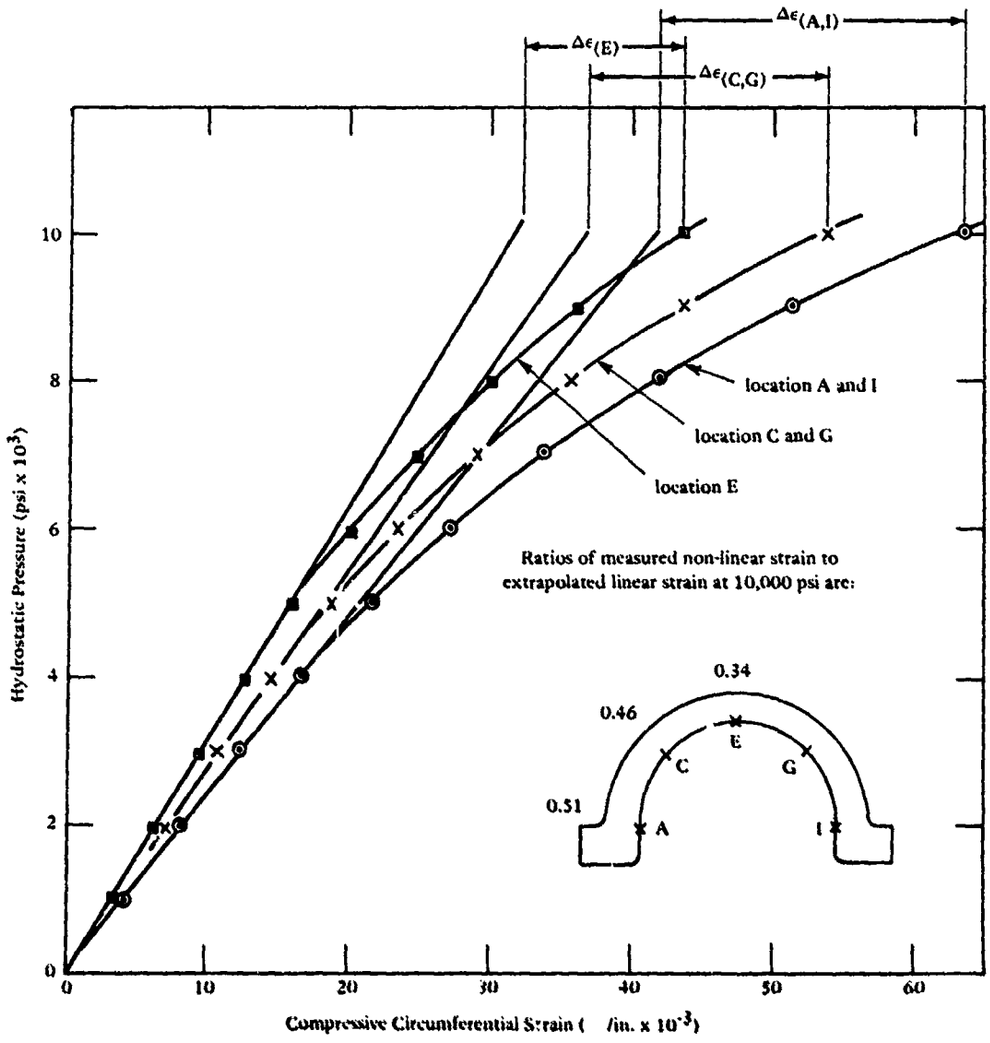

Figure 15. Magnitude of nonlinearity in strains measured on the interior face of Type I window J during short-term pressurization at 74°F to 10,000 psi.

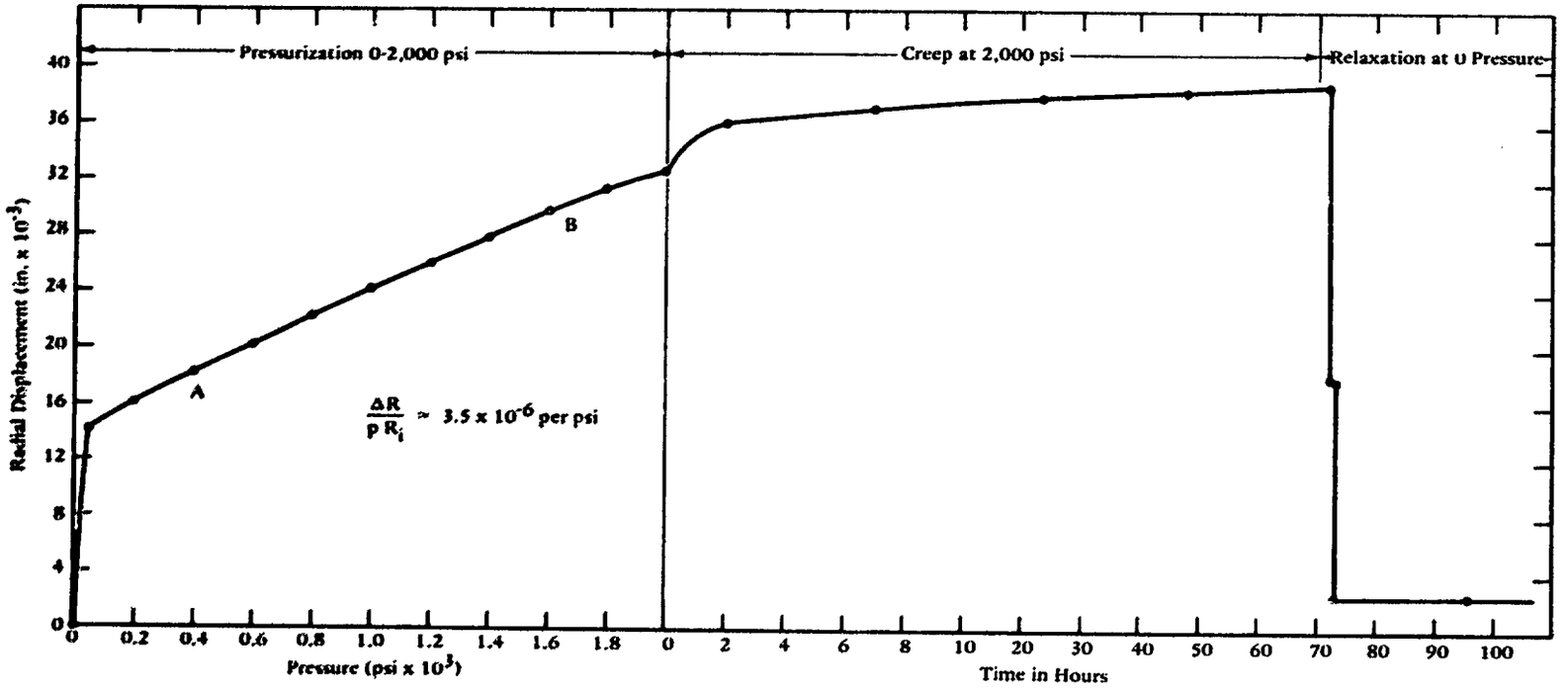

Figure 16. Radial displacement of apex on Type VI window W during short-term pressurization to and sustained pressure loading at 2,000 psi; 72°F.

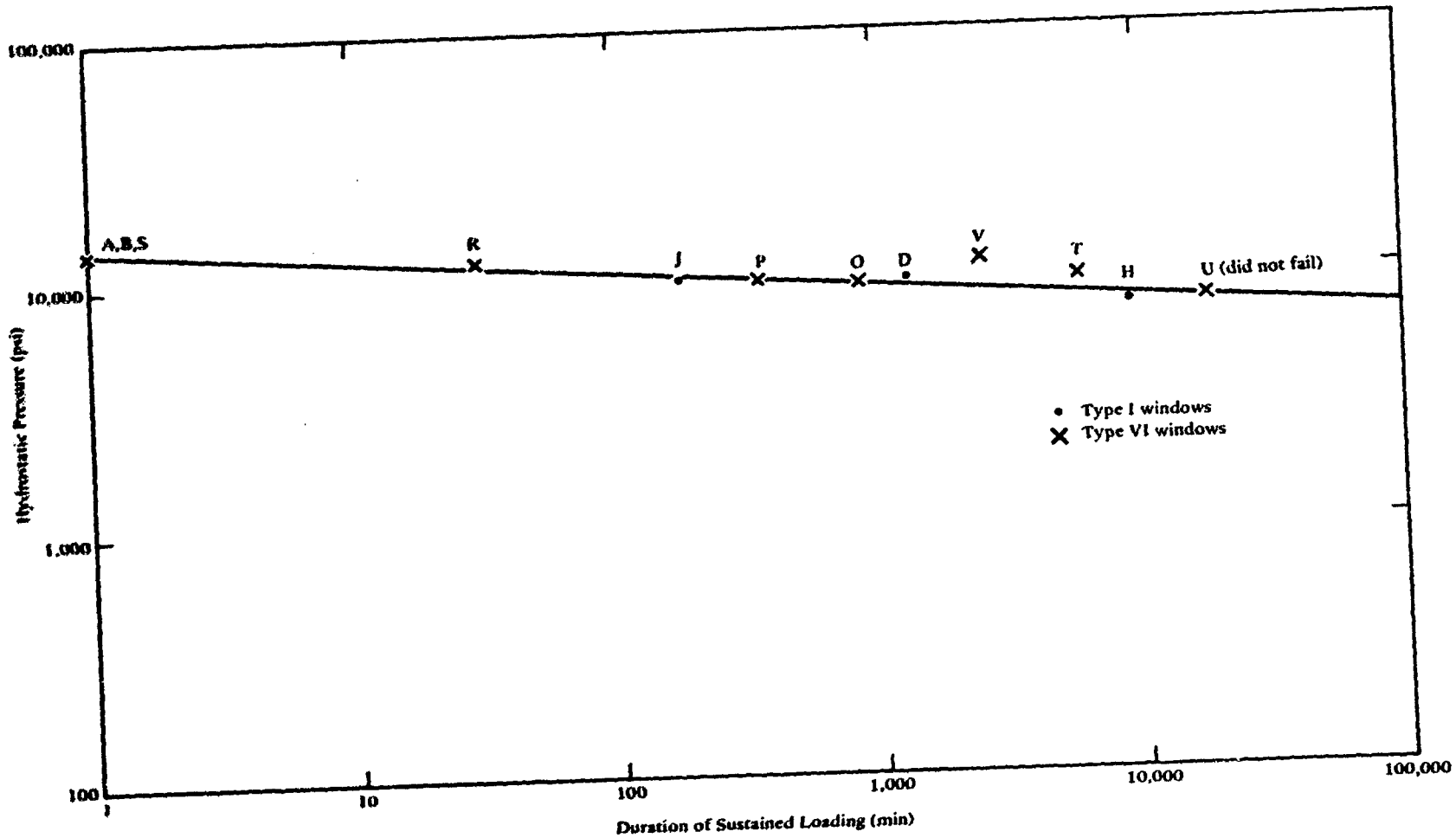

Figure 17. Long-term critical pressures of Type I and Type VI windows tested to catastrophic failure under sustained hydrostatic loading at 65-75°F ambient temperature.

Figure 18. Window H, Type I after 153 hours of sustained pressure loading at 8,000 psi; note the separation of flange.

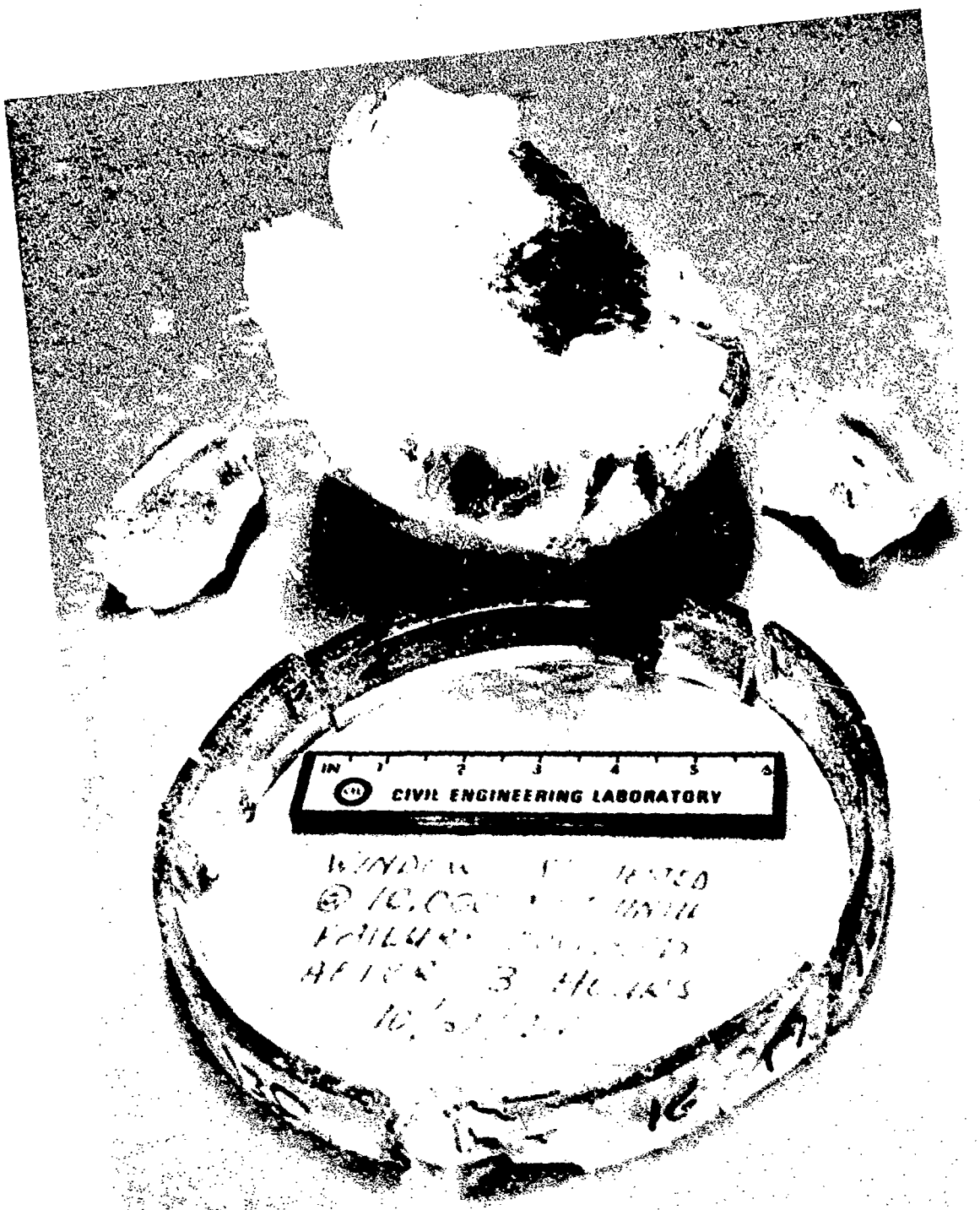

Figure 19. Window J, Type I after 3 hours of sustained pressure loading at 10,000 psi; note the undistorted flange fragments indicating that they broke off immediately after pressurization, before the window deformed plastically.

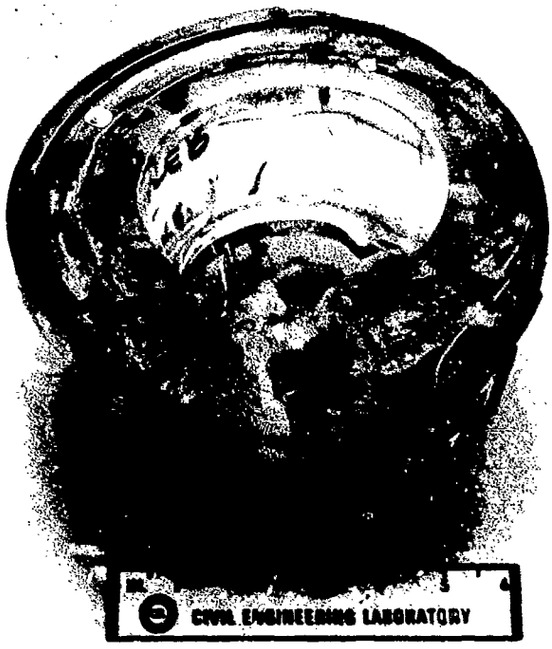

Figure 20. Window R, Type VI after 30 minutes of sustained pressure loading at 12,000 psi; note the extensive lamination and partial separation of flange.

Figure 21. Same window as Figure 20; note the partial separation of flange and large scale plastic deformation midway between the flange and apex that led to the plastic instability failure of the window.

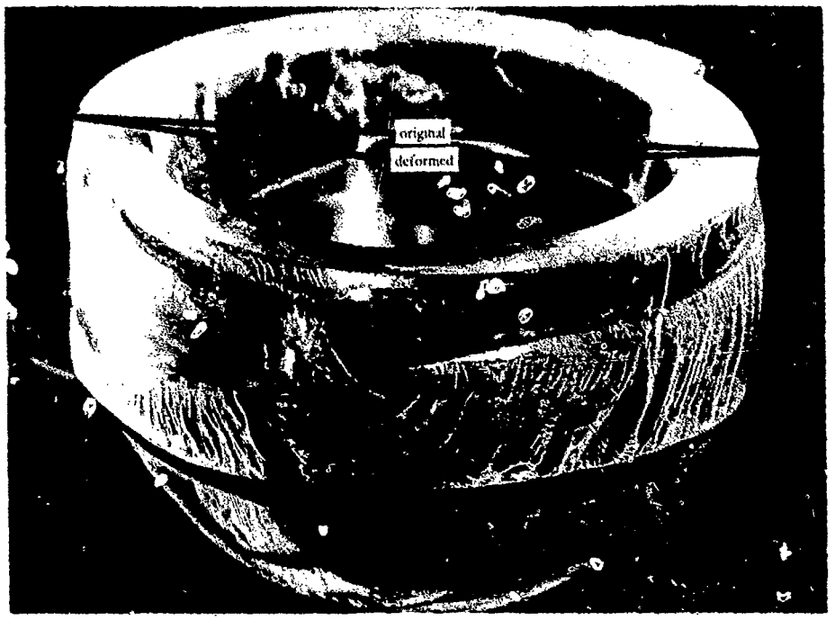

Figure 22. Window U, Type VI after 312 hours of sustained pressure loading at 8,000 psi; note that (a) the flange has separated even though the window did not implode yet and (b) the bearing surface on the window has deformed plastically giving it the appearance of a very shallow cone.

Figure 23. Same window as in Figure 22; note that the separated flange remains intact indicating that (a) the circumferential cracks initiate sooner and propagate faster than radial cracks and (b) the separation occurs before extensive plastic deformations occur.

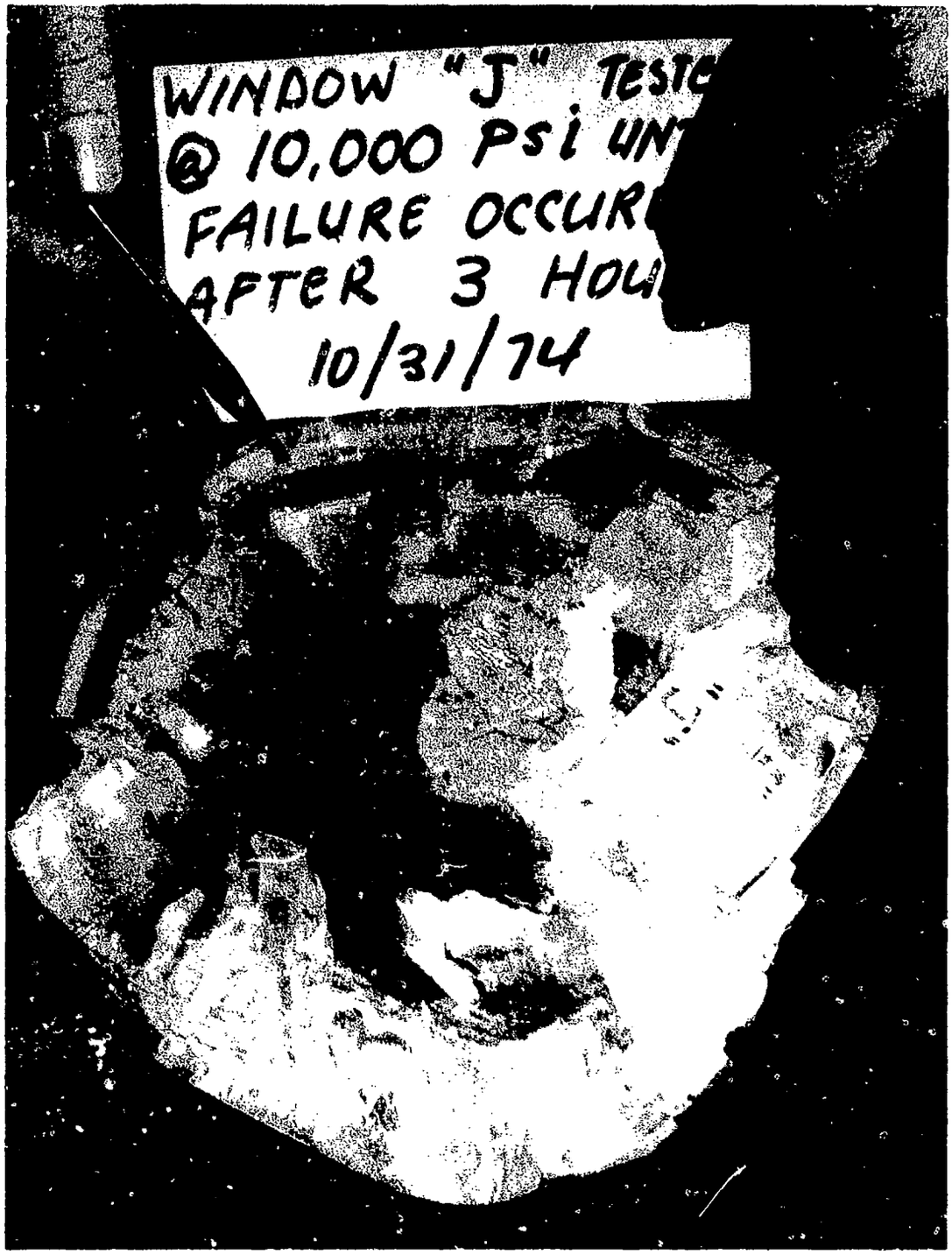

Figure 24. Window J, Type VI after 3 hours of sustained pressure loading at 10,000 psi; note the extensive lamination of the dome at the apex.

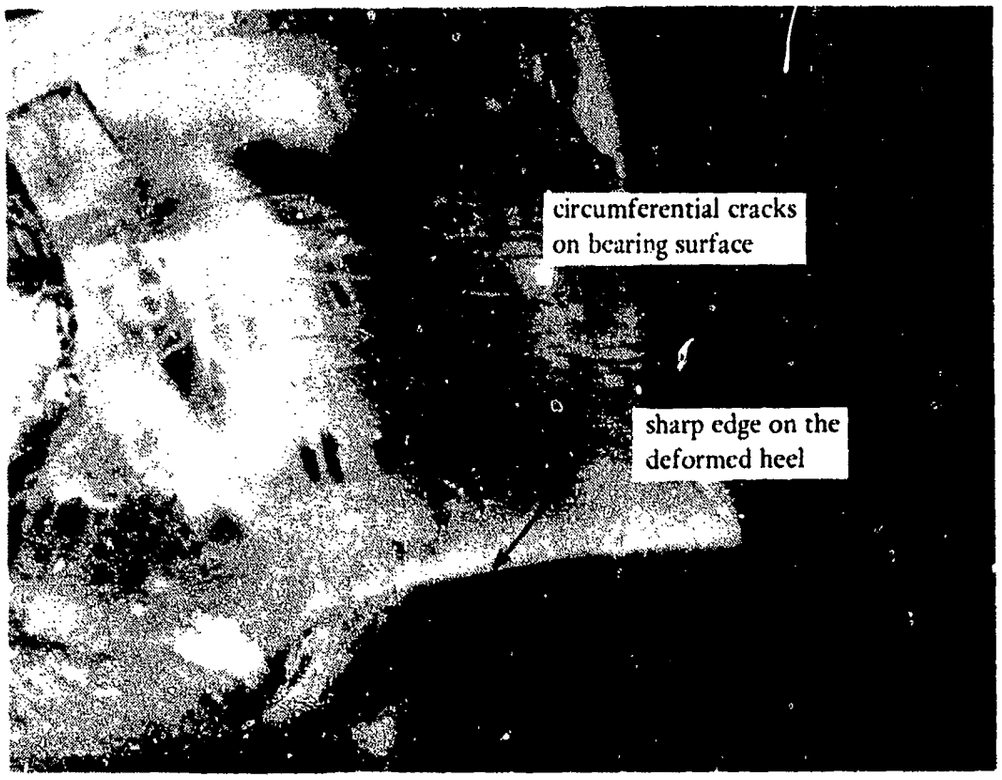

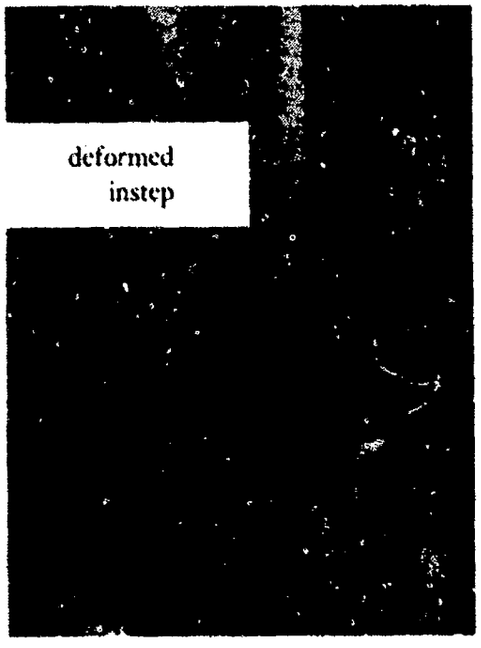

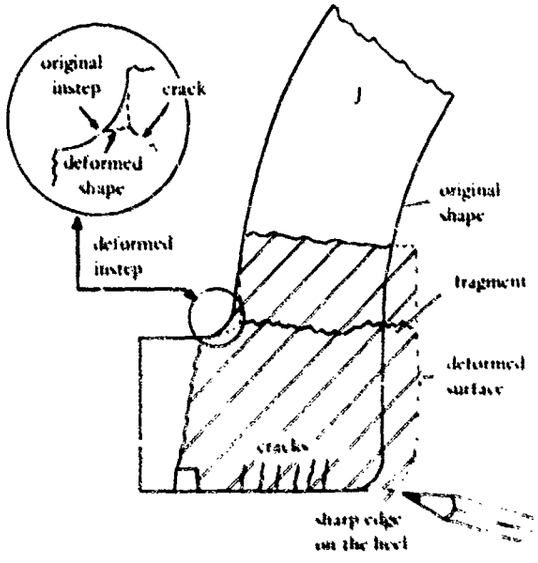

Figure 25. Same window as in Figure 24; note the presence of circumferential cracks in the bearing surface of the flange and the plastic transformation of the rounded heel into a sharp edge and the fillet on the instep into a sharp corner.

Figure 26. Window H, after 154 hours of sustained pressure loading at 8,100 psi; note the increase in wall thickness of the window near the flange due to plastic flow of acrylic under biaxial compression.

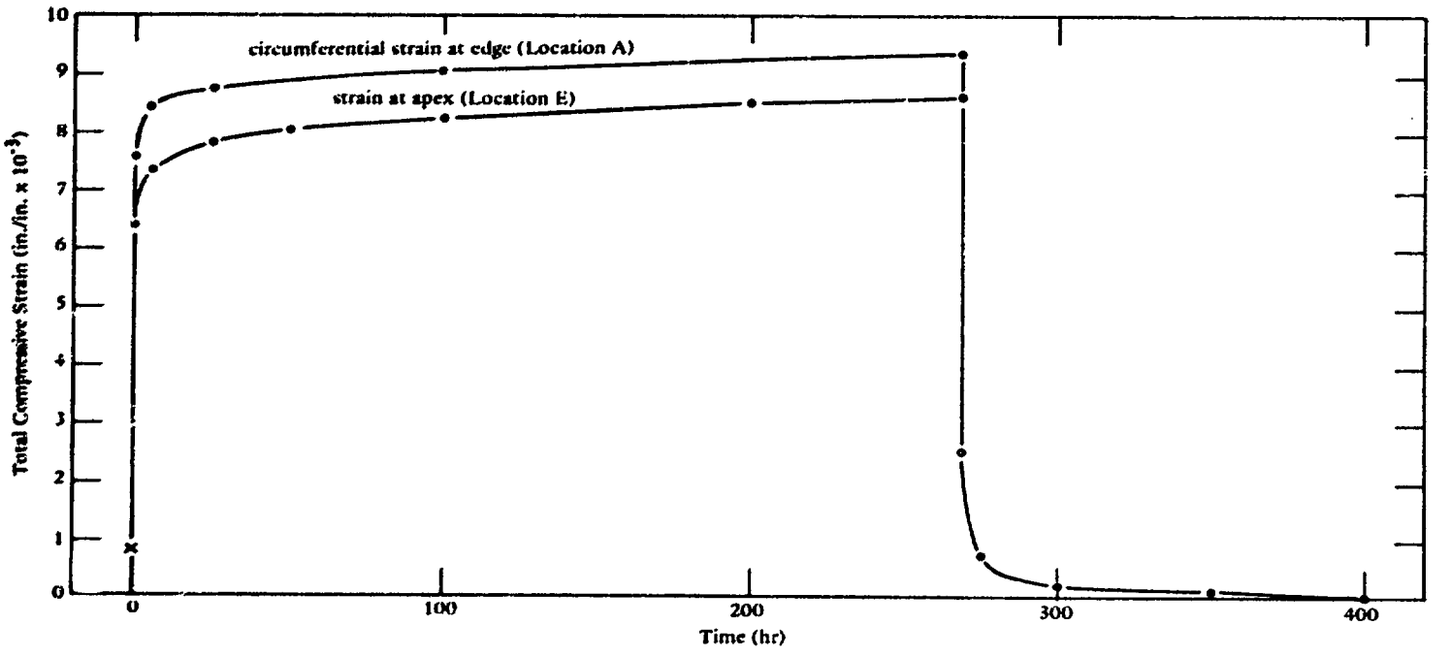

Figure 27. Typical total deformation and relaxation of Type I window I under sustained pressure loading of 2,000 psi.

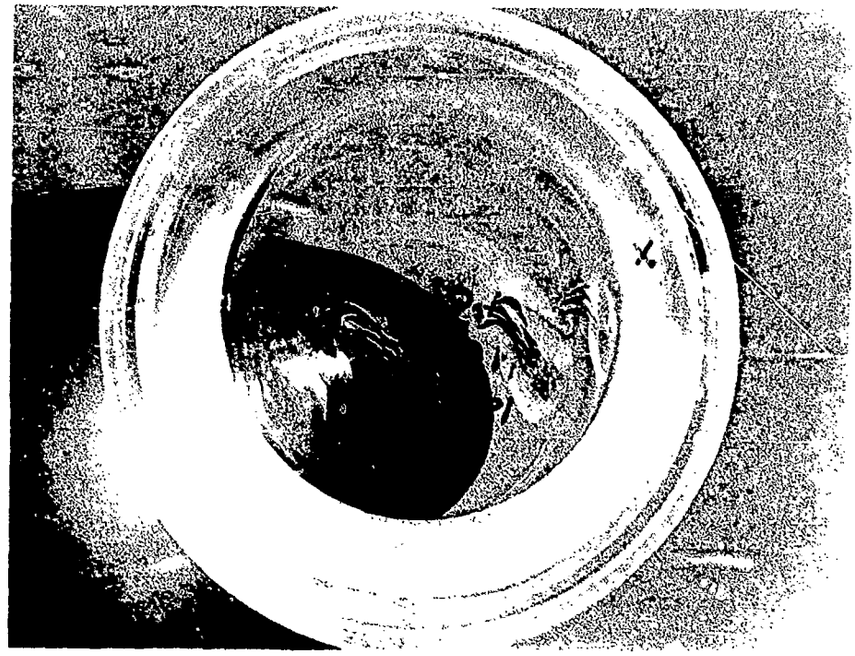

Figure 28. Extensive crazing and minor cracking on the bearing surface of Type VI window R after 262 hours of sustained pressure loading at 4,000 psi.

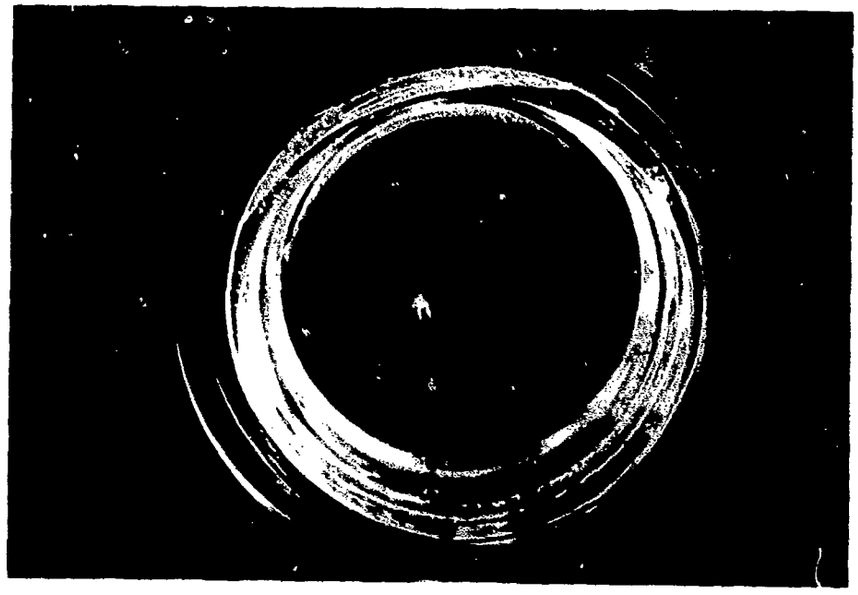

Figure 29. Extensive crazing and a major circumferential crack on the bearing surface of Type VI window Q after 139 hours of sustained pressure loading at 7,000 psi.

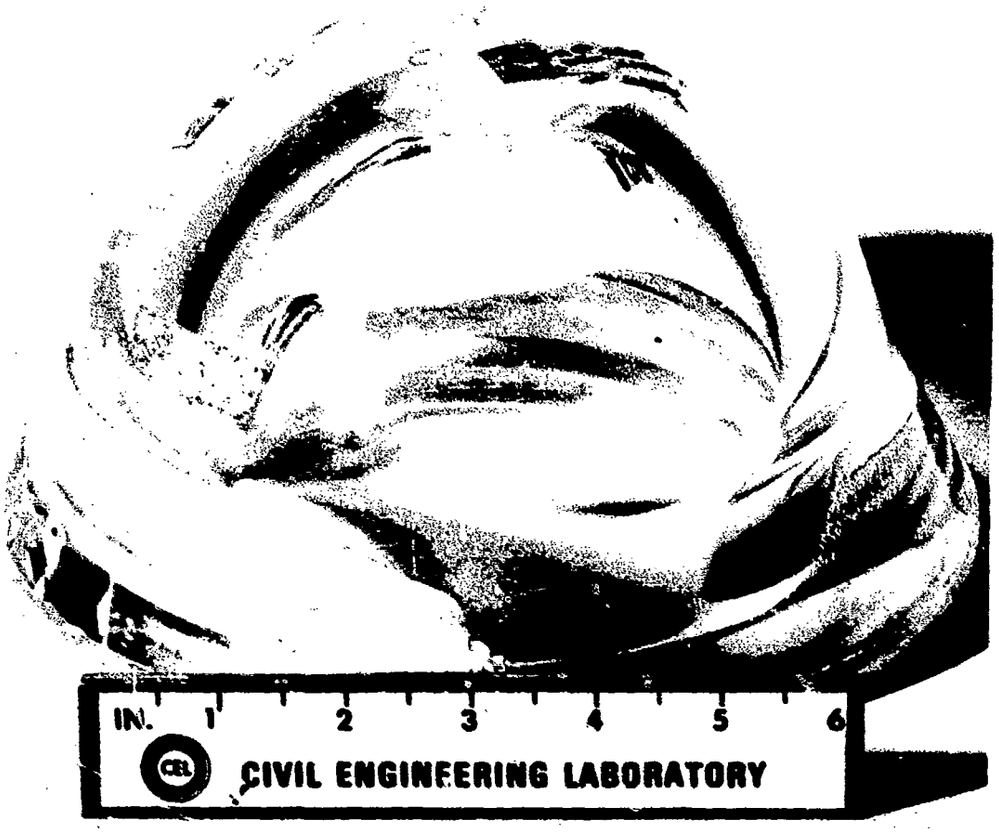

Figure 30. Same window as in Figure 29; note that the circumferential crack has completely penetrated the flange and the flange remains attached to the body of the window only at one place.

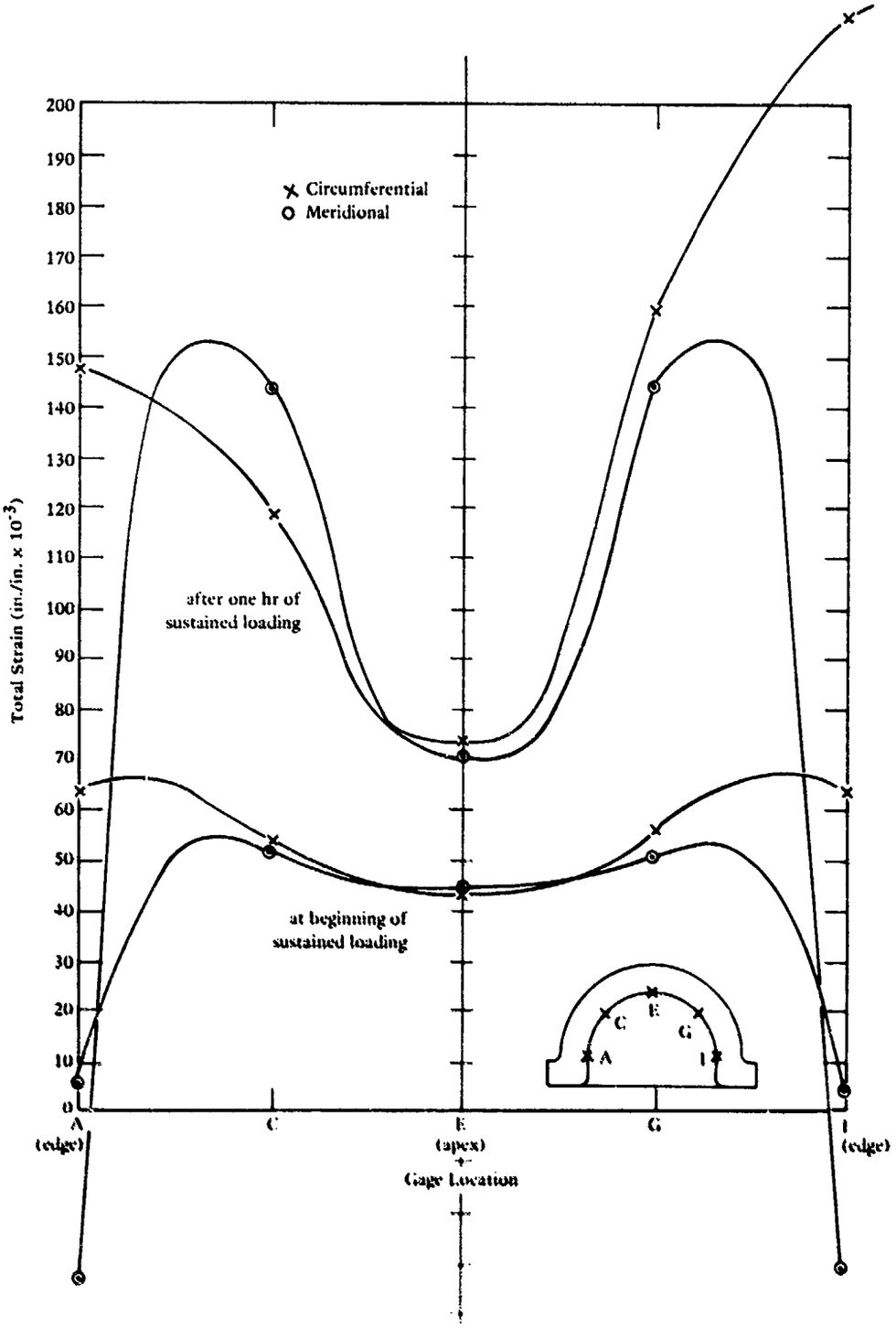

Figure 31. Change in magnitude and distribution of strains with duration of sustained pressure loading at 10,000 psi; window J, Type 1; 75°F.

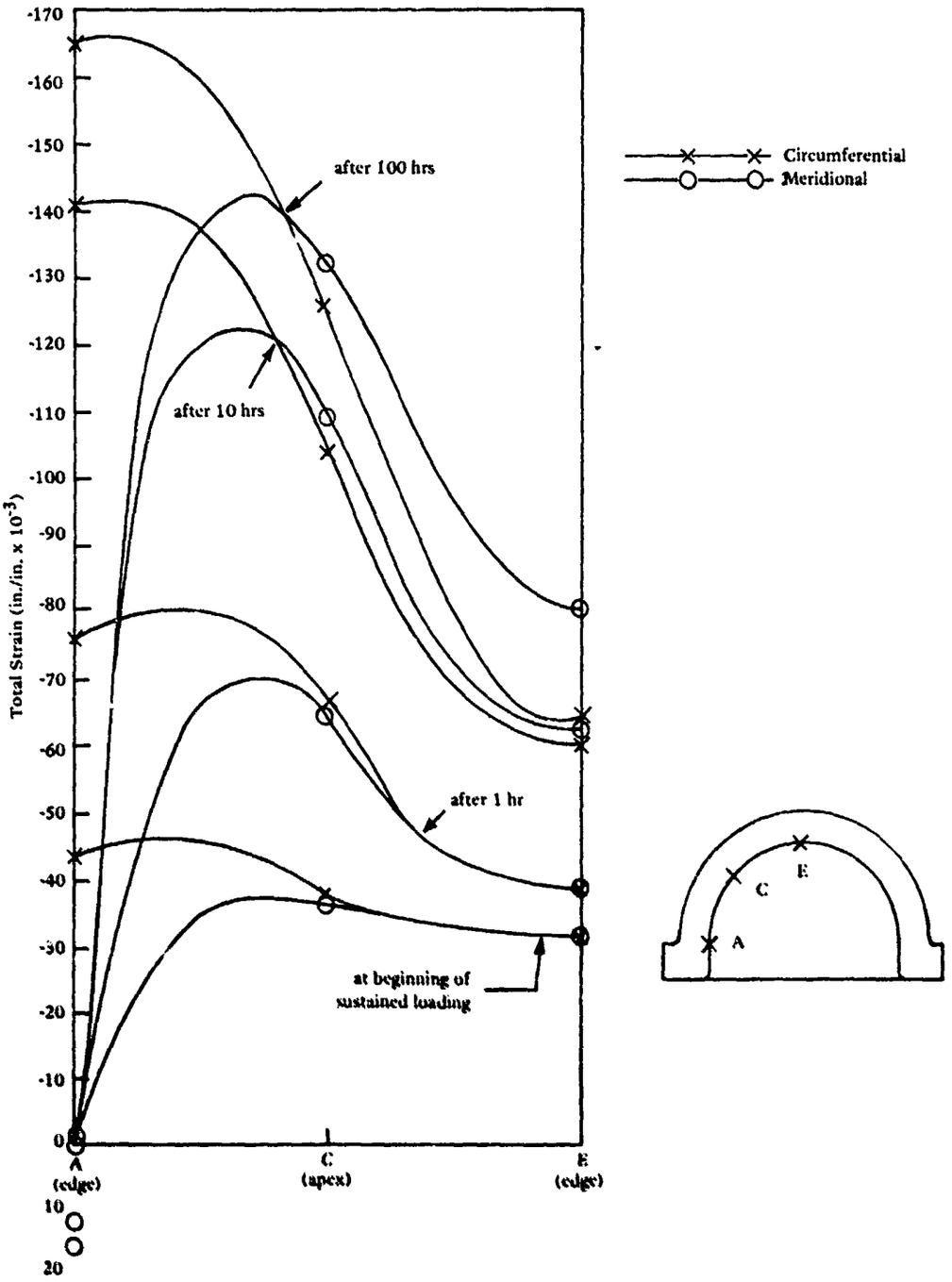

Figure 32. Change in magnitude and distribution of strains with duration of sustained pressure loading at 8,000 psi; window H, Type I; 75°F.

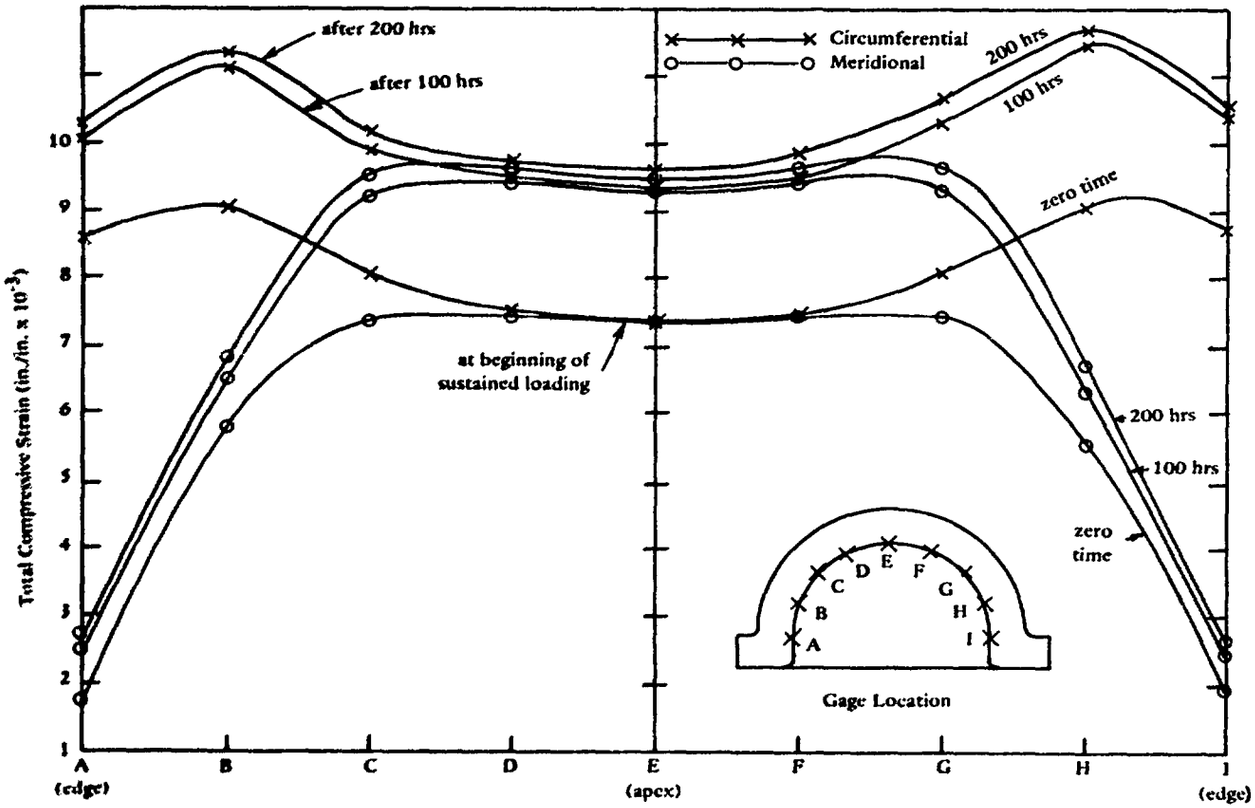

Figure 33. Change in magnitude and distribution of strains with duration of sustained pressure loading at 2,000 psi; window I, Type I; 76°F.

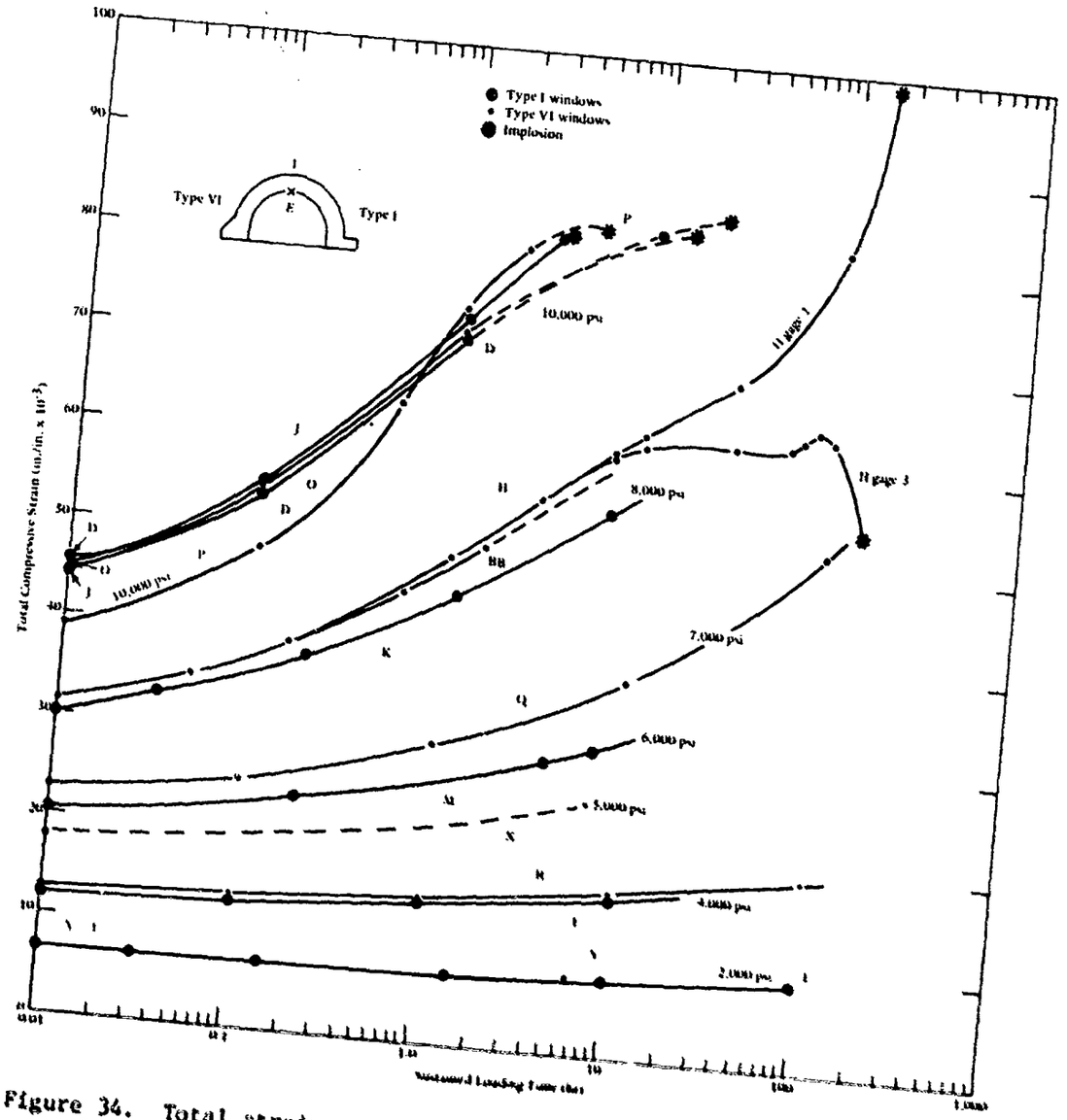

Figure 34. Total strain at the apex as a function of time and magnitude of pressure under sustained loading.

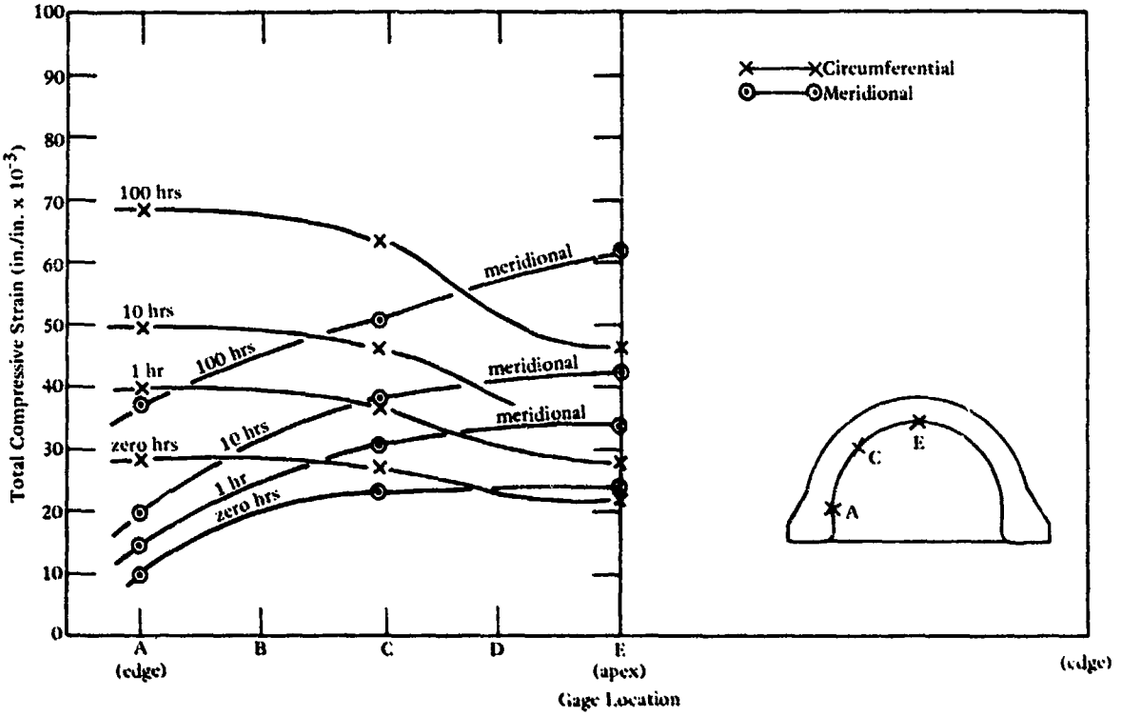

Figure 35. Total strain as a function of loading duration under 7,000 psi pressure; window Q, Type VI.

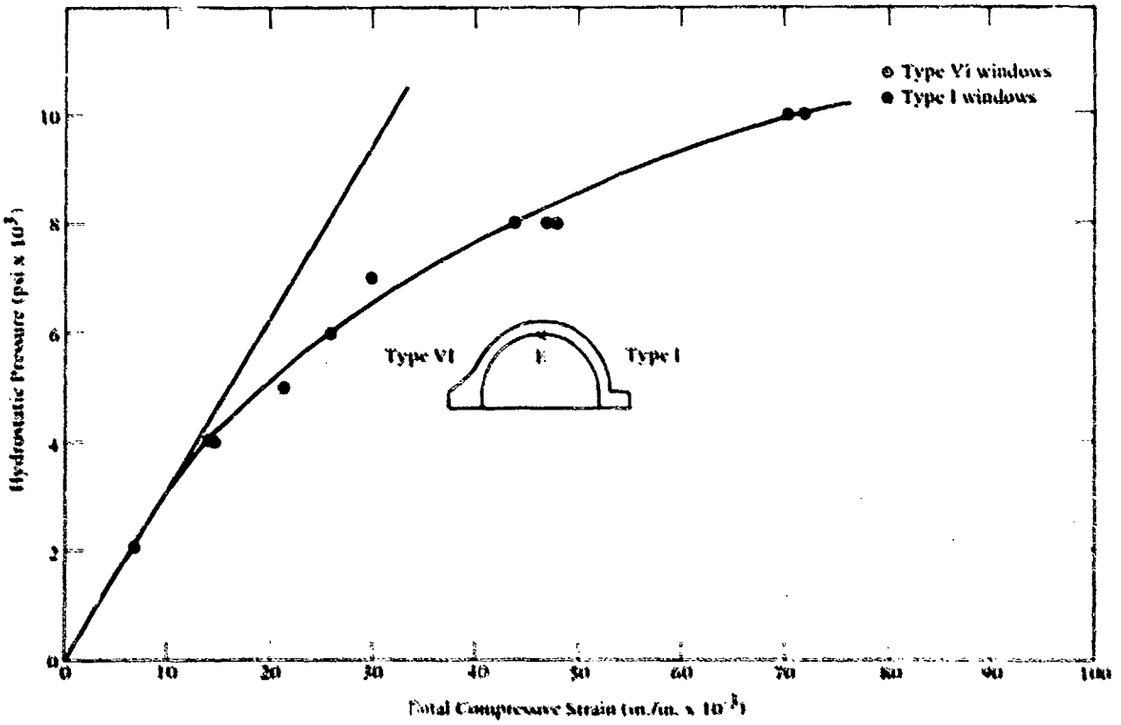

Figure 36. Typical nonlinearity in window deformation under short-term pressure loading.

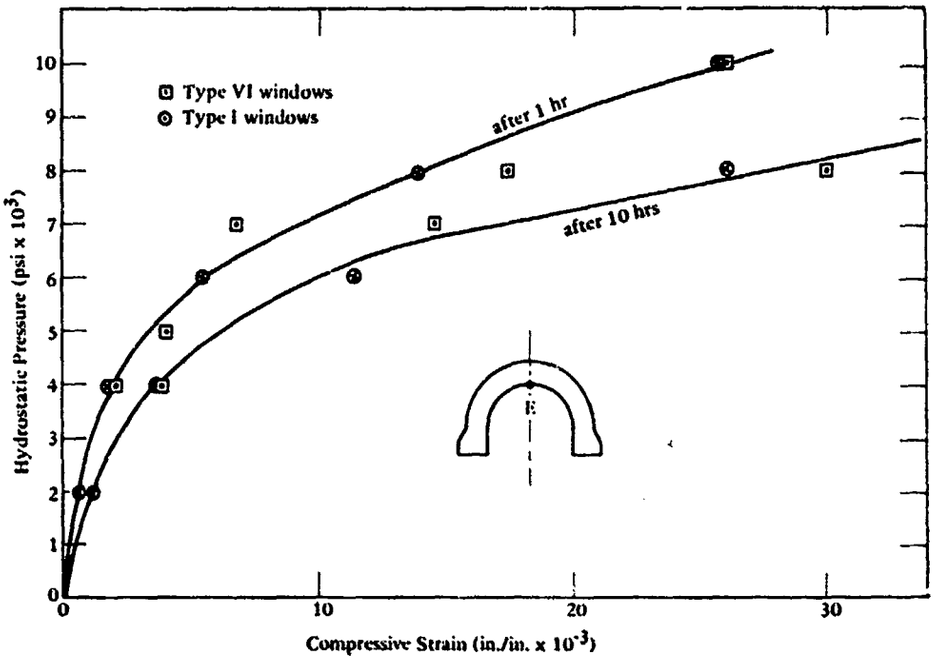

Figure 37. Time-dependent strain (creep) as a function of sustained pressure loading.

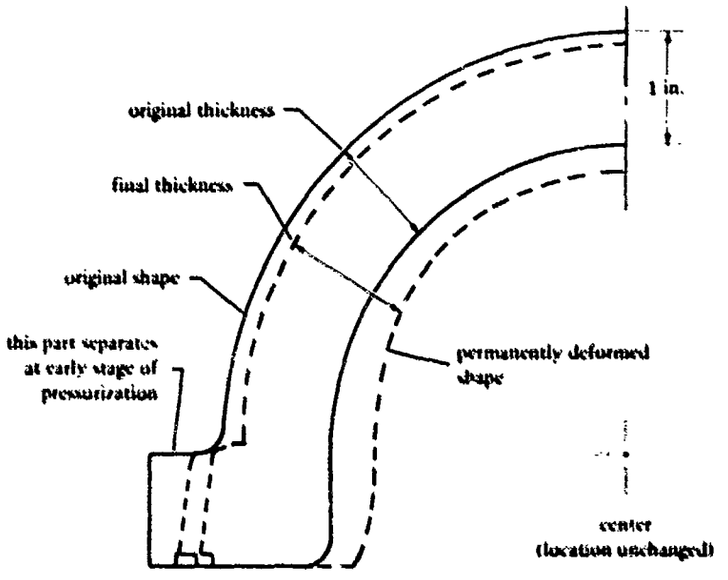

Figure 38. Typical plastic deformation of Type I windows, subjected to long-term pressure loading of sufficient magnitude to cause imploding; windows J and H, Type I.

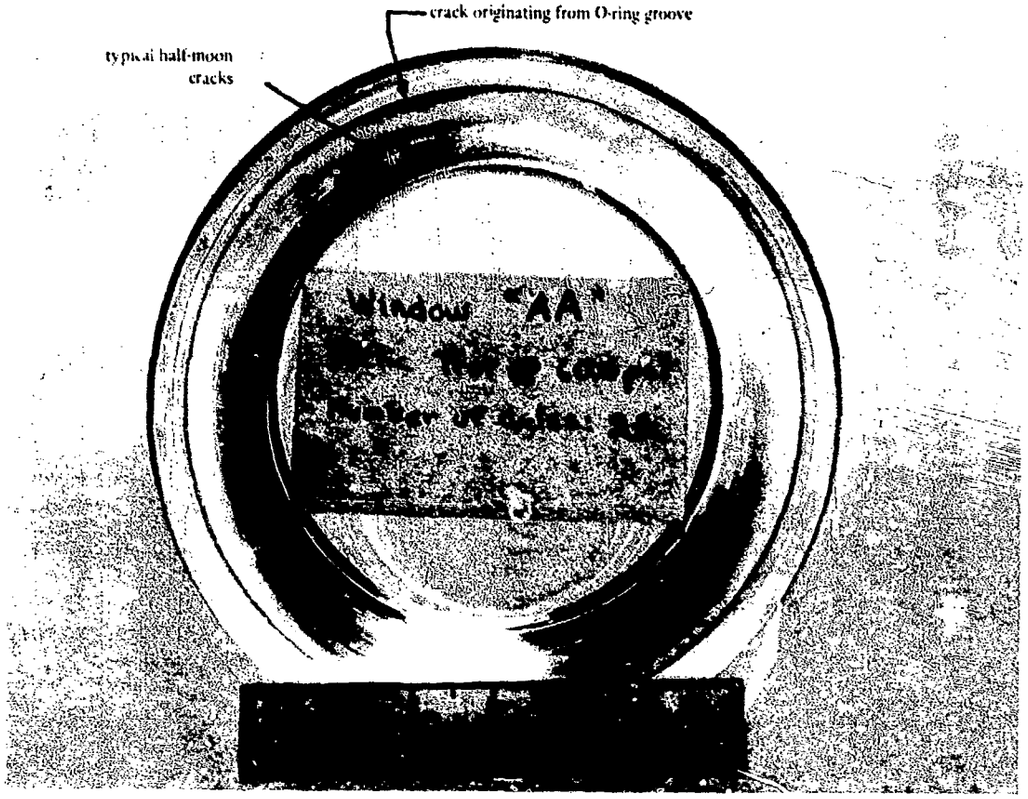

Figure 39. Typical cyclic fatigue cracks on the flange bearing surface; window AA, Type VI after 22 standard pressure cycles to 6,000 psi. Note that major crack originates at O-ring groove.

Figure 40. Same window as in Figure 39; note the shape of the typical cyclic fatigue crack in the bearing surface on the flange. Similar cracks were observed in bearing surfaces of acrylic windows subjected to cyclic pressure loading in other studies [2,8,10]. This peculiar shape is probably caused by expansion of grease or water trapped in the crack during relaxation phases of pressure cycling.

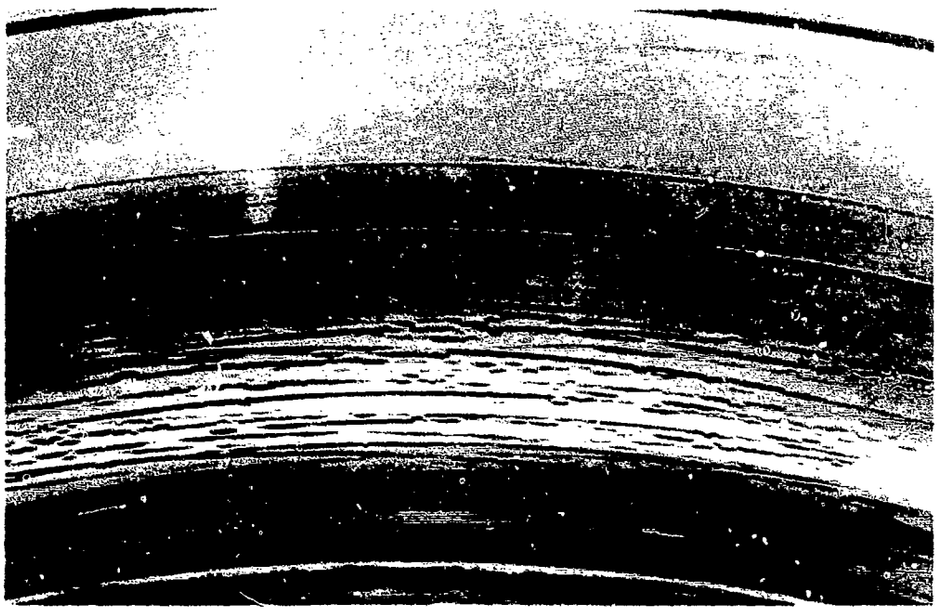

Figure 41. Same window as in Figure 39; note that the circumferential crazing on the bearing surface of the flange appears primarily near the heel of the flange and not the O-ring groove.

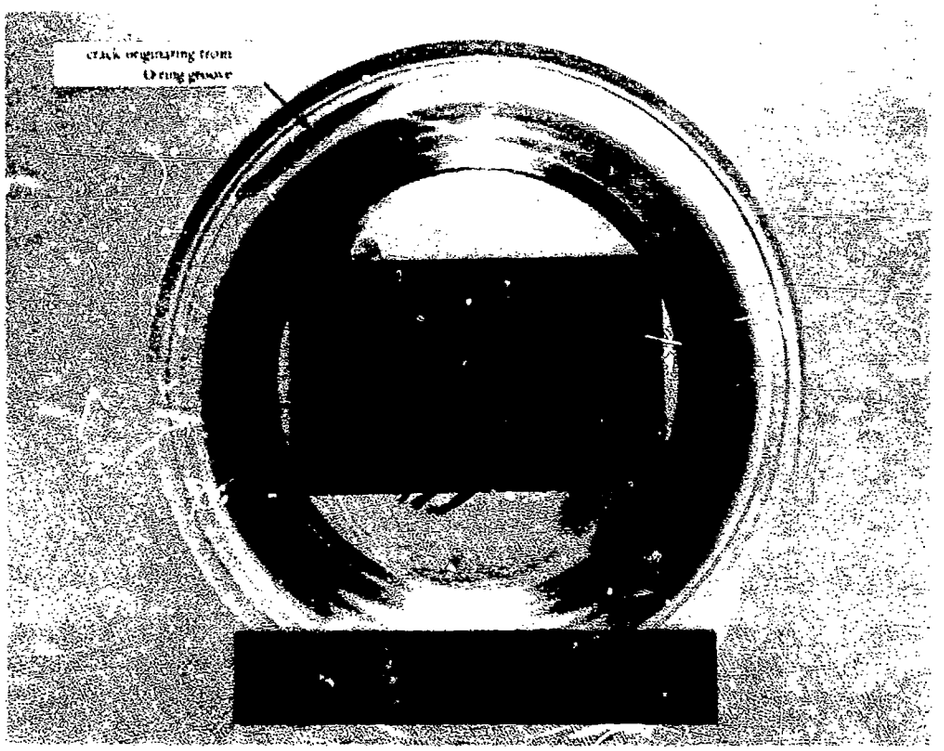

Figure 42. Typical cyclic fatigue cracks on the flange bearing surface; window I, Type I after 38 standard pressure cycles to 3,000 psi. Note that the crack originates at O-ring groove.

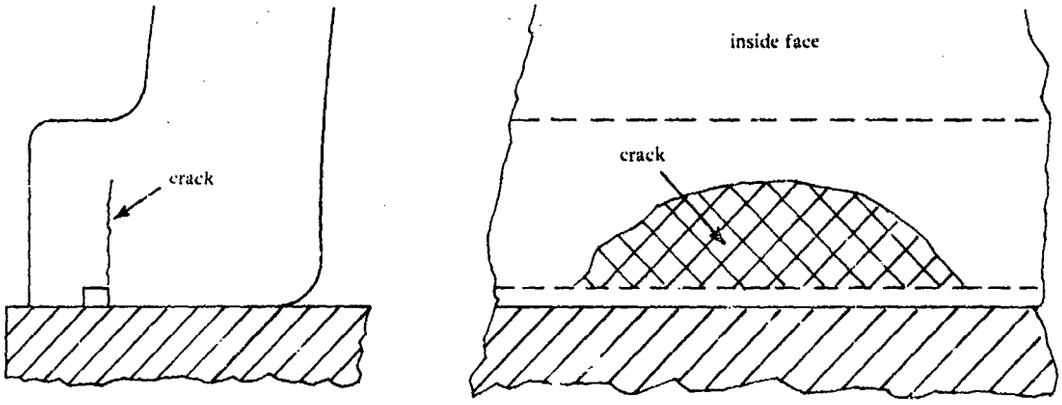

Figure 43. Cracks found in windows AA and I.

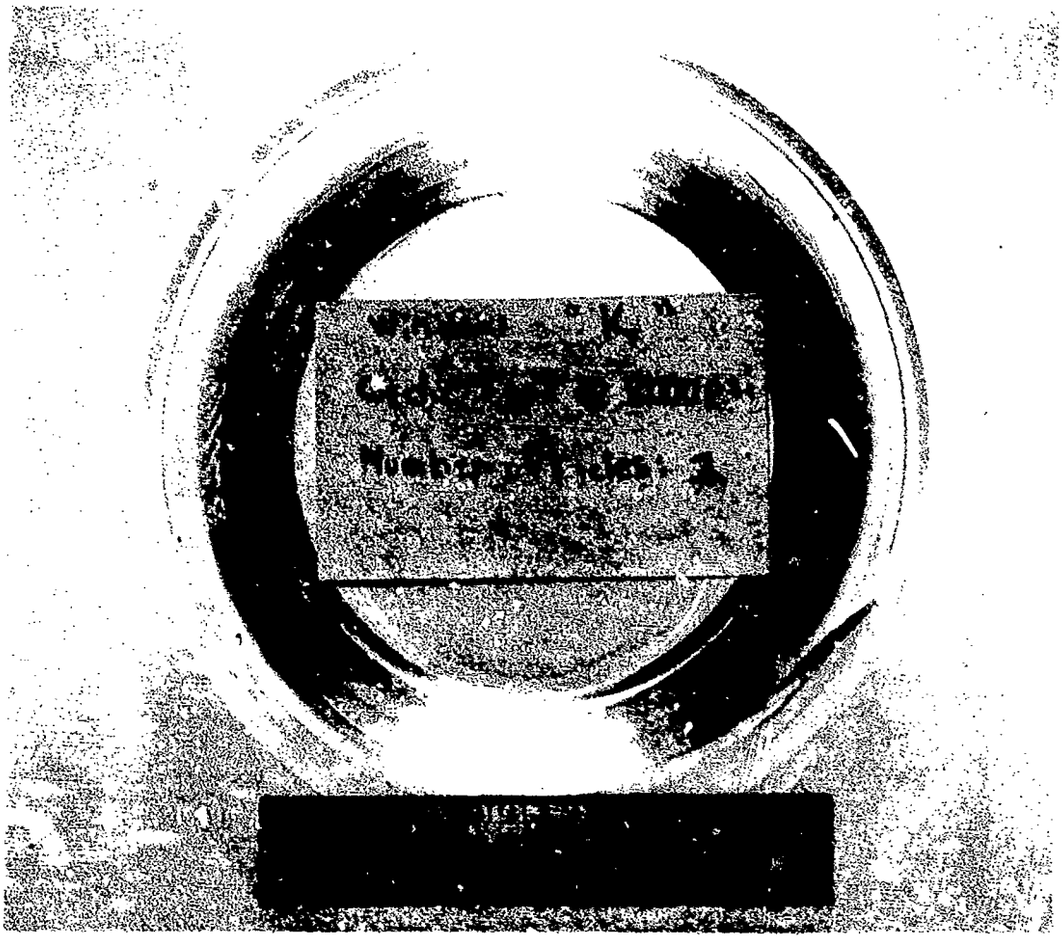

Figure 44. Typical cyclic fatigue cracks on the flange bearing surface; window K, Type I after one standard pressure cycle to 8,000 psi. Note major circumferential crack between the heel of the flange and the O-ring groove.

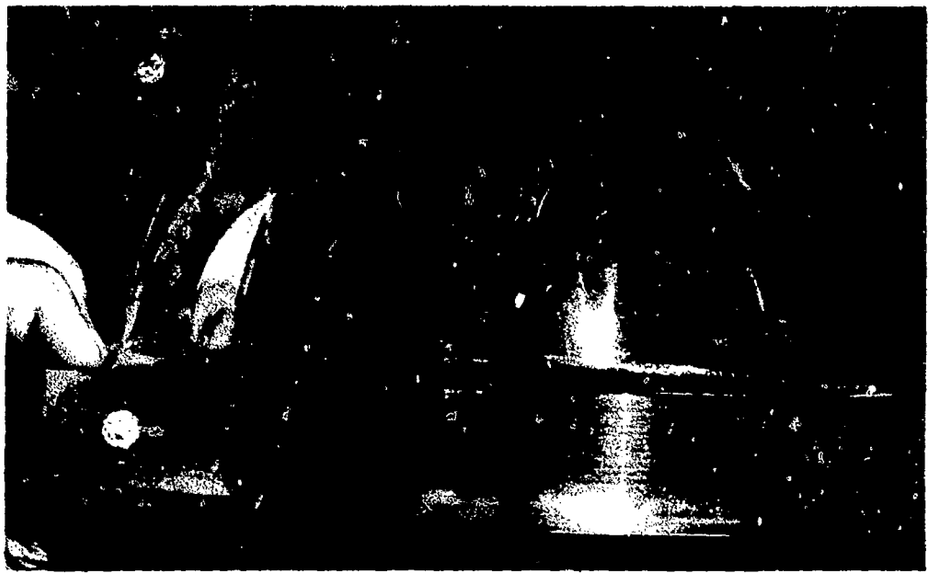

Figure 45. Same window as in Figure 44; note how the circumferential crack has penetrated the whole thickness of the flange.

Figure 46. Typical cyclic fatigue cracks on the flange bearing surface; window BB, Type VI after two standard pressure cycles to 8,000 psi. Note many circumferential cracks between heel of the flange and O-ring groove.

Figure 47. Same window as in Figures 39, 40, and 41; note that cyclic fatigue cracks on the flange bearing surface originating not at the O-ring groove have a characteristic mushroom shape.

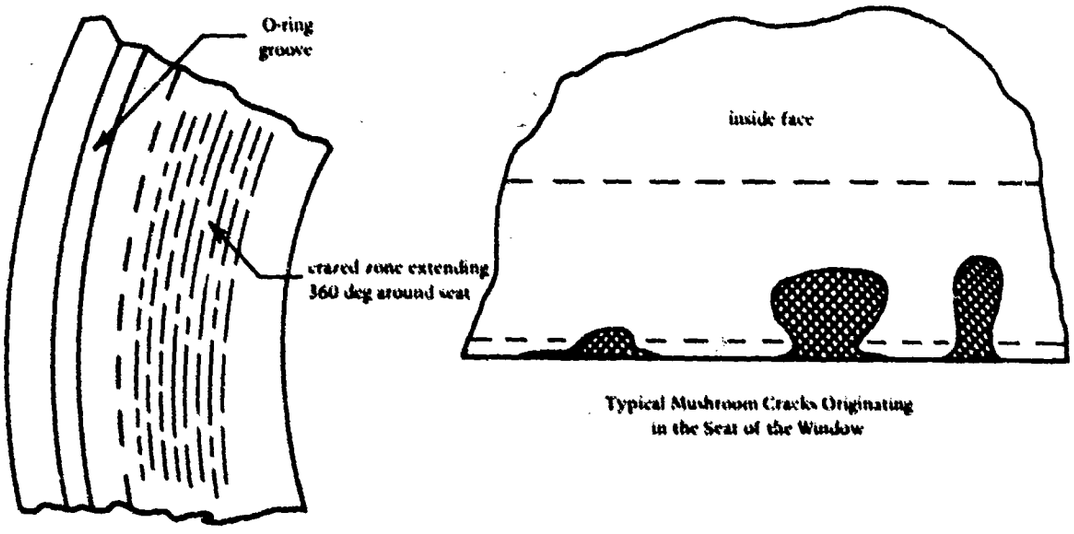

Figure 48. Two characteristic forms of window fracturing.

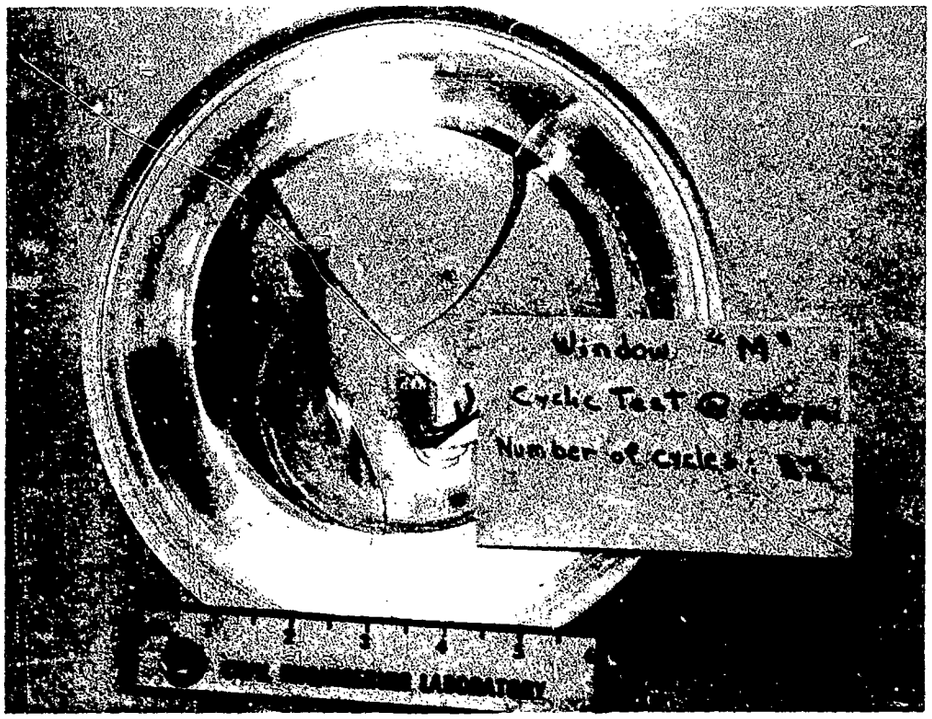

Figure 49. Typical cyclic fatigue meridional cracks on the interior face of window M, Type I window after 22 standard pressure cycles to 6,000 psi; note that the meridional cracks do not penetrate through the whole thickness of the window or flange.

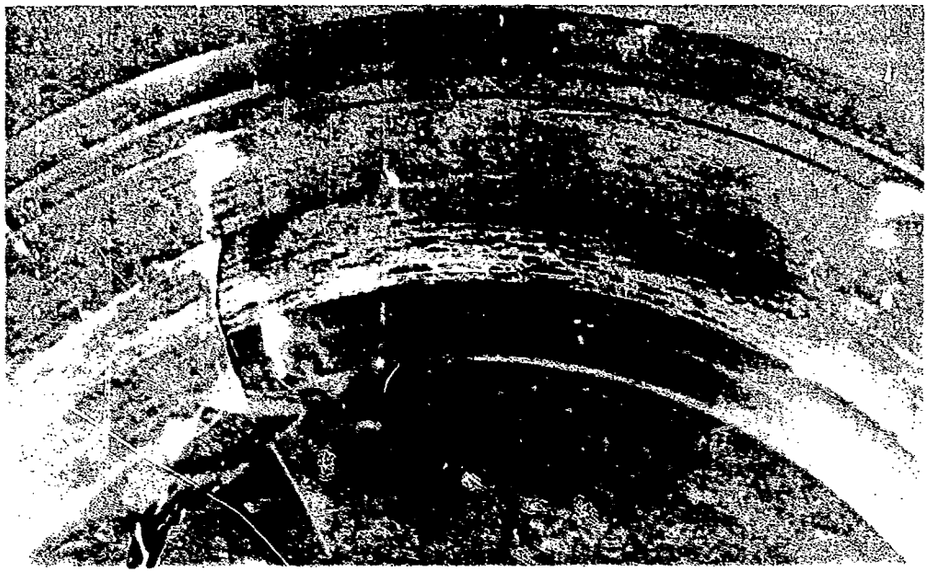

Figure 50. Same window as in Figure 49; note the presence of extensive crazing and small circumferential cracks on the bearing surface of the flange that appeared prior to the meridional cracks.

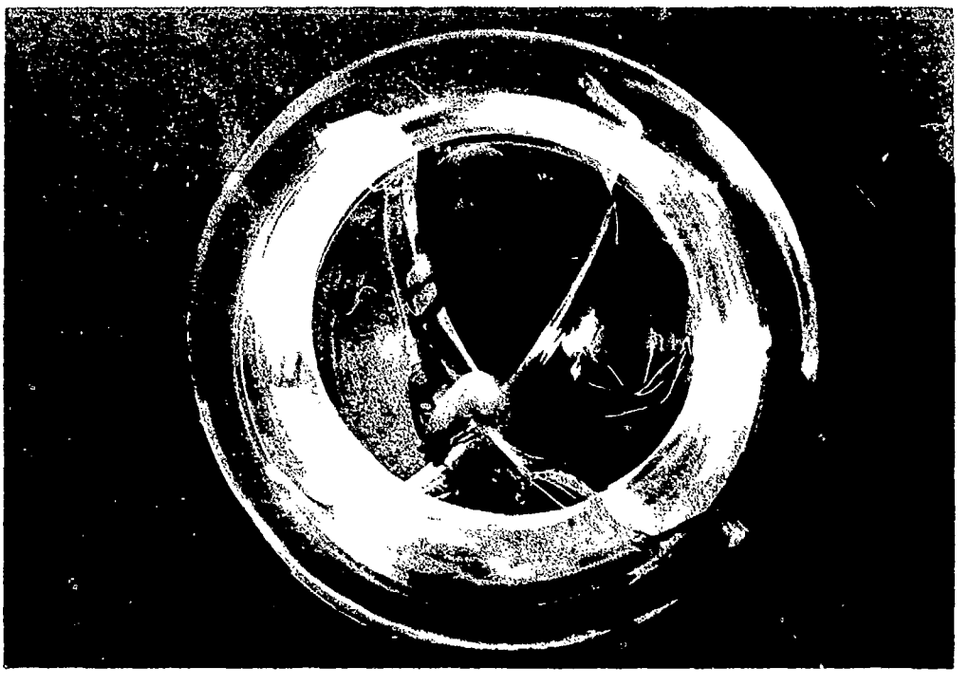

Figure 51. Typical cyclic fatigue meridional cracks on the interior face of window E, Type I (modified) after one standard pressure cycle to 8,000 psi; note that the cracks do not penetrate through the whole thickness of the window.

Figure 52. Same window as in Figure 51; note the wide crack between surfaces and that the width of the crack is widest on the interior face of the window indicating that the crack originated on the interior face and subsequently propagated outward toward exterior face.

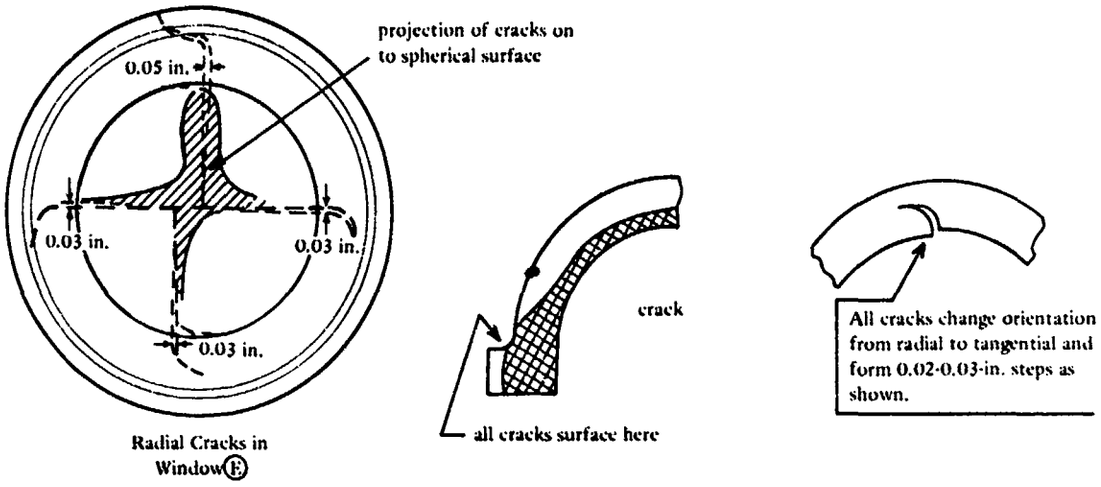

Figure 53. Cracking in Window Ⓔ.

Figure 54. Typical cyclic fatigue circumferential cracks on the bearing surfaces of Type I flanges that cause the window to leak after a few pressure cycles; window K, Type I after one standard pressure cycle to 8,000 psi.

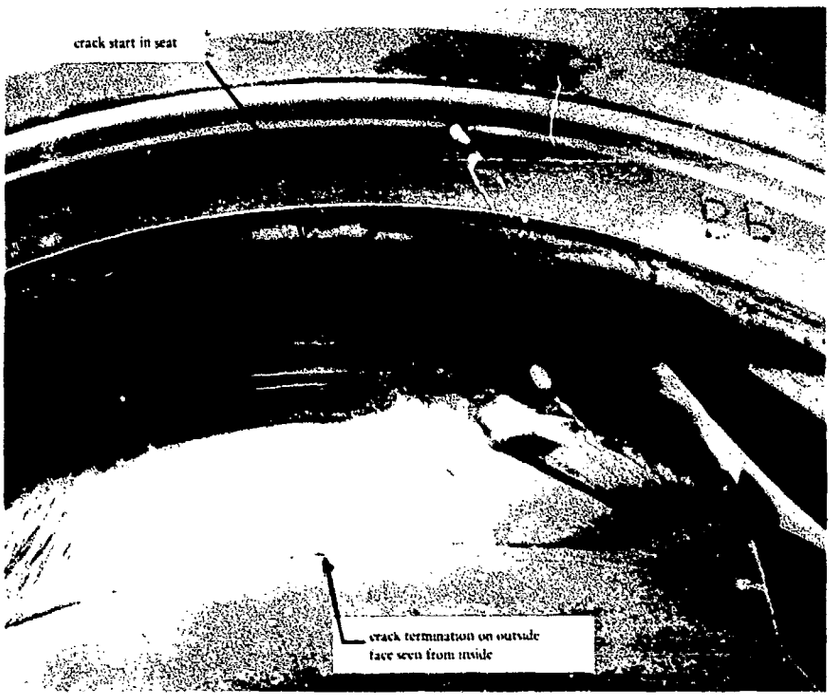

Figure 55. Typical cyclic fatigue circumferential cracks on the bearing surfaces of Type VI flanges that cause the window to leak after a few pressure cycles; window BB, Type VI after two standard pressure cycles to 8,000 psi.

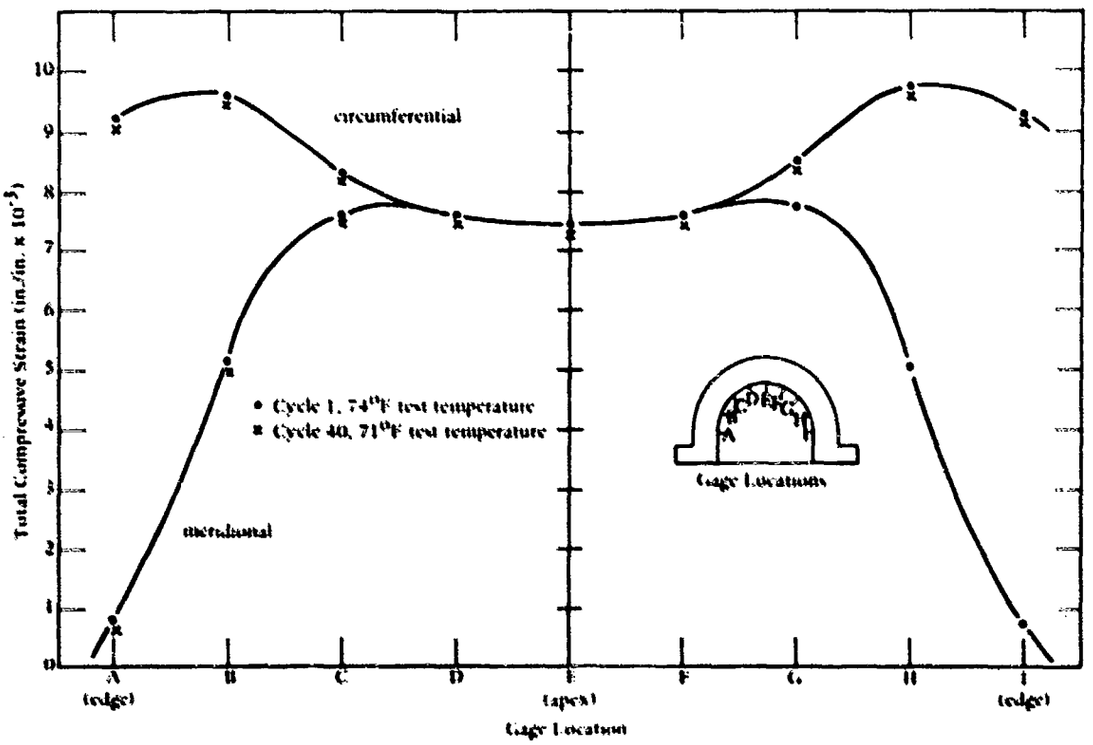

Figure 56. Distribution of compressive strains on the interior face of Type I windows at the end of 7-hour sustained pressure loading phase at 2,000 psi in a standard pressure cycle, window 1.

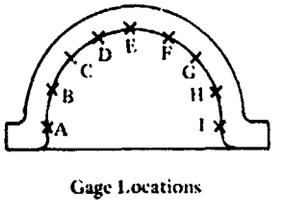

Gage Locations

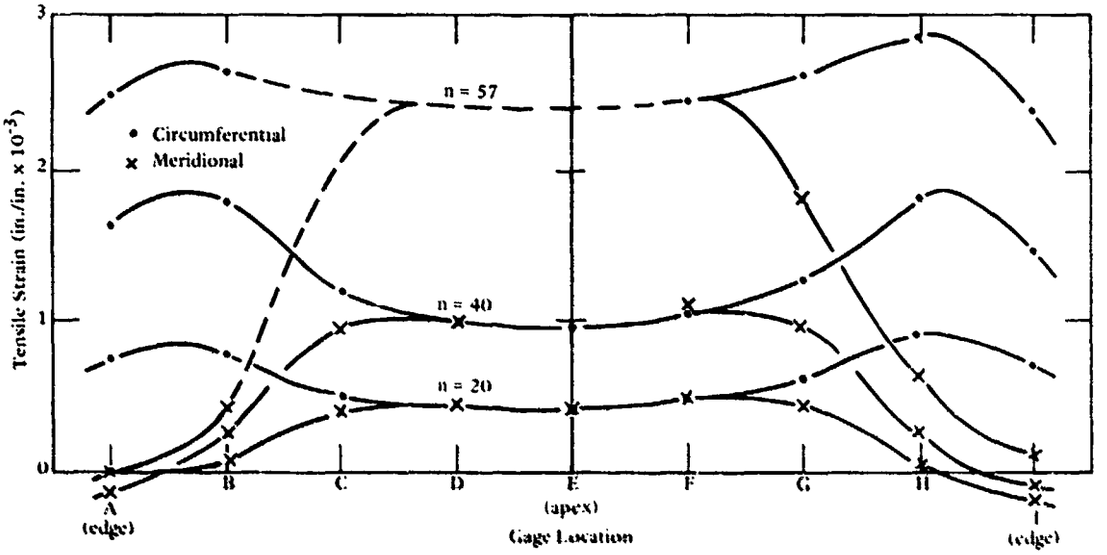

Figure 57. Distribution of residual tensile strains on the interior face of Type I window at the end of 17-hour-long relaxation phases at 0 psi in standard pressure cycles to 2,000 psi, window 1. All residual strains are measured from the strain level prior to first pressure cycle; 70-75°F.

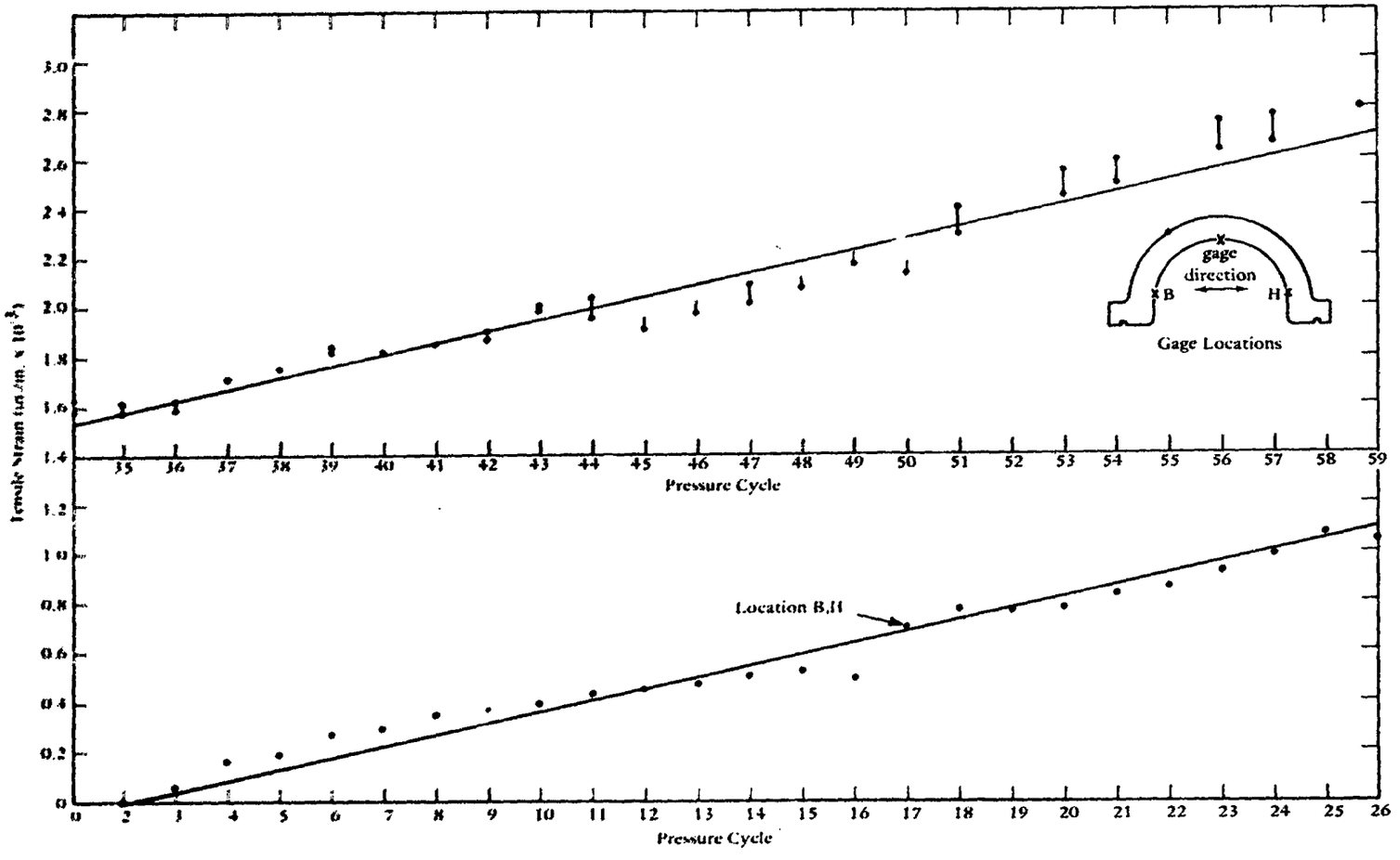

Figure 58. Rate of increase for residual tensile strains on the interior face of type I window at the end of 17-hour-long relaxation phases at 0 psi in standard pressure cycles to 2,000 psi, window I. All residual strains are measured from the strain datum prior to the first cycle.

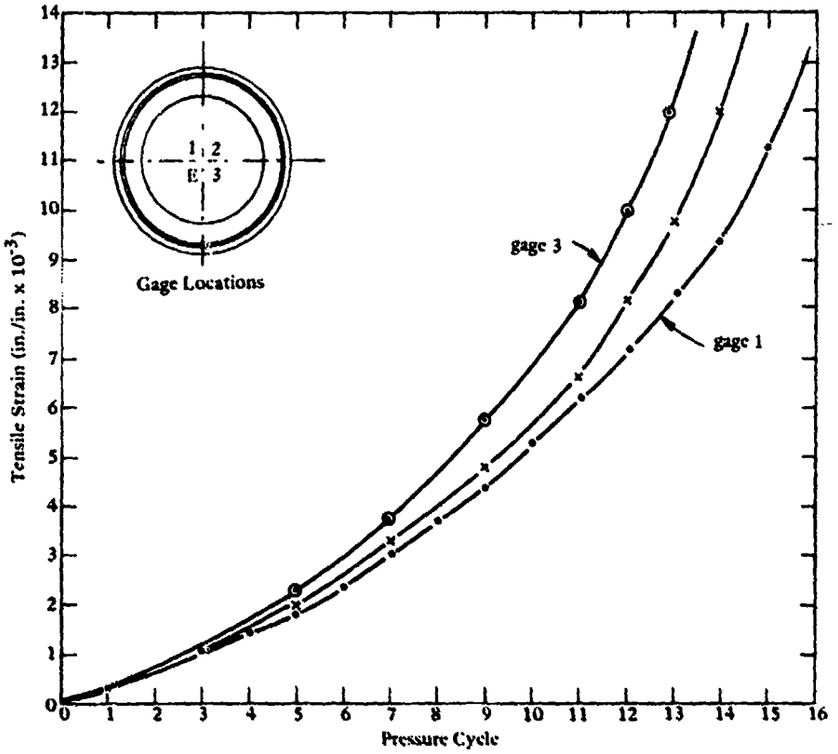

Figure 59. Rate of increase for residual tensile strains on interior face of Type VI window at the end of 17-hour-long relaxation phases at 0 psi in standard pressure cycles to 5,000 psi, window X. All residual strains are measured from the strain level prior to first pressure cycle; 68-73°F.

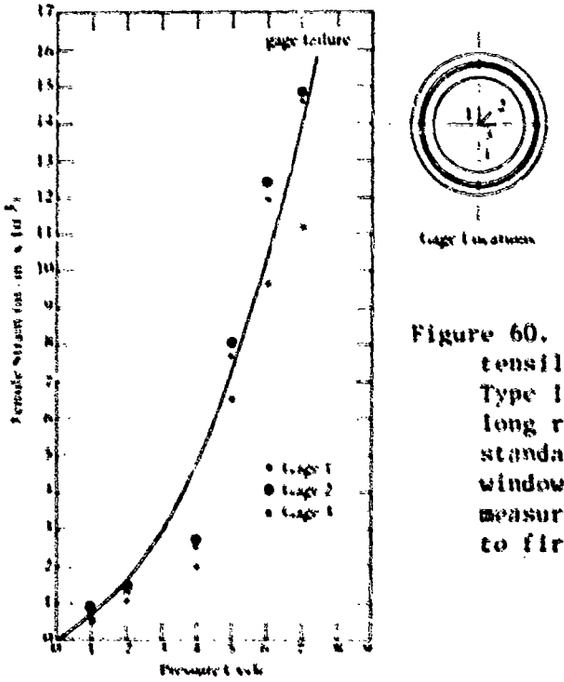

Figure 60. Rate of increase for residual tensile strains on interior face of Type I window at the end of 17-hour-long relaxation phases at 0 psi in standard pressure cycles to 6,000 psi, window N. All tensile strains are measured from the strain level prior to first pressure cycle.

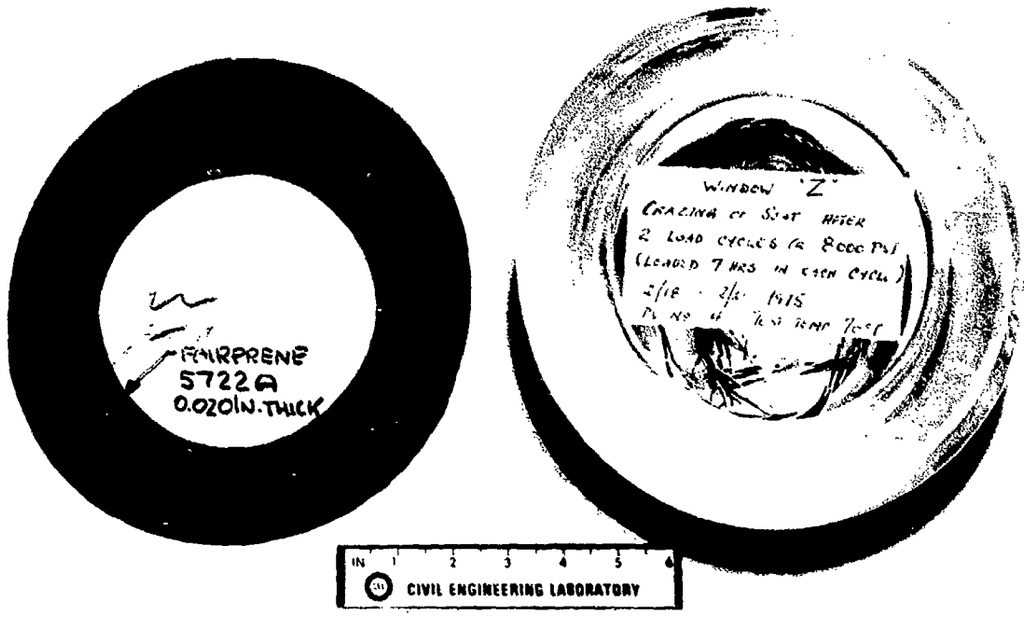

Figure 61. Window Z, Type VI after two standard pressure cycles to 8,000 psi on a neoprene-coated nylon cloth gasket; note the absence of major cracks, also compare to window BB, Type VI (Figures 46 and 55) that was tested under identical cyclic conditions but without a gasket.

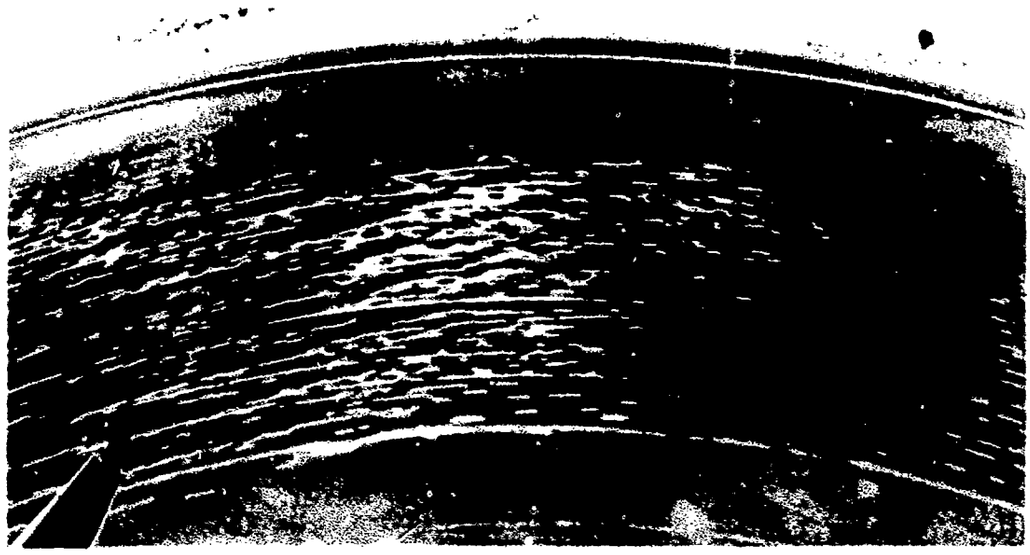

Figure 62. Same window as in Figure 61; note that only minor crazing is present on the bearing surface indicating the beneficial effect of the gasket.

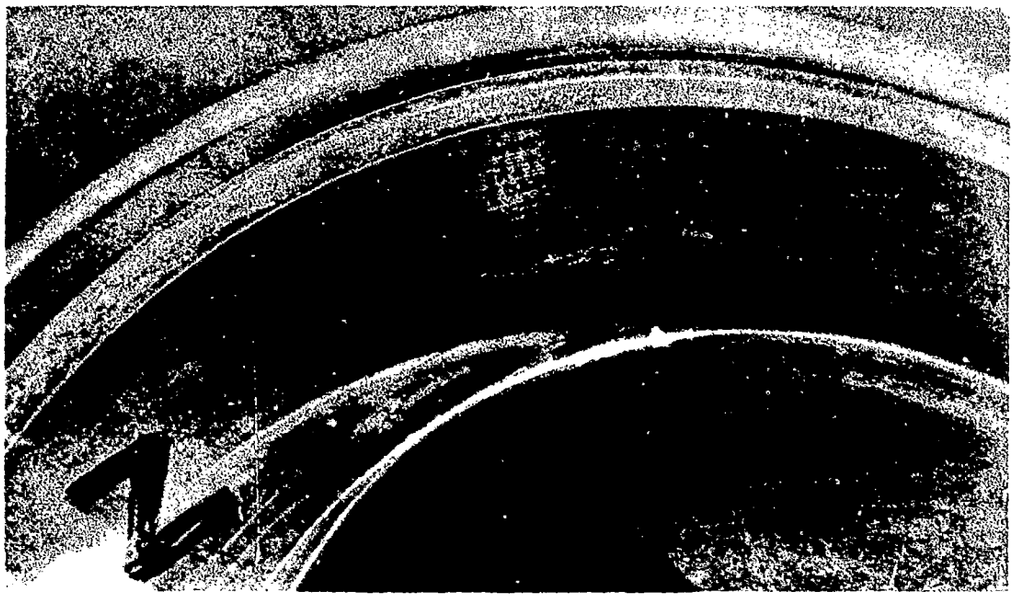

Figure 63. Window Z, Type VI after two standard pressure cycles to 8,000 psi on a neoprene-coated nylon cloth gasket and 200 hours of relaxation at 0 pressure. Note the absence of crazing at the termination of second pressure cycle (Figure 62).

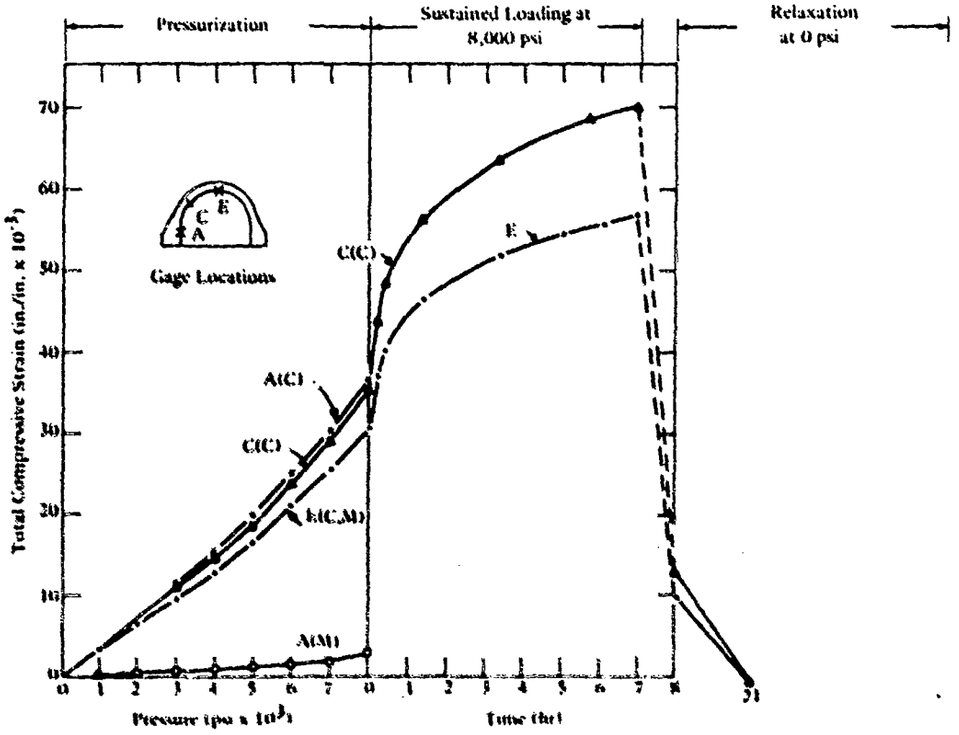

Figure 64. Distribution of strain in window Z, Type VI when pressure cycled to 8,000 psi on a neoprene-coated nylon cloth gasket.

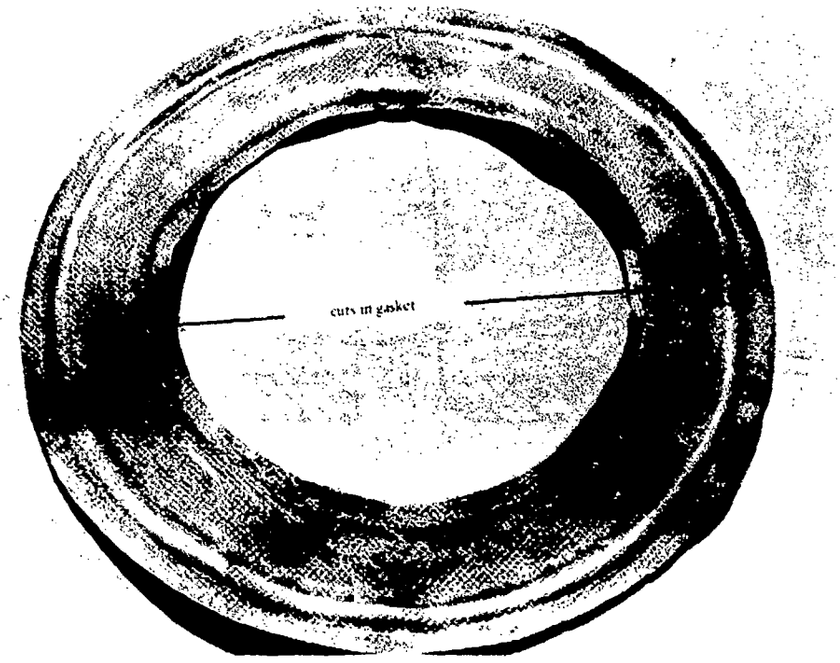

Figure 65. Cuts in neoprene-coated nylon cloth gasket by window Z, Type VI, subjected to two standard pressure cycles at 8,000 psi.

Gage Locations

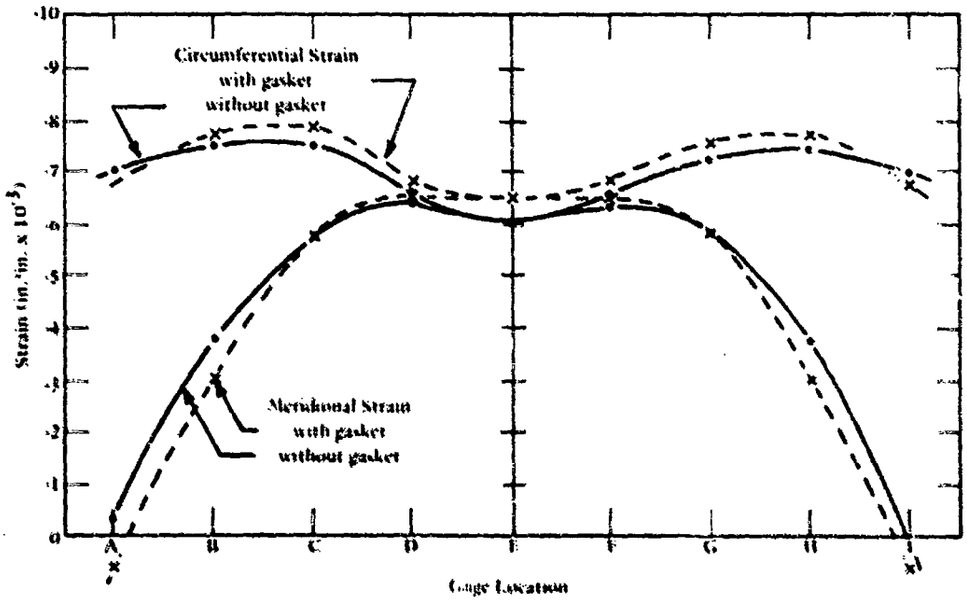

Figure 66. Comparison of short-term strain distributions for the same window Y, Type VI pressurized to 2,000 psi with and without a neoprene-coated nylon cloth bearing gasket.

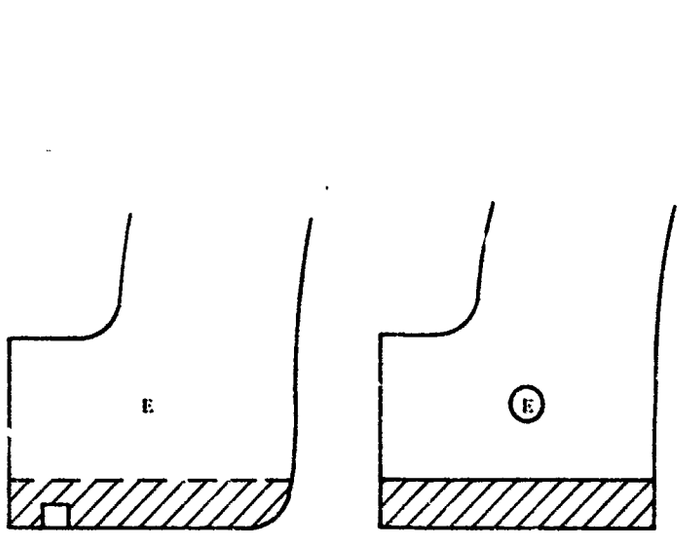

Figure 67. Shaded area machined off and replaced with a bonded-in-place acrylic disc.

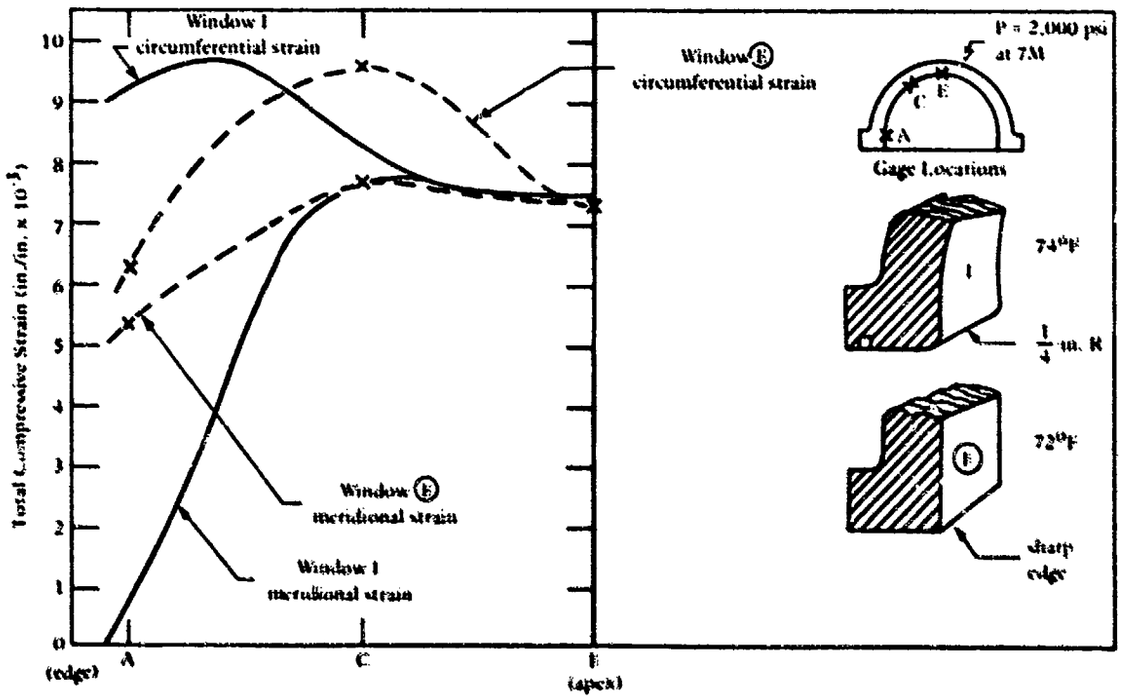

Figure 68. Comparison of strains in Type I windows with rounded and sharp heels after 7 hours of sustained pressurization to 2,000 psi; windows I and E, respectively.

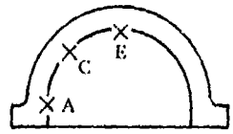

Gage Locations

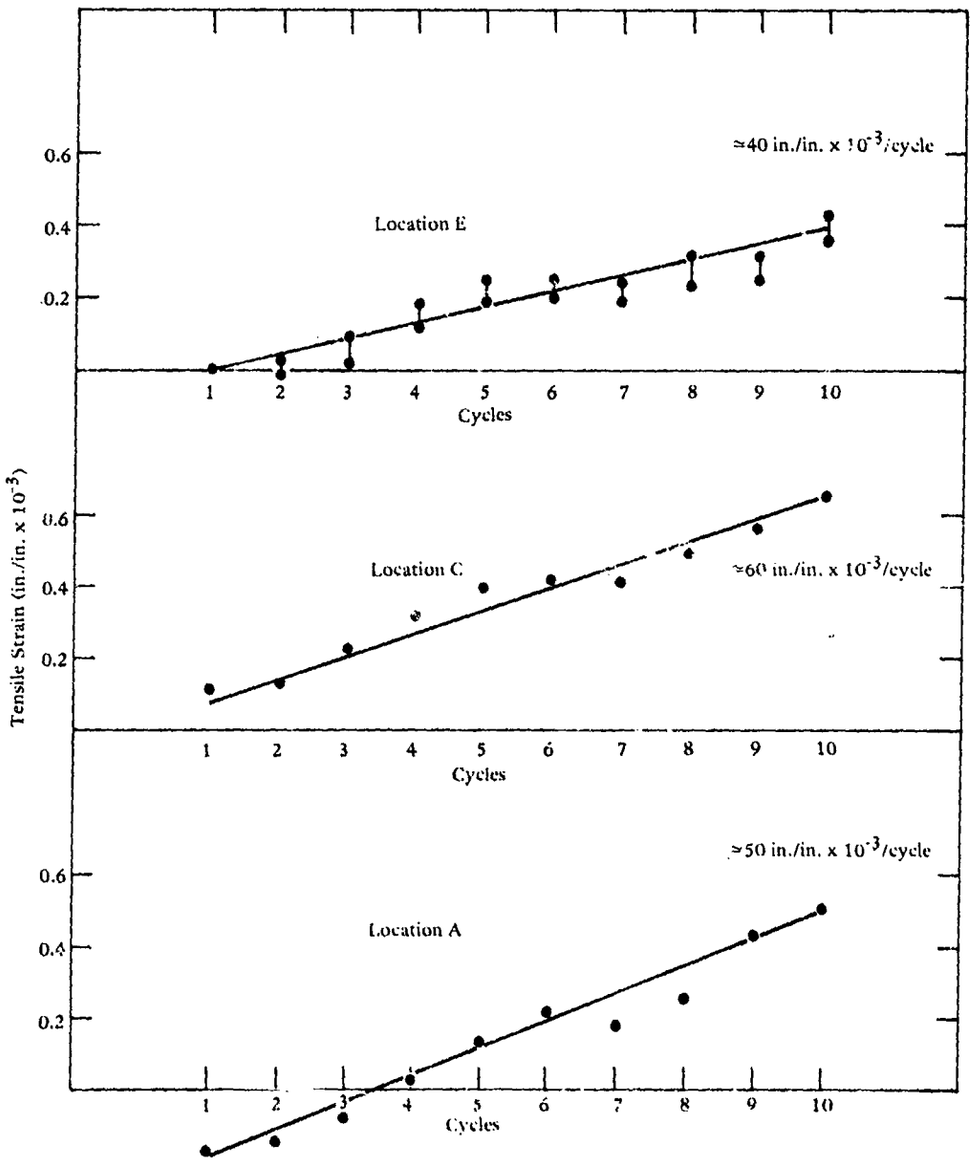

Figure 69. Rate of increase for residual tensile circumferential strains on the interior face of window (E), Type I with sharp heel at the end of 17-hour-long relaxation phases at 0 psi in standard pressure cycles to 2,000 psi.

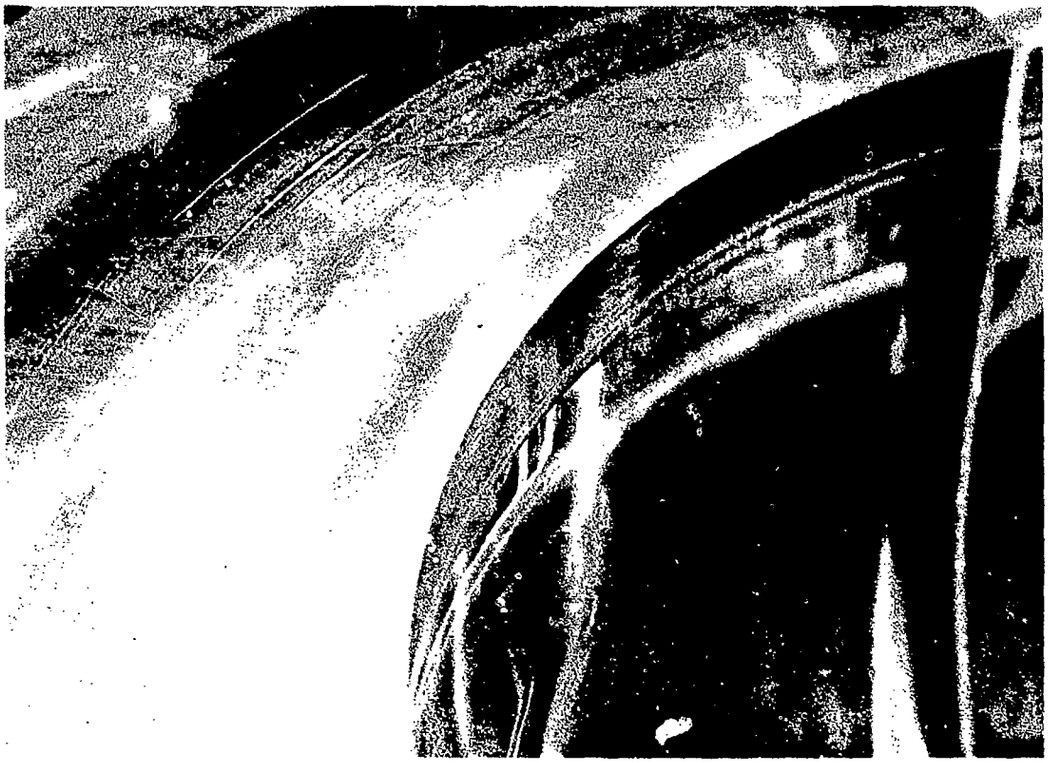

Figure 70. Sharp edge on the heel of modified Type I, window Ⓔ after one standard pressure cycle to 8,000 psi; note the absence of deformation.

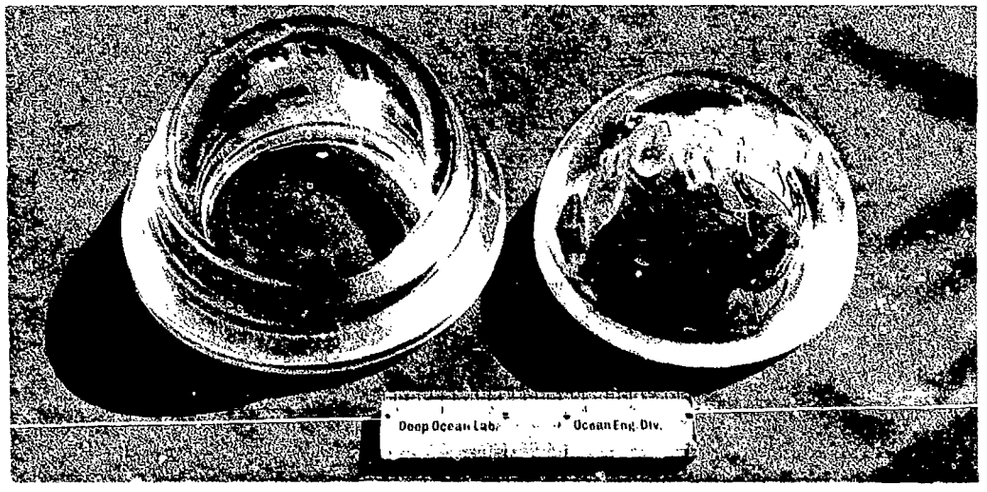

Figure 71. Type VI window prior to and after removal of flange by machining.

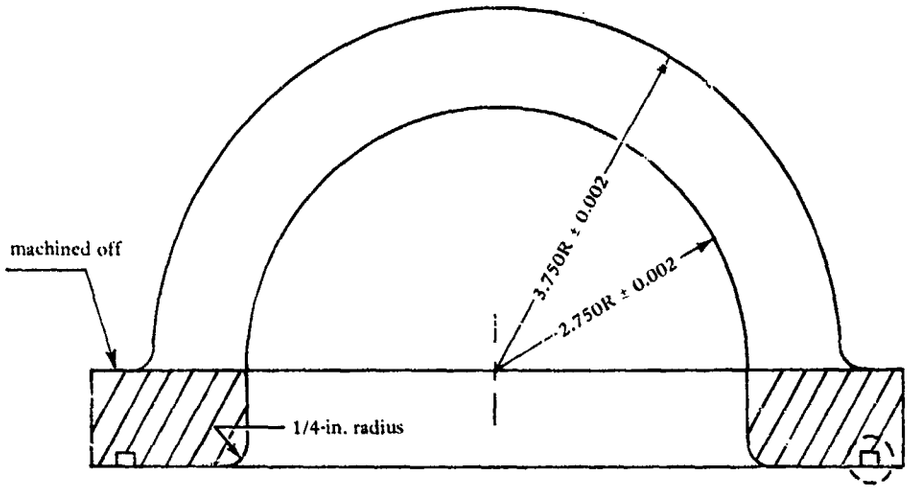

Figure 72. Machining of window I to remove flange.

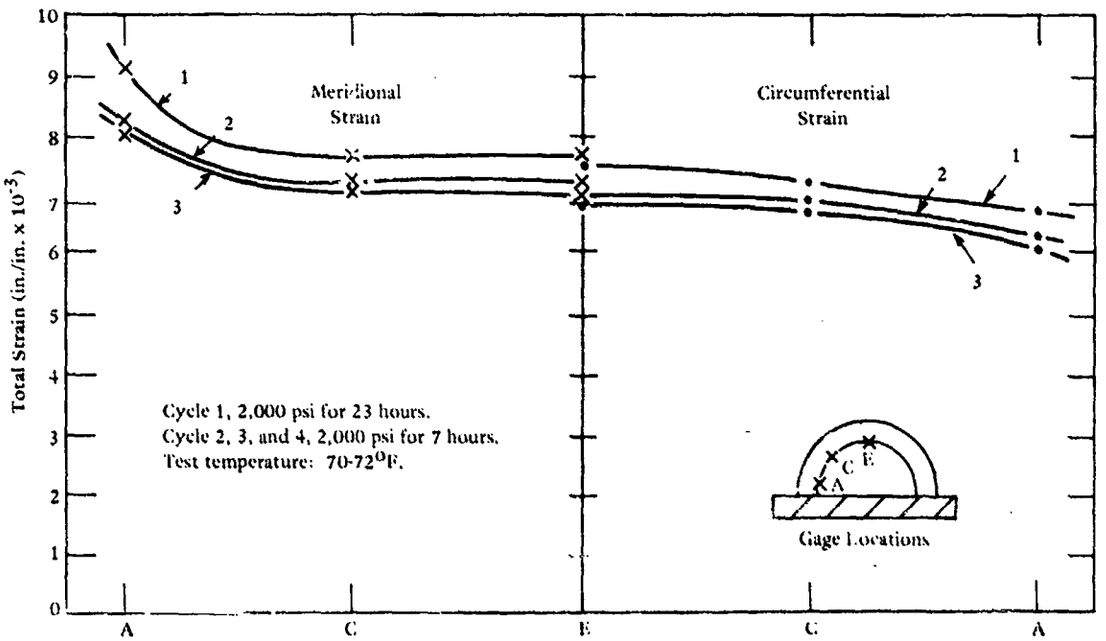

Figure 73. Distribution of strains on the interior face of flangeless hemispherical window I during sustained loading phases of pressure cycling to 2,000 psi; note that the strains on the interior face between the edge and apex are more uniform than in Type I and Type VI windows (Figures 56 and 66).

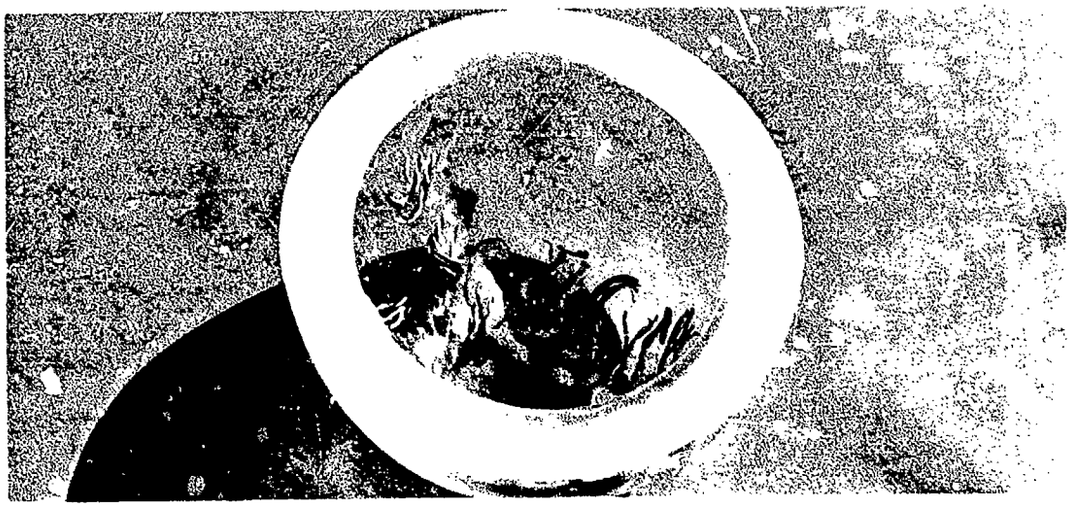

Figure 74. Flangeless window I after two standard pressure cycles to 8,000 psi without a bearing gasket.

Figure 75. Same window as in Figure 74; note absence of cracks and only very minor crazing on the bearing surface.

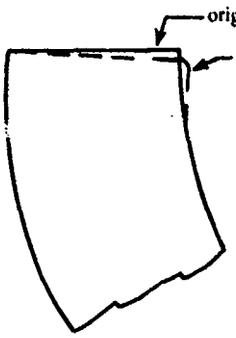

Figure 76. Seat deformation in window I after testing to 8,000 psi.

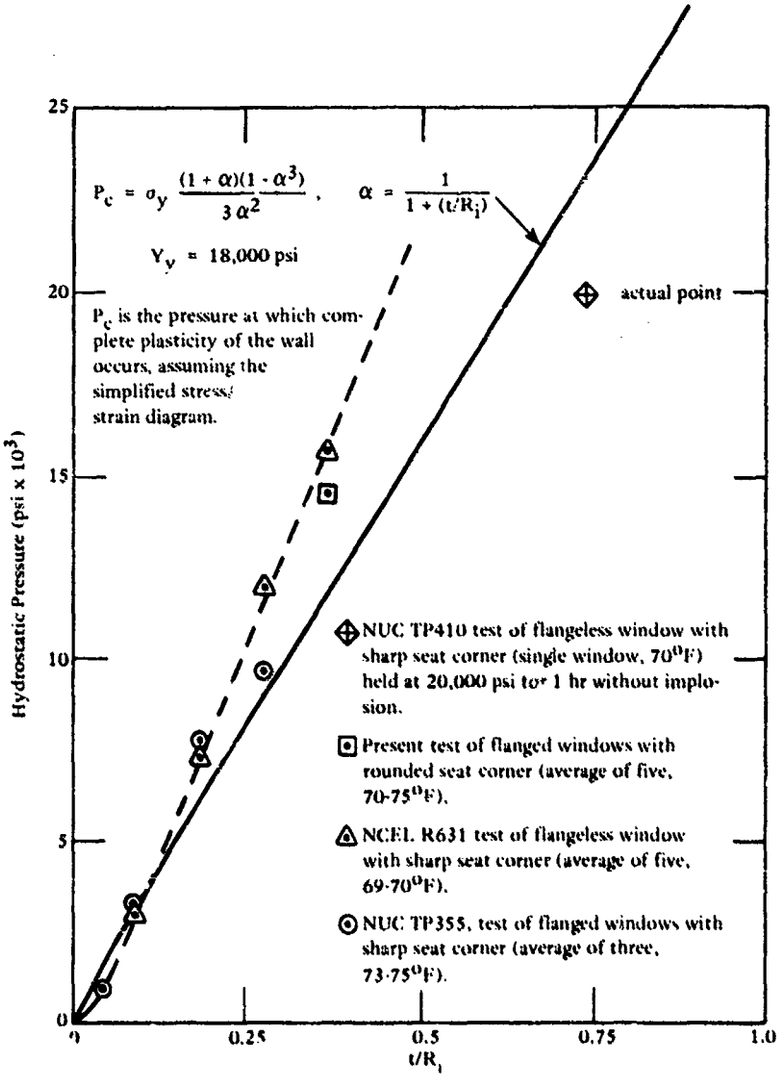

Figure 77. Comparison of actual and calculated critical pressures for hemispherical windows under short-term hydrostatic loading.

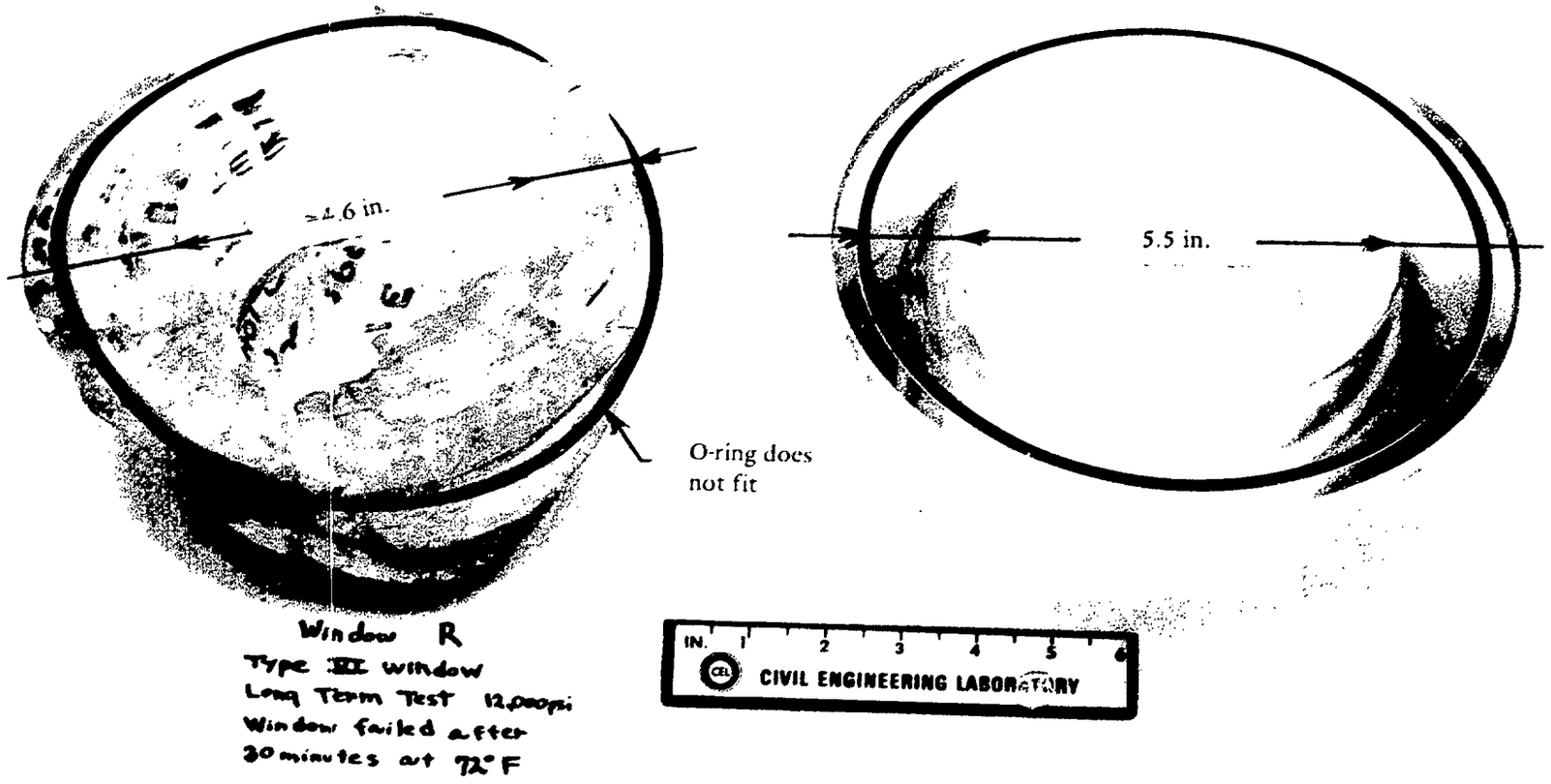

Figure 78. Plastic flow of acrylic plastic resulting in significant diametral deformation of windows prior to implosion under long-term pressure loading.

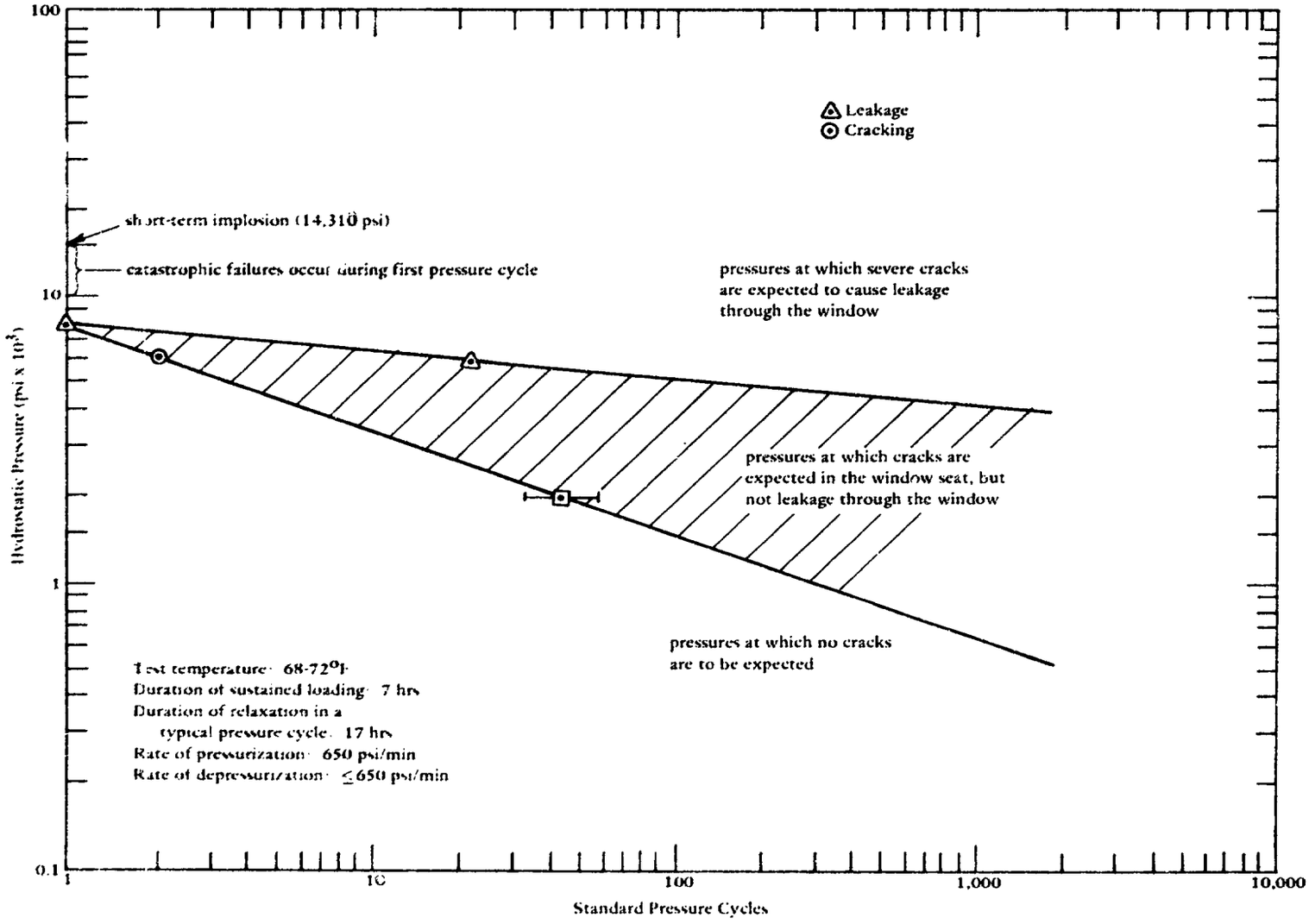

Figure 79. Cyclic fatigue life of hemispherical windows with Type I flanges without bearing gaskets when subjected to standard pressure cycles in room temperature range.

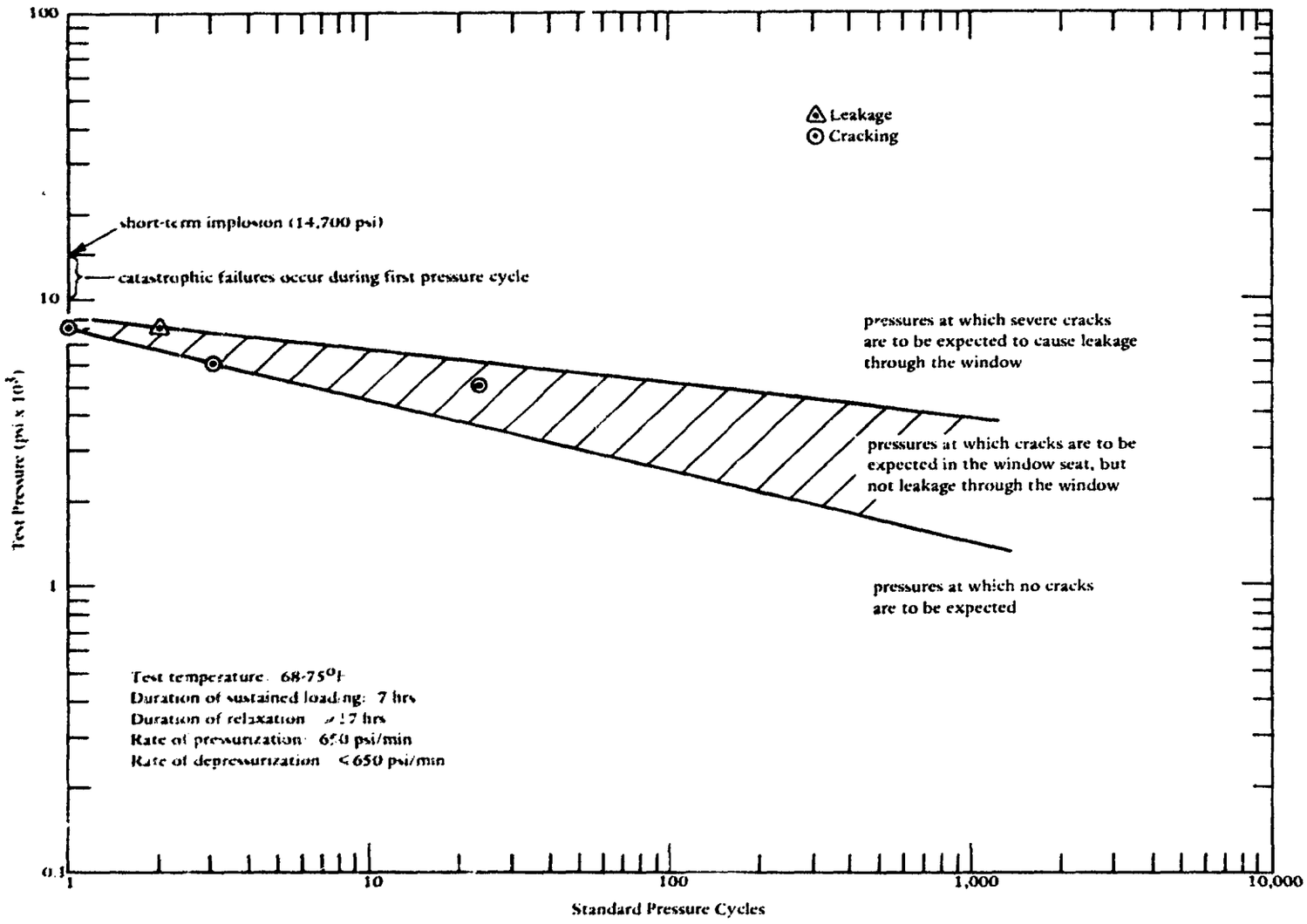

Figure 80. Cyclic fatigue life of hemispherical windows with Type VI flanges without bearing gasket when subjected to standard pressure cycles in room temperature range.

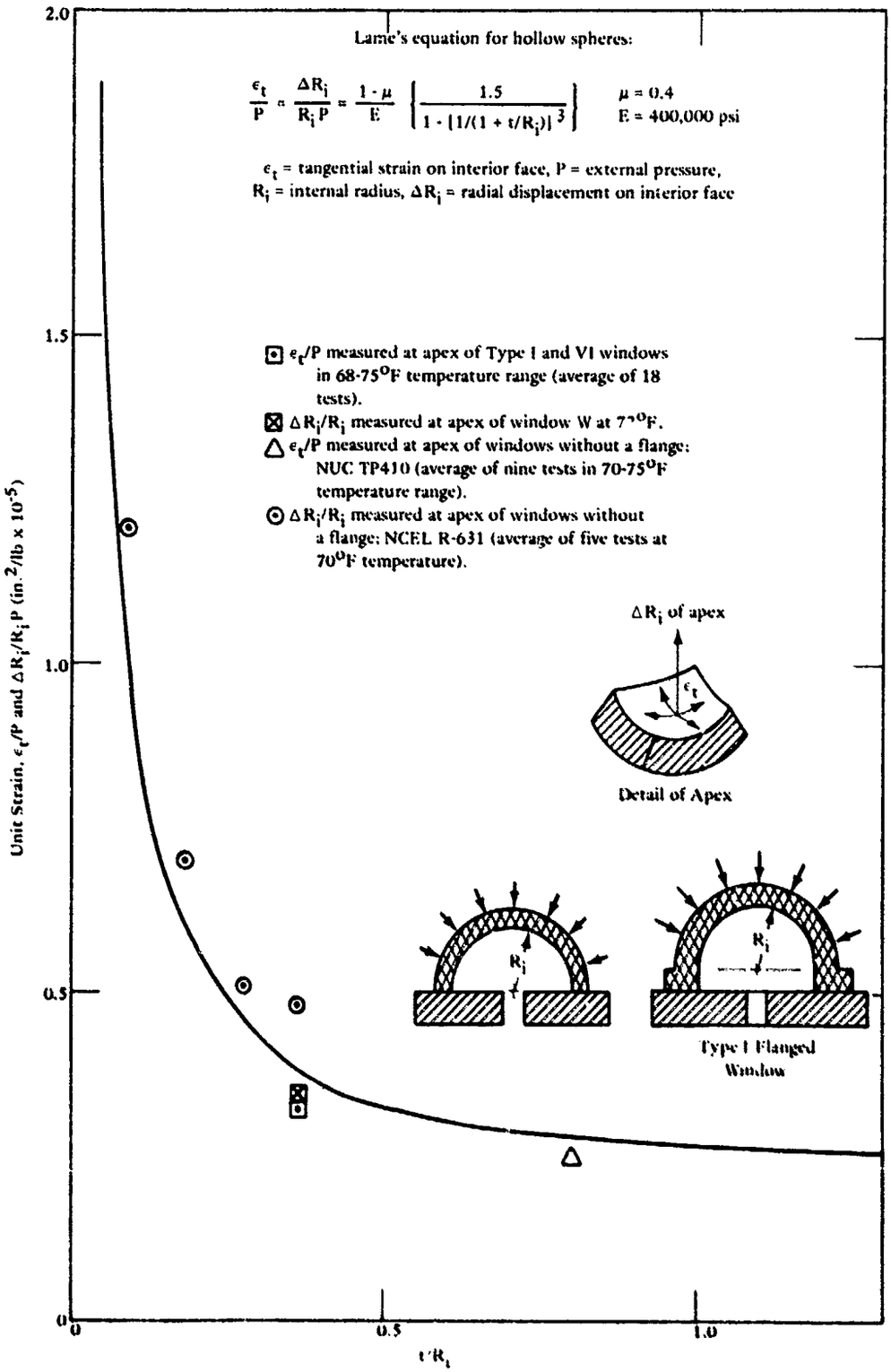

Figure 81. Comparison of measured and calculated strains in linear range of the apex of hemispherical windows with different t/R_i ratios when subjected to short-term external hydrostatic loading.

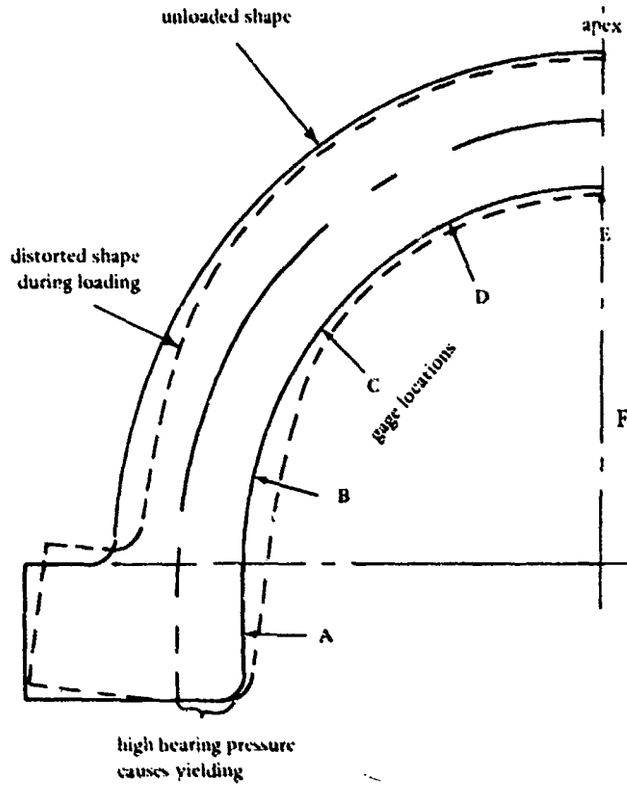

Figure 82. Reconstruction of Type I window deformation in the elastic range when subjected to external short-term hydrostatic loading.

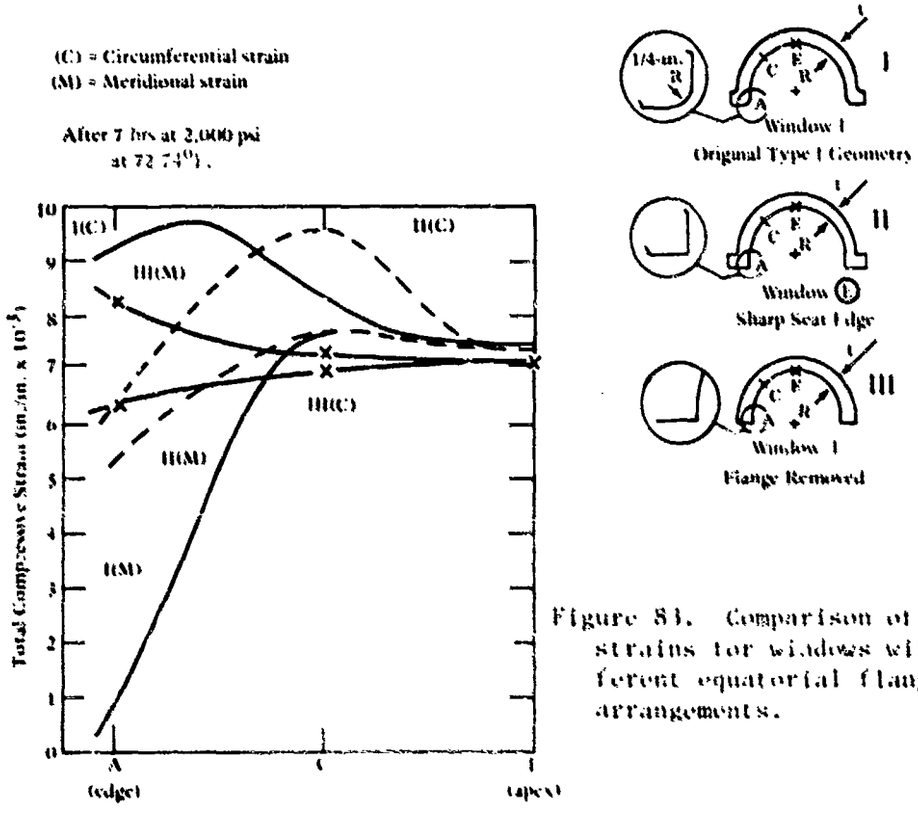

Figure 81. Comparison of measured strains for windows with different equatorial flange arrangements.

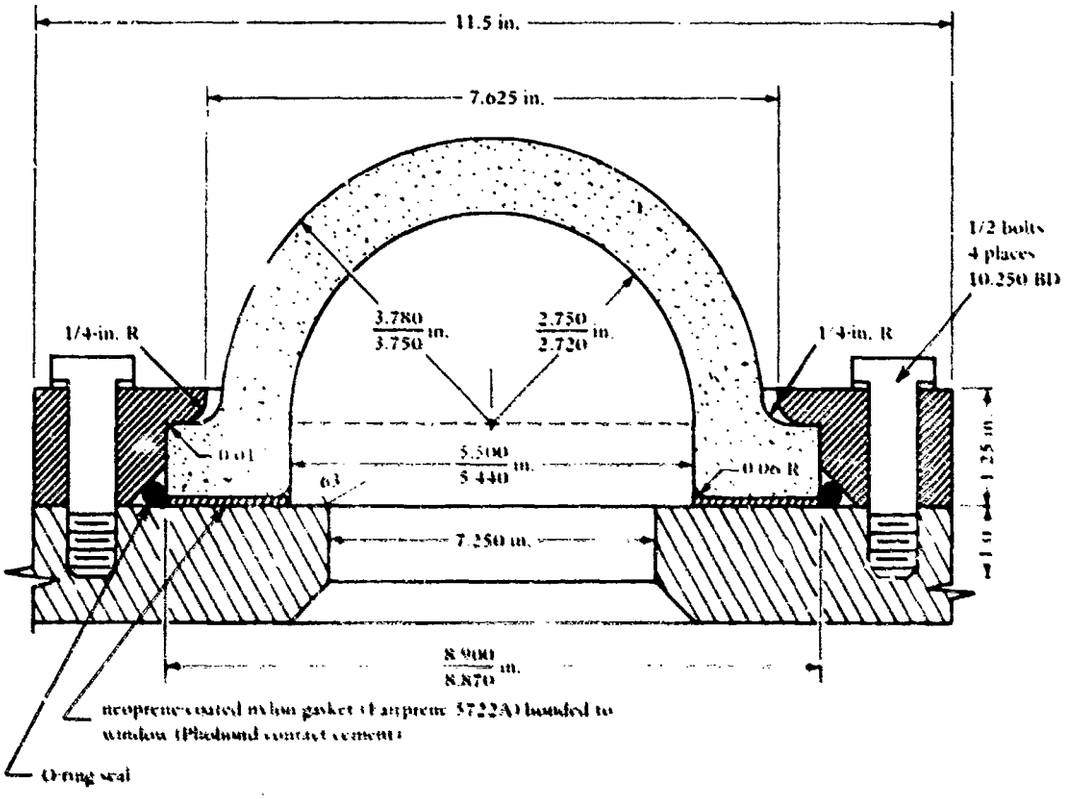

Figure 84. Recommended seat and seal design for modified Type I (Type II) windows.

Appendix

DETAILED DATA

Although the body of the report presents summaries of strain distributions in Type I and Type VI windows under different kinds of hydrostatic loadings, there often is a need for detailed knowledge of strains at each strain gage location. To satisfy this requirement, detailed plots of strains are shown for representative windows of Type I and Type VI.

Figures 85 and 86 afford a direct comparison between strains on the same window subjected to short-term loading with and without a neoprene bearing gasket. Figures 87 and 88 allow a comparison, on the other hand, between strains on Type I and Type VI windows under short-term loading.

Figures 89 and 90 permit a comparison of creep strains on Type I and Type VI windows under the same sustained loading condition, that is, 10,000 psi. The effect of sustained loading magnitude on the rate of creep and subsequent relaxation in Type VI window can be observed by comparing Figures 91, 92, 93, and 94.

Figure 95 presents graphically the strain history of the concave surface at the apex for a Type VI window during sustained loading at 4,000 psi and subsequent relaxation.

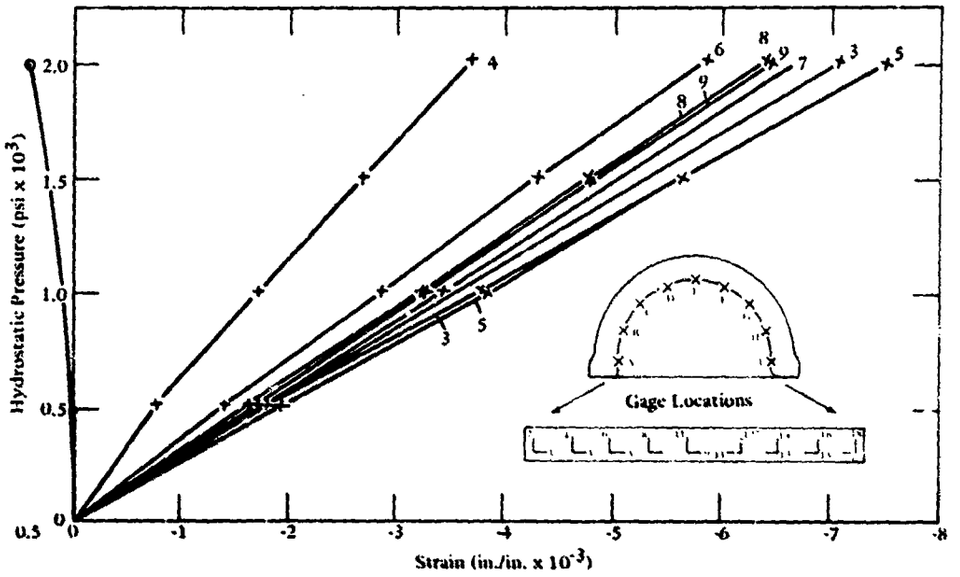

(a) For gages 1 through 9.

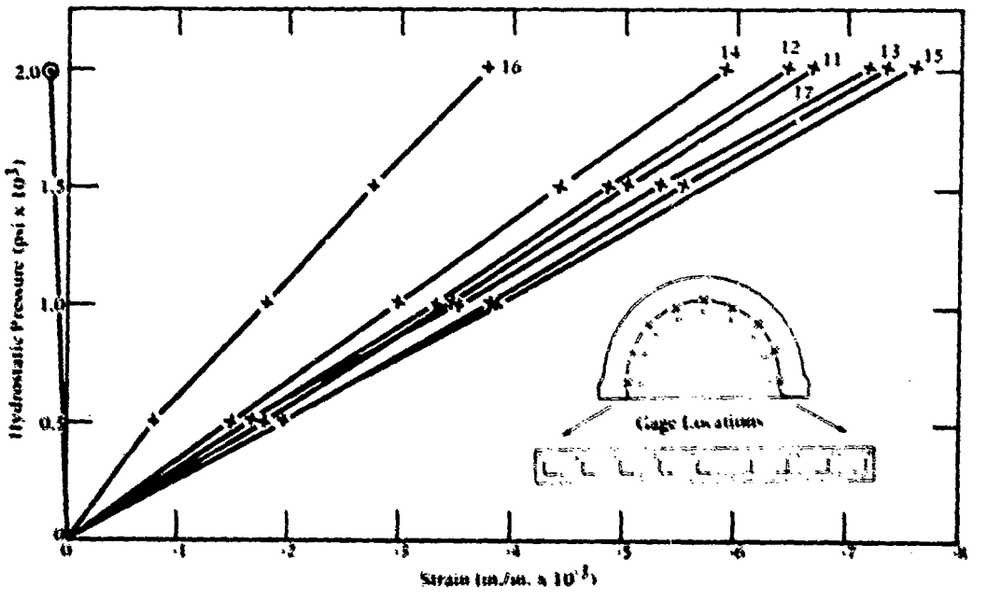

(b) For gages 11 through 18.

Figure 85. Window Y, Type VI under short-term loading without a neoprene bearing gasket.

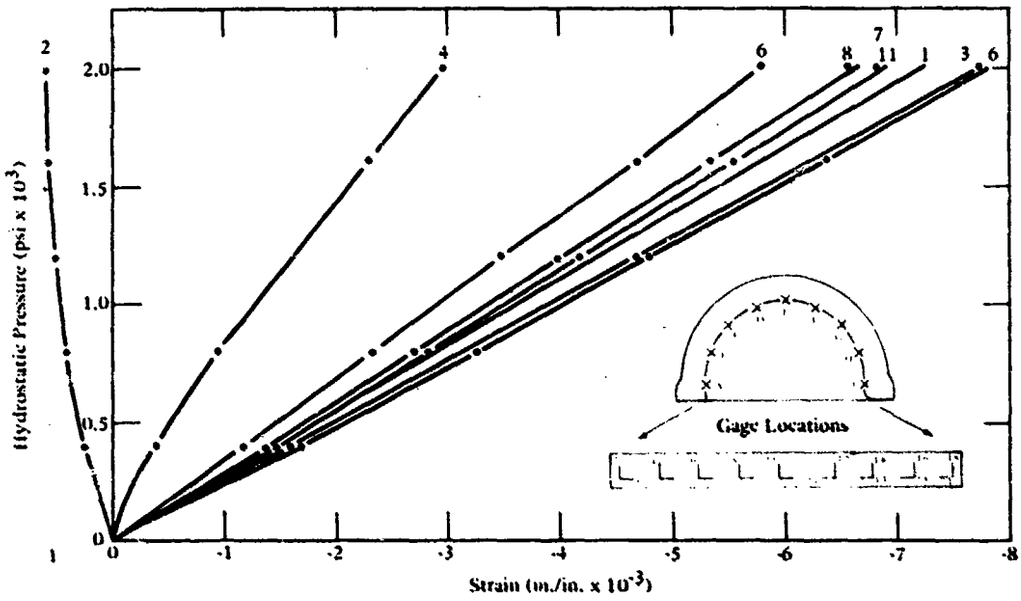

(a) For gages 1 through 8 and gage 11.

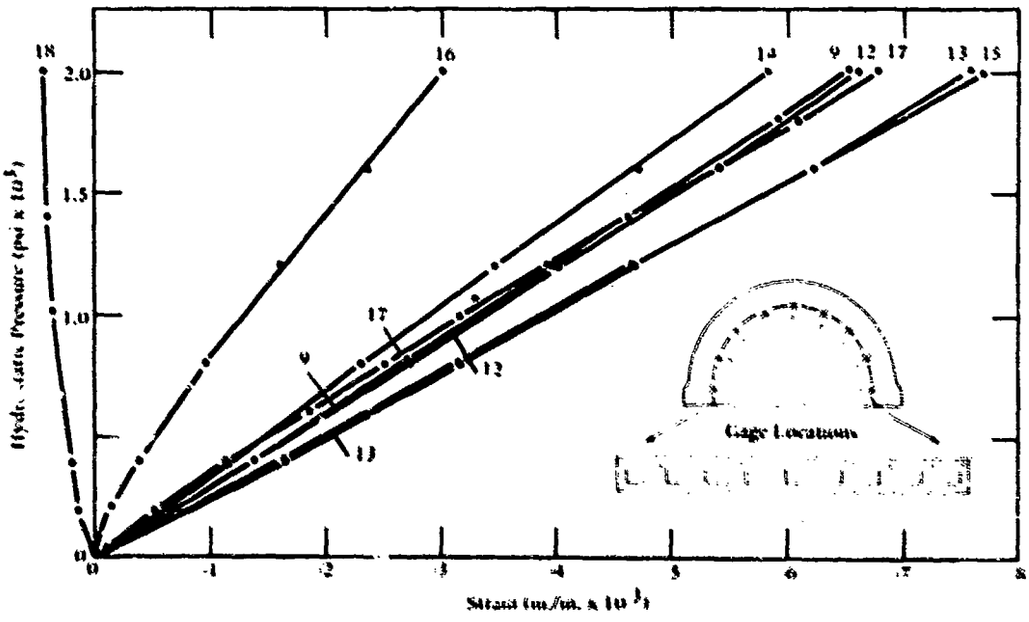

(b) For gage 9 and gages 12 through 18.

Figure 86. Window Y, Type VI under short-term loading when resting on a 5722A Fairprene bearing gasket.

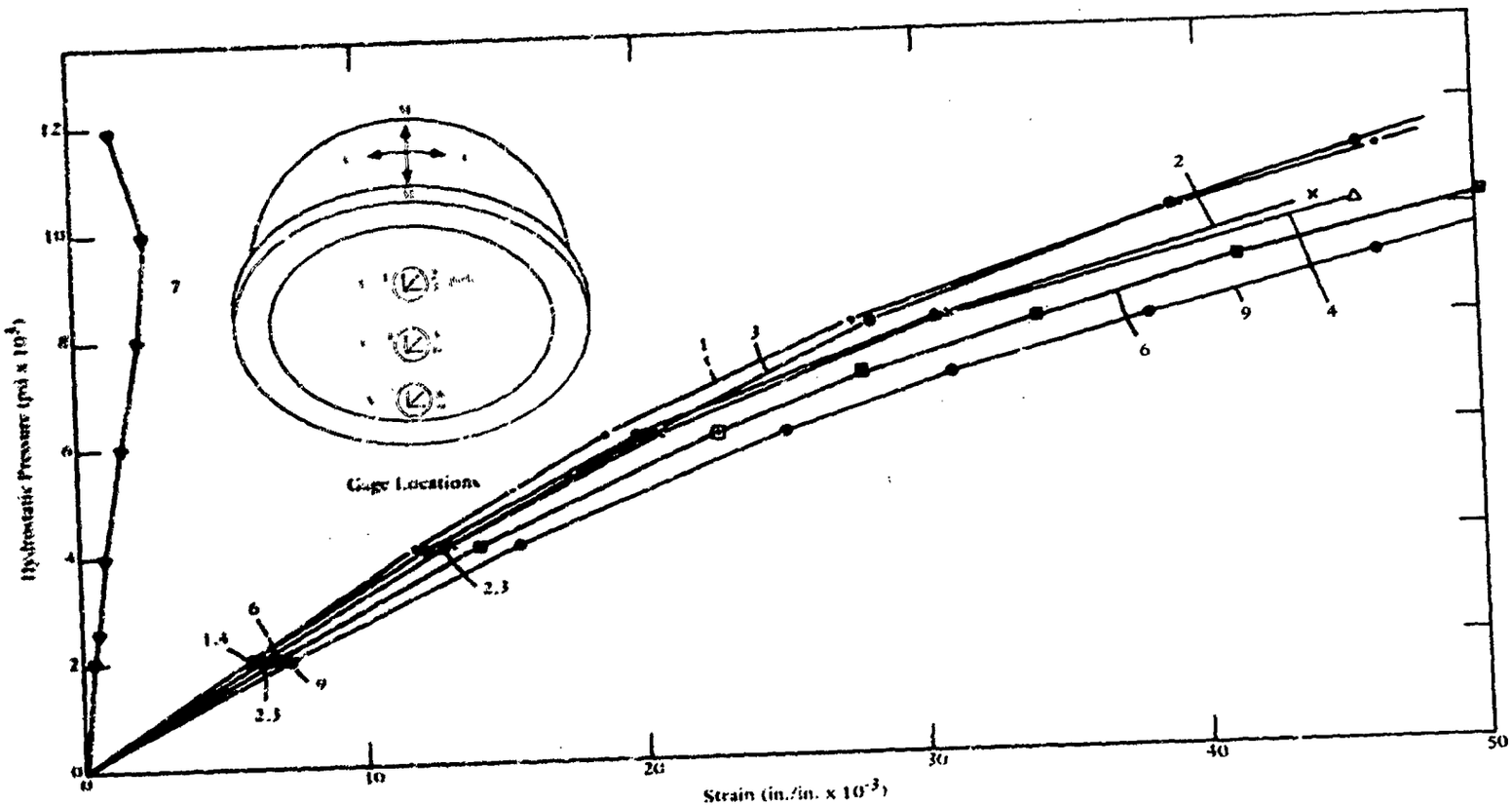

Figure 87. Window C, Type I under short-term loading.

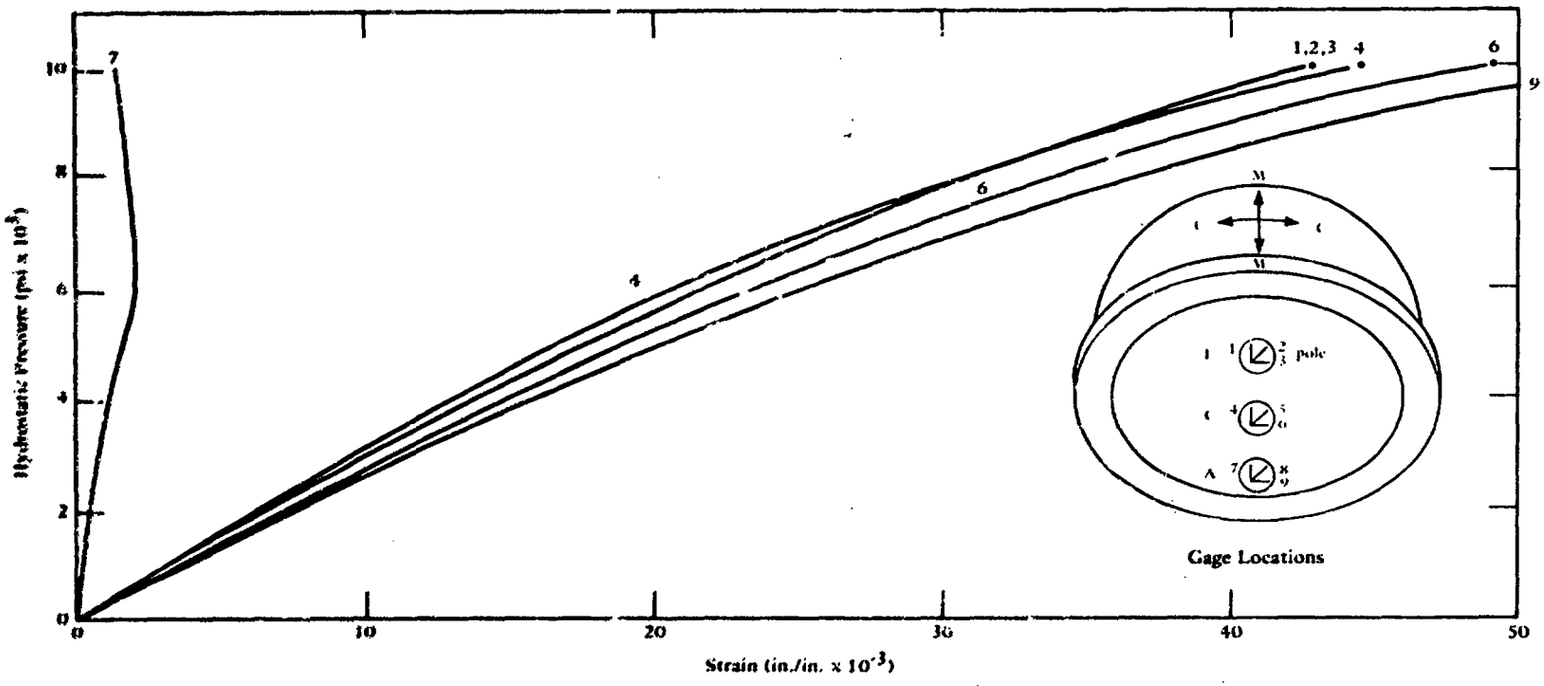

Figure 88. Window O, Type VI under short-term loading.

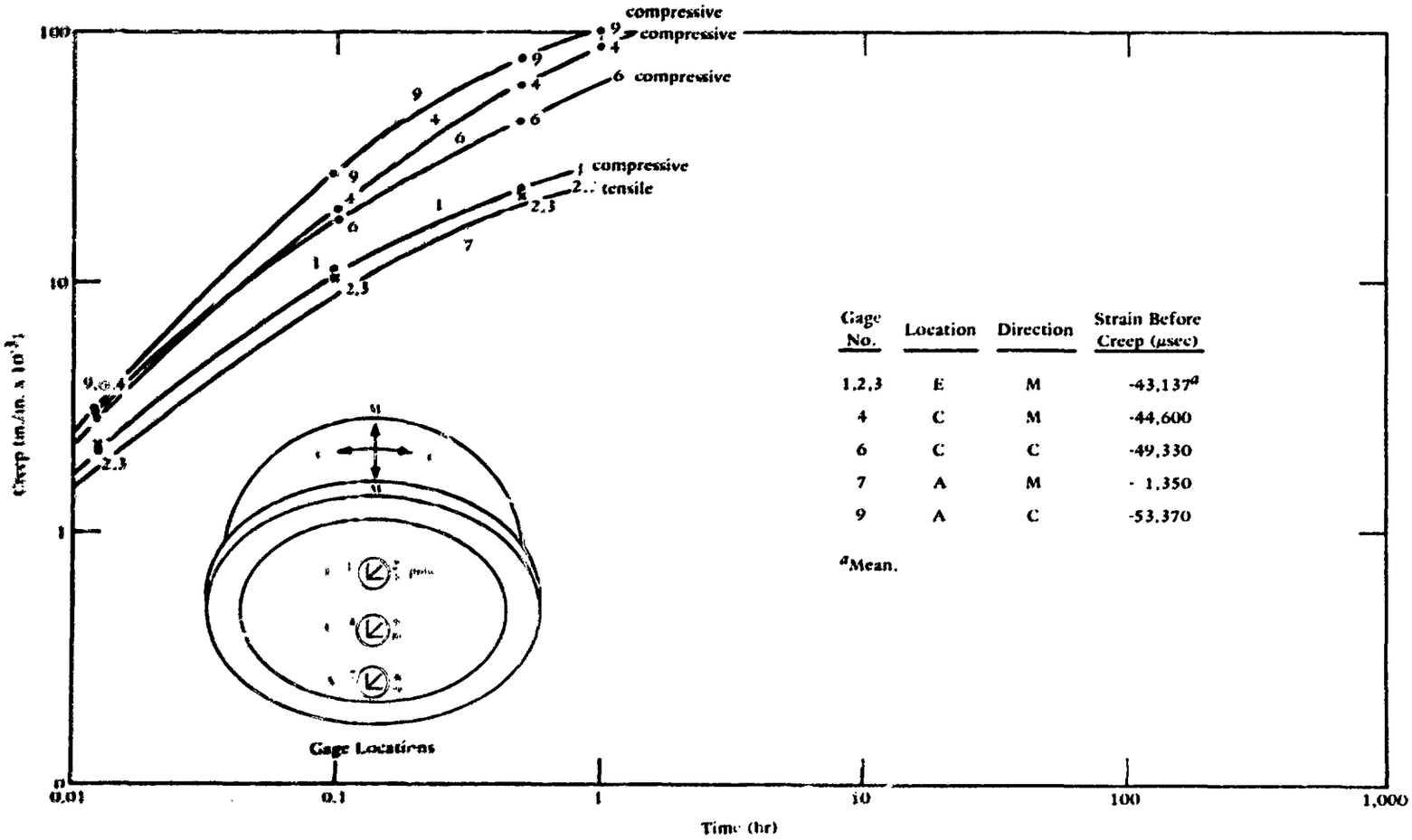

Gage No.	Location	Direction	Strain Before Creep (μsec)
1,2,3	E	M	-43,137[a]
4	C	M	-44,600
6	C	C	-49,330
7	A	M	- 1,350
9	A	C	-53,370

[a]Mean.

Figure 89. Window O, Type VI under sustained loading at 10,000 psi.

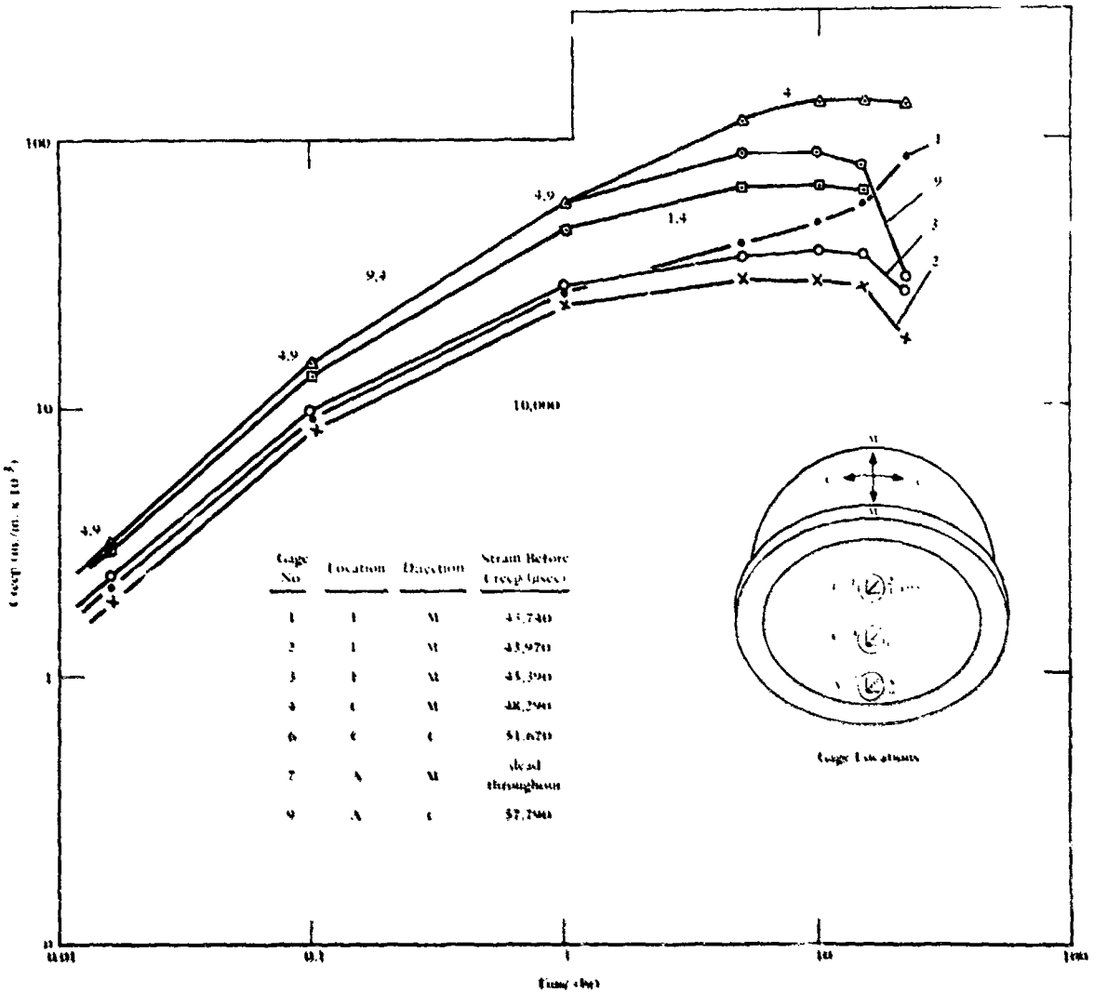

Figure 90. Window D, Type I under sustained loading at 10,000 psi.

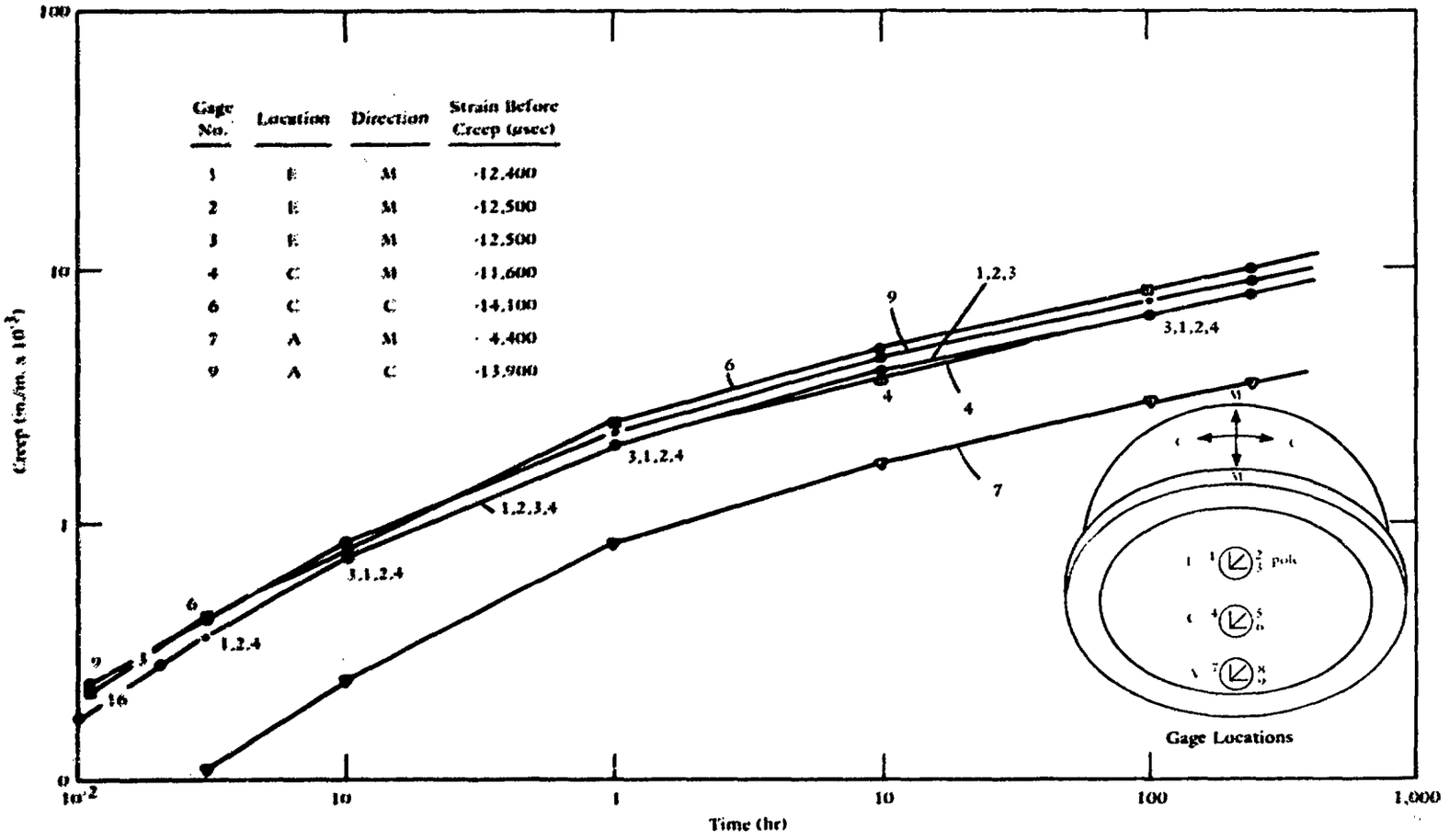

Figure 91. Window R, Type VI under sustained loading at 4,000 psi.

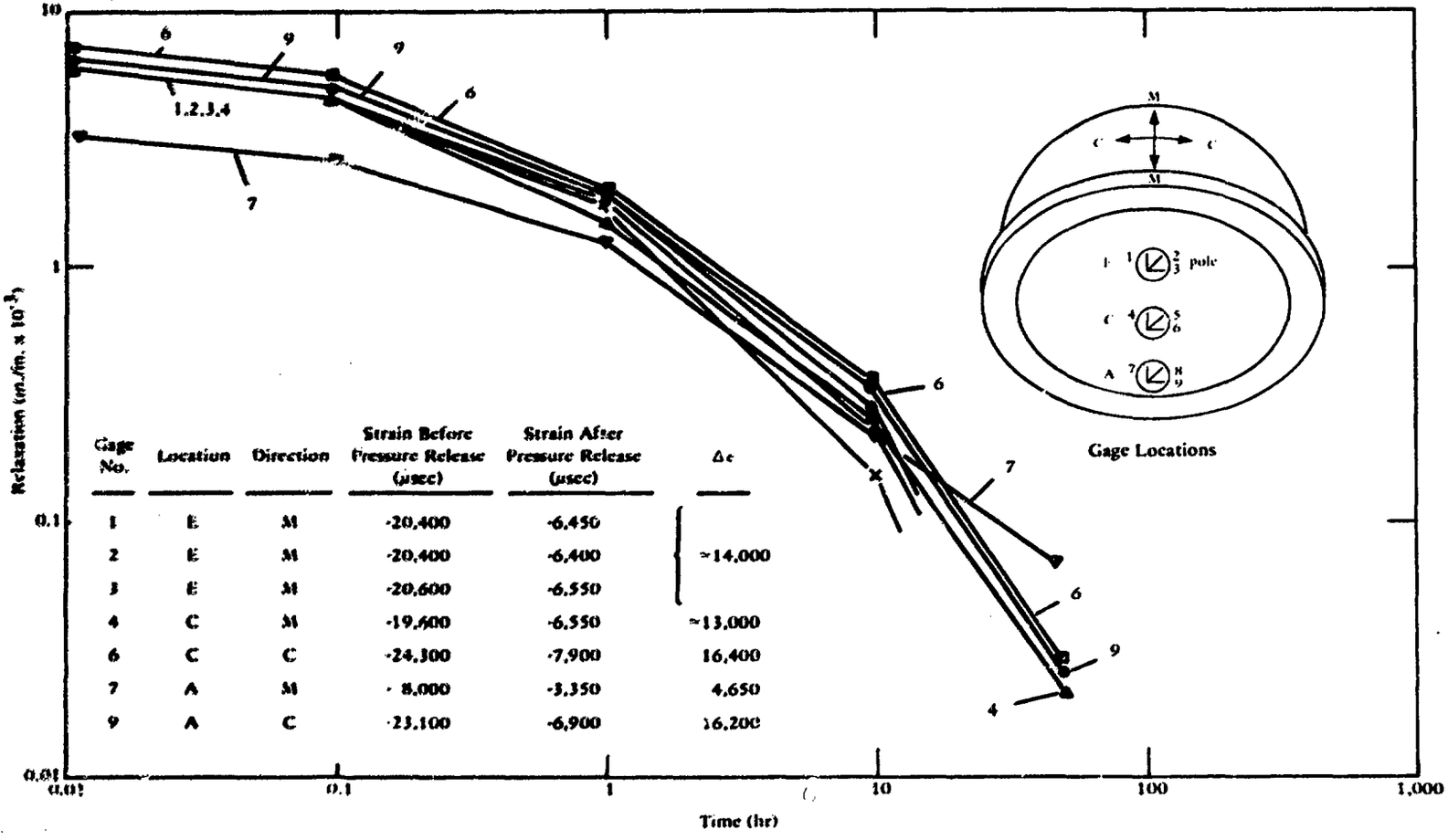

Gage No.	Location	Direction	Strain Before Pressure Release (μsec)	Strain After Pressure Release (μsec)	Δε
1	E	M	-20,400	-6,450	
2	E	M	-20,400	-6,400	≈14,000
3	E	M	-20,600	-6,550	
4	C	M	-19,600	-6,550	≈13,000
6	C	C	-24,300	-7,900	16,400
7	A	M	- 8,000	-3,350	4,650
9	A	C	-23,100	-6,900	16,200

Figure 92. Window R, Type VI during relaxation from sustained loading at 4,000 psi.

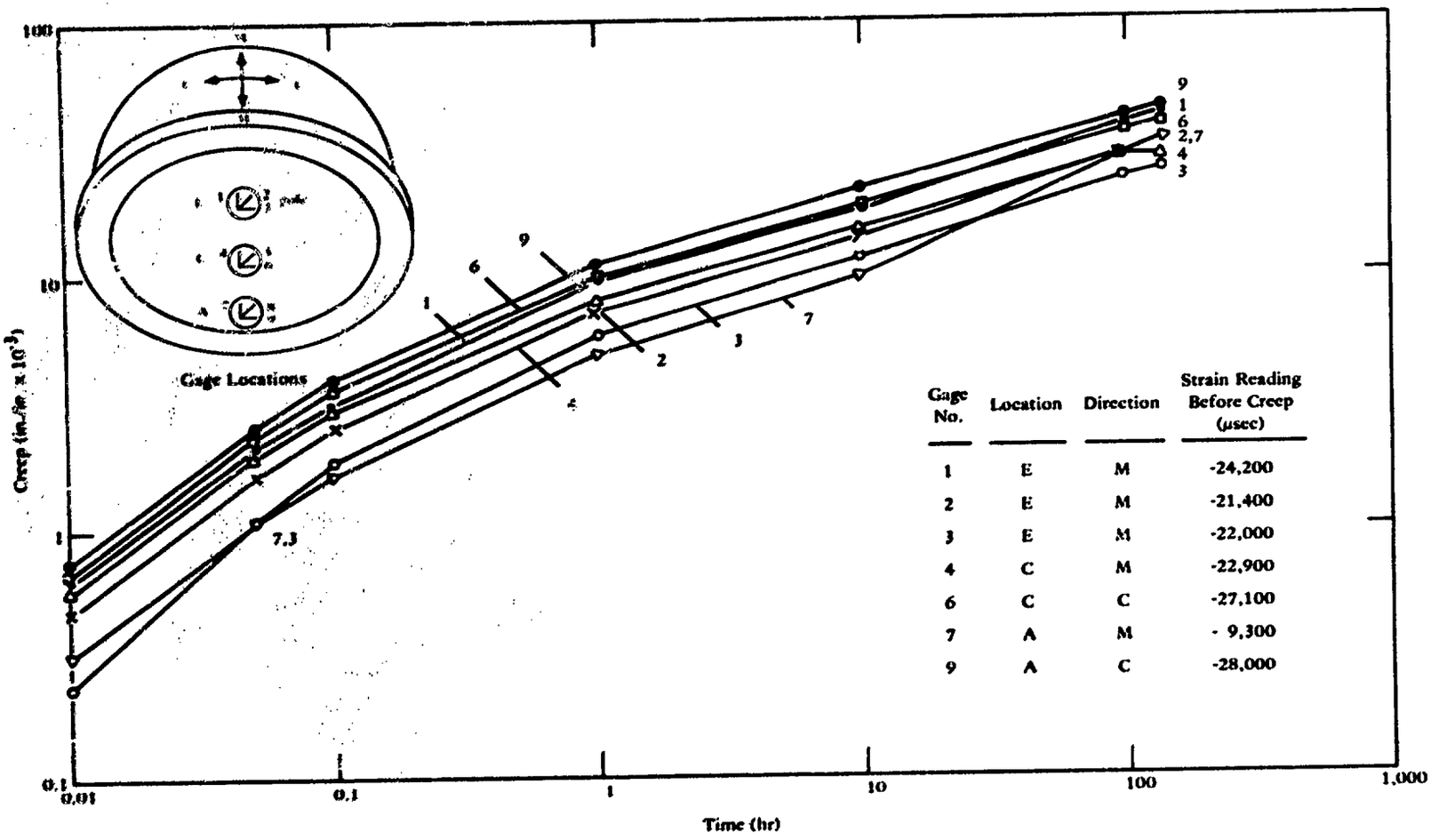

Figure 93. Window Q, Type VI during sustained loading at 7,000 psi.

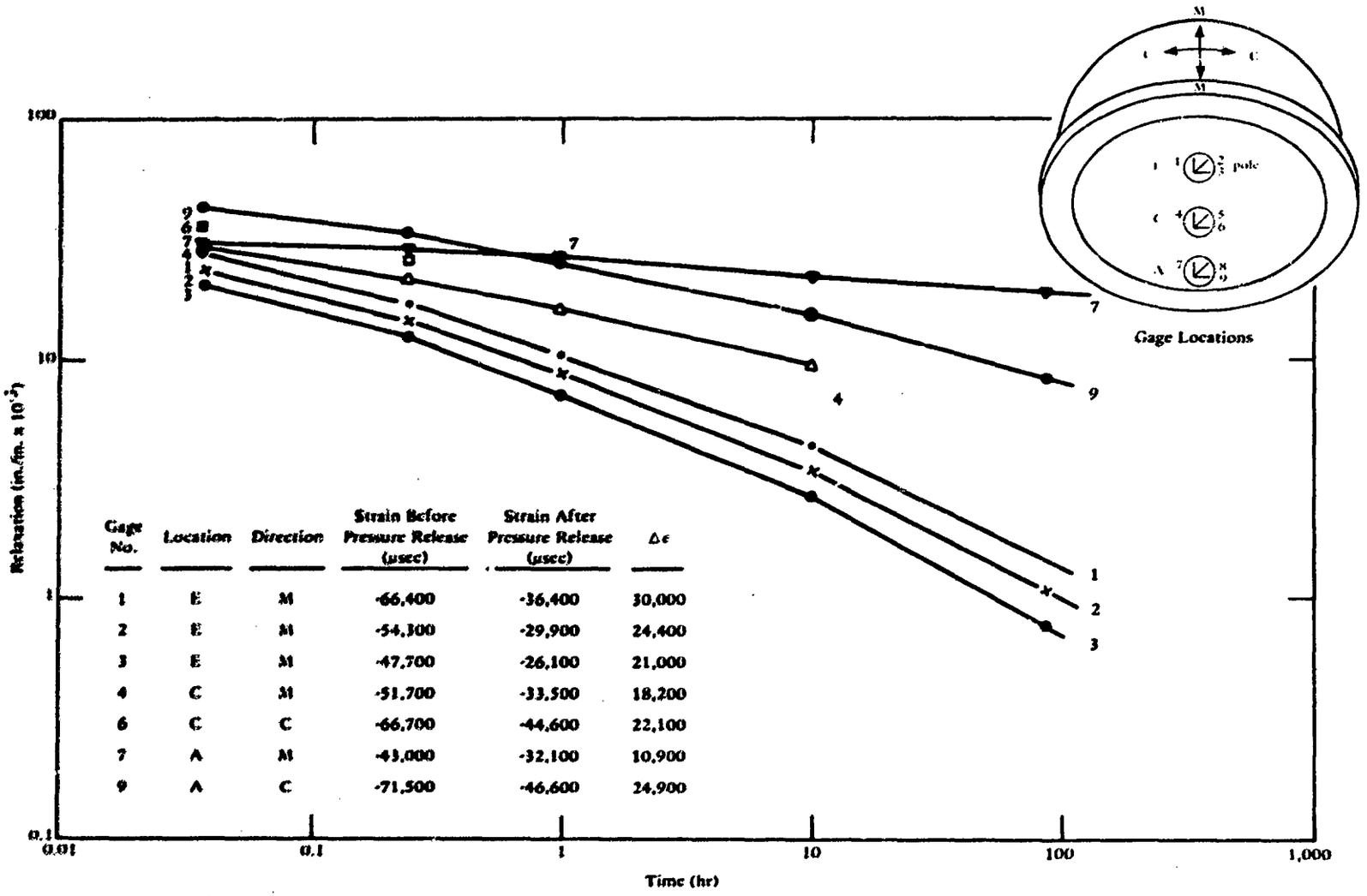

Gage No.	Location	Direction	Strain Before Pressure Release (μsec)	Strain After Pressure Release (μsec)	Δε
1	E	M	-66,400	-36,400	30,000
2	E	M	-54,300	-29,900	24,400
3	E	M	-47,700	-26,100	21,000
4	C	M	-51,700	-33,500	18,200
6	C	C	-66,700	-44,600	22,100
7	A	M	-43,000	-32,100	10,900
9	A	C	-71,500	-46,600	24,900

Figure 94. Window Q, Type VI during relaxation from sustained loading at 7,000 psi.

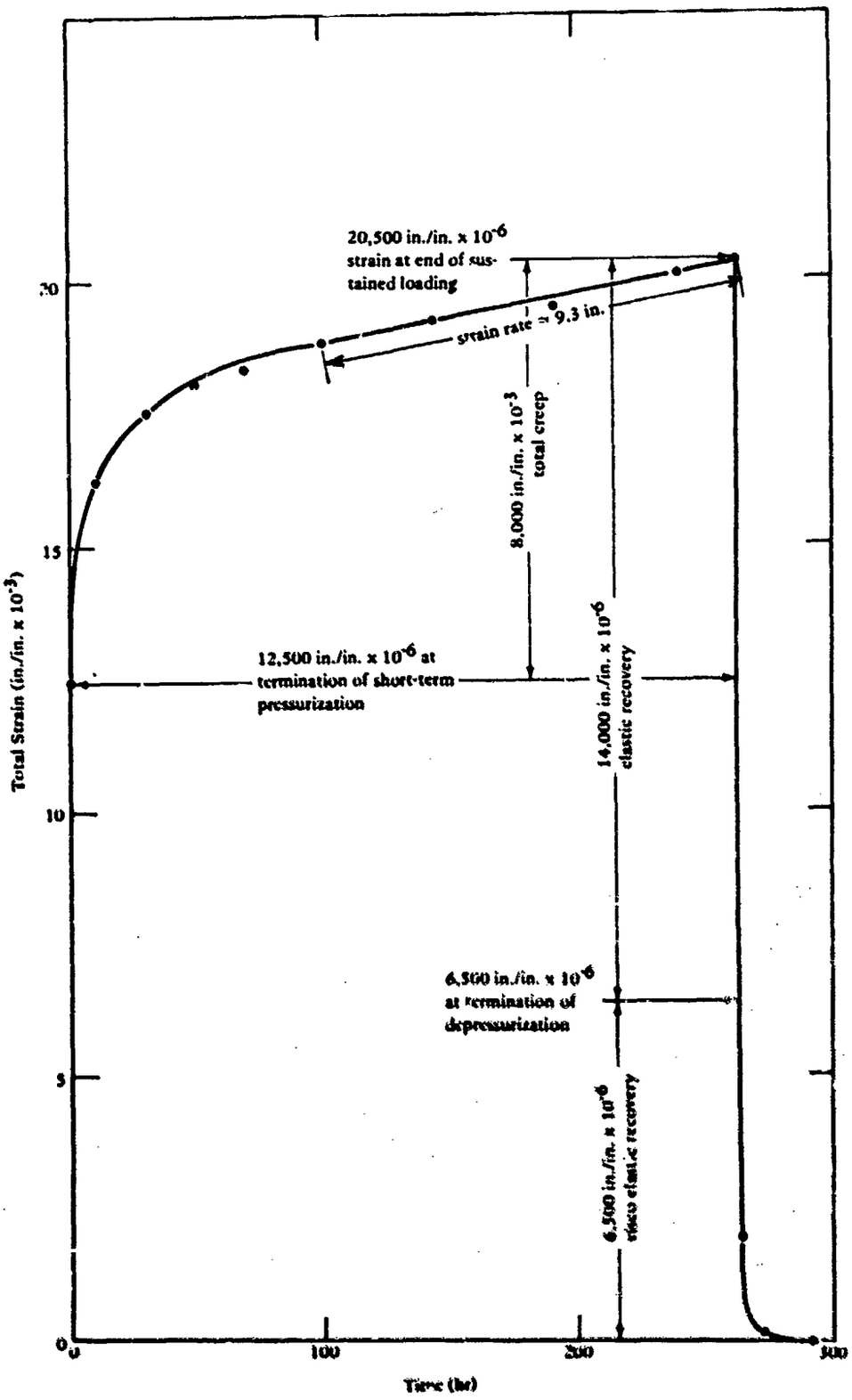

Figure 95. Window R, Type VI during a sustained pressure loading and the subsequent relaxation; strain on the interior face at the apex.

short-term loading	increasing the hydrostatic pressure at 650 psi/minute rate
short-term critical pressure (STCP)	pressure at which catastrophic failure of the window occurs when subjected to short-term hydrostatic loading at 75°F (24°C) ambient temperature
long-term or static loading	pressurizing the window to a specified pressure at 650 psi/minute rate and maintaining that pressure for specified number of hours
cyclic loading	pressurizing the window repeatedly to a specified pressure at 650 psi/minute rate, maintaining this pressure for a specified number of hours, depressurizing at 650 psi per minute to 0 psi and allowing the window to relax for a specified number of hours before repeating the procedure
strain	unit deformation, in./in. of original length
creep	time dependent deformation of material under sustained loading of constant magnitude; in./in. of original length
relaxation	time dependent restoration of material to its original dimensions under absence of external loading; in./in. of original length
hoop orientation of strains or stresses	direction parallel to the edge of spherical sector window
meridional orientation of strains or stresses	direction at right angle to the hoop direction; meridional lines pass through the apex
total strain	total deformation of material, includes both the short term and creep components of strain; in./in. of original length
short-term strain	deformation of material under short-term loading; in./in. of original length
radial displacement	displacement of the interior surface at the apex towards the center of curvature for the hemisphere
normalized strain	strain per unit increase of pressure under short-term loading; in./in./psi

DISTRIBUTION LIST

AFB CESCH, Wright-Patterson, Stinfo Library, Offutt NE
ARMY BMDSC-RC (H. McClellan, Huntsville AL
ARMY BALLIST RSCH LABS AMXBR-XA-LB, Aberdeen Proving Ground MD
ARMY COASTAL ENGR RSCH CEN Fort Belvoir VA
ARMY CORPS OF ENGR Seattle Dist. Library, Seattle WA
ARMY CRREL A. Kovacs, Hanover NH
ARMY MATERIALS & MECHANICS RESEARCH CENTER Dr. Lenoe, Watertown MA
ASST SECRETARY OF THE NAVY Spec. Assist Energy (P. Waterman), Washington DC, Spec. Assist Submarines, Washington DC
BUREAU OF RECLAMATION Code 1512 (C. Selander) Denver CO
MCB ENS S.D. Keesling, Quantico VA
CNO Code OPNAV 90H, OP987P4 (B. Petrie), Pentagon
COMFLEACT PWO, Okinawa Japan
COMSUBDEVGRUCNE Operations Offr, San Diego, CA
DEFENSE DOCUMENTATION CTR Alexandria, VA
DEFENSE INTELLIGENCE AGENCY Dir., Washington DC
DTNSRDC Code 1548 (T. Tsai), Bethesda MD, Code 1706, Bethesda MD
DTNSRDC Code 284 (A. Rufolo), Annapolis MD
ENERGY R&D ADMIN. INEL Tech. Lib (Reports Section), Idaho Falls ID
NAD Code 011B-1, Hawthorne NV
NAS PWD Maint. Div., New Orleans, Belle Chasse LA, PWO
NAVAIRSYSCOM J. C. W. Hall, Washington DC
NAVAL FACILITY PWO, Centerville Bch, Ferndale CA
NAVARCLAB Library, Pt Barrow AK
NAVCOASTSYSLAB Code 710 (R. Elliott), Code 710.5 (J. Mettleman), Code 710.5 (J. Quirk), Library
NAVCOMMSTA PWO, Adak AK
NAVFACENGCOM Code 04 UB, Code 0451, Code 04B5, Code 101, PC-22 (E. Spencer), PI-2
NAVFACENGCOM - CHES DIV, Code 403 (H. DeVoe), Code FPO-1 (Olsen), Code FPO-1C2
NAVFACENGCOM - LANT DIV, RDT&ELO 09P2, Norfolk VA
NAVFACENGCOM - NORTH DIV, Code 1028, RDT&ELO, Philadelphia PA
NAVFACENGCOM - PAC DIV, Code 402, RDT&L, Pearl Harbor HI, Commanders
NAVFACENGCOM - SOUTH DIV, Code 90, RDT&ELO, Charleston SC
NAVFACENGCOM - WEST DIV, Codes 09PA, 09P20
NAVHOSP L T R, Ebberud, Puerto Rico
NAVOCEANO Code 1600, Code 3412 (J. DePalma), Washington DC
NAVPHIBASE Code S3L, Norfolk VA, OIC, UCT I
NAVSCOLCECOFF C35
NAVSHIPYD Code 400, Puget Sound, PWO
NAVSTA CO, PWD Engr Div, Puerto Rico, PWO, Puerto Rico
NAS OIC, CBU 412, Oak Harbor WA, PWD (ENS E.S. Agonoy), Crane Field, Beeville TX
NATL OCEAN AND ATMOS ADMIN Libraries Div (D823), Silver Spring MD
NATL RESEARCH COUNCIL Naval Studies Board, Washington DC
NAVACT PWO, London UK
NAVCOMMSTA PWO
NAVCONSTRACEN CO (CDR C.L. Seugen), Port Hueneme, CA
NAVELEXSYSCOM Code PME-124-61, Washington DC
NAVEODFAC Code 605, Indian Head MD
NAVFACENGCOM CDR L.K. Dunwoody, Alexandria VA, Code 0453 (D. Potter)
NAVFACENGCOM - CHES DIV Code 402 (R. Morrow), Code FPO-1 (C. Bailey), Code FPO 1SP3 (C.F. Sullivan)
NAVFACENGCOM CONTRACTS Eng Div dir, Southwest Pac, PI, TRIDENT (CDR J.R. Jacobsen), Brem., ton WA 98310
NAVMARCORESTRANCEN ORU 1113 (Cdr D.R. Lawson), Denver CO
NAVSEASYSCOM Code SEA 00C
NAVSEC Code 6034 (Library), Washington DC
NAVSHIPYD Code 202.4, Long Beach CA, Code 202.5 (Library) Puget Sound, Bremerton WA, Code Portsmouth NH, PWD (L.T.S.B. Hall), Long Beach CA

NAVSUPPACT AROICC (LT R.G. Hocker), Naples Italy
NAVWPNSUPPCEN PWO
NAVXDIVINGU LT A.M. Parisi, Panama City FL
NCBC CEL (CDR N.W. Petersen), Port Hueneme, CA, Code 10
NCBU 411 OIC, Norfolk VA
NMCB One, LT F.P. Digeorge
NTC Code 54 (ENS P. G. Jackel), Orlando FL
NUC Code 4099 (E. Hamilton), San Diego CA, Code 65 (H. Talkington), Code 6302 (R. Jones), Code 8035 (Tech. Lib.), San Diego CA
NUSC Code EA123 (R.S. Munn), New London CT, Code S332, B-80 (J. Wilcox), Code TA131 (C. de la Cruz), New London CT
OCEANAV Mangmt Info Div., Arlington VA
OFFICE OF NAVAL RESEARCH CDR Harlett, Boston MA
ONR Code 484, Arlington VA, Dr. A. Laufer, Pasadena CA
PLASTICS TECH EVAL CTR PICATINNY ARSENAL A. Anzalone, Dover NJ
PMTC Pat. Counsel, Point Mugu CA
PWC ENS J.E. Surash, Pearl Harbor HI, ACE Office (LTJG St. Germain), Code 120C (A. Adams), ENS J.A. Squatrito, San Francisco Bay, Oakland CA
SUBASE NEW LONDON LTJG D. W. Peck Groton CT
USCG MMT-4, Washington DC
USCG ACADEMY LT N. Stramana5, New London CT
USCG R&D CENTER CO, D. Motherway, Groton CT, Tech. Dir.
USNA Ch. Mech. Engr. Dept. Sys. Engr Dept (Dr. Mooney), Annapolis MD
CALIFORNIA INSTITUTE OF TECHNOLOGY PASADENA, CA (SCOTT)
CALIFORNIA STATE UNIVERSITY LONG BEACH, CA (CHELAPATI)
CITY OF CERRITOS Cerritos CA (J. Adams)
COLORADO STATE UNIV., FOOTHILL CAMPUS Engr Sci. Branch, Lib., Fort Collins CO
CORNELL UNIVERSITY Ithaca NY (Serials Dept, Engr Lib.)
DAMES & MOORE LIBRARY LOS ANGELES, CA
FLORIDA ATLANTIC UNIVERSITY BOCA RATON, FL (MC ALLISTER), Boca Raton FL (Ocean Engr Dept., C. Lin)
FLORIDA ATLANTIC UNIVERSITY Boca Raton FL (W. Tessin)
GEORGIA INSTITUTE OF TECHNOLOGY Atlanta GA (School of Civil Engr., Kahn), Atlanta GA (B. Mazanti)
INSTITUTE OF MARINE SCIENCES Morehead City NC (Director)
IOWA STATE UNIVERSITY Ames IA (CE Dept, Handy)
LEHIGH UNIVERSITY BETHLEHEM, PA (MARINE GEOTECHNICAL LAB., RICHARDS), Bethlehem PA (Fritz Engr. Lab No. 13, Beedle), Bethlehem PA (Linderman Lib. No. 30, Fleckenstein)
LIBRARY OF CONGRESS WASHINGTON, DC (SCIENCES & TECH DIV)
MAINE MARITIME ACADEMY CASTINE, ME (LIBRARY)
MASSACHUSETTS INST. OF TECHNOLOGY Cambridge MA (Rm 10-500, Tech. Reports, Engr. Lib.), Cambridge MA (Rm 14 E210, Tech. Report Lib.), Cambridge MA (Whitman)
MICHIGAN TECHNOLOGICAL UNIVERSITY HOUGHTON, MI (HAAS)
MIT Cambridge, MA (Harleman)
NATL ACADEMY OF ENG, ALEXANDRIA, VA (SEARLE, JR.)
OREGON STATE UNIVERSITY CORVALLIS, OR (CE DEPT, BELL), Corvalis OR (School of Oceanography), LT R.B. Steiner, NROTC Unit, Corvallis OR
PENNSYLVANIA STATE UNIVERSITY STATE COLLEGE, PA (SNYDER), UNIVERSITY PARK, PA (GOTOLSKI)
PURDUE UNIVERSITY LAFAYETTE, IN (ALTSCHAEFFL), LAFAYETTE, IN (CE LIB), Lafayette IN (Leonards)
RUTGERS UNIVERSITY New Brunswick NH (Civil & Environ Engr Dept., du Bouchet)
SAN DIEGO STATE UNIV, Dr. Krishnamurthy, San Diego CA
SCRIPPS INSTITUTE OF OCEANOGRAPHY LA JOLLA, CA (ADAMS), San Diego, CA (Marine Phy. Lab. Spess)
STANFORD UNIVERSITY STANFORD, CA (DOUGLAS)
TEXAS A&M UNIVERSITY COLLEGE STATION, TX (CE DEPT), College TX (CE Dept, Herbich)
BONNEVILLE POWER ADMIN Los Angeles CA (Hancock Lib. of Bio. & Ocean)
UNIVERSITY OF CALIFORNIA BERKELEY, CA (CE DEPT, MITCHELL), BERKELEY, CA (OFF. BUS. AND FINANCE, SAUNDERS), DAVIS, CA (CE DEPT, TAYLOR), SAN DIEGO, CA, LA JOLLA, CA (SEIBOLD)
UNIVERSITY OF DELAWARE Newark, DE (Dept of Civil Engineering, Chewon)
UNIVERSITY OF HAWAII HONOLULU, HI (SCIENCE AND TECH. DIV.)

UNIVERSITY OF ILLINOIS URBANA, IL (LIBRARY)
UNIVERSITY OF MASSACHUSETTS (Heronemus), Amherst MA CE Dept
UNIVERSITY OF MICHIGAN Ann Arbor MI (Richart)
UNIVERSITY OF NEBRASKA-LINCOLN LINCOLN, NE (SPLETTSTOESSER)
UNIVERSITY OF NEW HAMPSHIRE DURHAM, NH (LAVOIE)
UNIVERSITY OF PENNSYLVANIA PHILADELPHIA, PA (SCHOOL OF ENGR & APPLIED SCIENCE, ROLL)
UNIVERSITY OF RHODE ISLAND KINGSTON, RI (PAZIS)
UNIVERSITY OF TEXAS Inst. Marina Sci (Library), Port Aransas TX
UNIVERSITY OF WASHINGTON SEATTLE, WA (APPLIED PHYSICS LAB), SEATTLE, WA (OCEAN ENG RSCH LAB, GRAY), SEATTLE, WA (PACIFIC MARINE ENVIRON. LAB., HALPERN)
US DEPT OF COMMERCE NOAA, Marine & Earth Sciences Lib., Rockville MD
UNIVERSITY OF CALIFORNIA Berkeley CA (E. Pearson), La Jolla CA (Acq. Dept, Lib. C-075A)
UNIVERSITY OF ILLINOIS Honolulu HI (Dr. Szilard)
UNIVERSITY OF RHODE ISLAND Narragansett RI (Pell Marine Sci. Lib.)
US GEOLOGICAL SURVEY Off. Marine Geology, Mailstop 915, Reston VA
AEROSPACE CORP. Acquisition Group, Los Angeles CA
ARCAIR CO. D. Young, Lancaster OH
ARVID GRANT OLYMPIA, WA
ATLANTIC RICHFIELD CO. DALLAS, TX (SMITH)
AUSTRALIA Dept. PW (A. Hicks), Melbourne
BECHTEL CORP. SAN FRANCISCO, CA (PHELPS)
BELGIUM NAECON. N.V., GEN.
BETHLEHEM STEEL CO. BETHLEHEM, PA (STEELE)
BROWN & ROOT Houston TX (D. Ward)
CANADA Can-Dive Services (English) North Vancouver, Lockheed Petrol. Srv. Ltd., New Westminster BC, Mem Univ Newfoundland (Chari), St Johns, Surveyor, Nenninger & Chenevert Inc.,
CHEVRON OIL FIELD RESEARCH CO. LA HABRA, CA (BROOKS)
COLUMBIA GULF TRANSMISSION CO. HOUSTON, TX (ENG. LIB.)
DILINGHAM PRECAST F. McHale, Honolulu HI
DRAVO CORP Pittsburgh PA (Giannino)
NORWAY DET NORSKE VERITAS (Library), Oslo
ESSO PRODUCTION RESEARCH CORP. HOUSTON, TX (RUNGE)
EVALUATION ASSOC. INC KING OF PRUSSIA, PA (FEDELE)
FRANCE P. Jensen, Boulogne, Pierre Launay, Boulogne-Billancourt, Roger LaCroix, Paris
GLOBAL MARINE DEVELOPMENT NEWPORT BEACH, CA (HOLLETT)
GOULD INC. Shady Side MD (Ches. Inst. Div., W. Paul)
GRUMMAN AEROSPACE CORP. Bethpage NY (Tech. Info. Ctr)
ITALY M. Caironi, Milan, Sergio Tattoni Milano
LAMONT-DOHERTY GEOLOGICAL OBSERV. Palisades NY (McCoy), Palisades NY (Selwyn)
LOCKHEED MISSILES & SPACE CO. INC. SUNNYVALE, CA (PHILLIPS)
MARATHON OIL CO Houston TX (C. Seay)
MARINE CONCRETE STRUCTURES INC. MEFAIRIE, LA (INGRAHAM)
NEWPORT NEWS SHIPBLDG & DRYDOCK CO. Newport News VA (Tech. Lib.)
NORWAY A. Torum, Trondheim, DET NORSKE VERITAS (Roren) Oslo, J. Creed, Ski, J.D. Holst, Oslo, Norwegian Tech Univ (Brandtzaeg), Trondheim
OCEAN DATA SYSTEMS, INC. SAN DIEGO, CA (SNODGRASS)
OCEAN ENGINEERS SAUSALITO, CA (RYNECKI)
OCEAN RESOURCE ENG. INC. HOUSTON, TX (ANDERSON)
OFFSHORE DEVELOPMENT ENG. INC. BERKELEY, CA. Berkeley CA
PORTLAND CEMENT ASSOC. Skokie IL (Rsch & Dev Lab, Lib.)
PRESCON CORP TOWSON, MD (KELLER)
PUERTO RICO Puerto Rico (Rsch Lib.), Mayaquez P R
RAND CORP. Santa Monica CA (A. Laupa)
SANDIA LABORATORIES Library Div., Livermore CA
SCHUPACK ASSOC SO. NORWALK, CT (SCHUPACK)
SEATECH CORP. MIAMI, FL (PERONI)
SHELL DEVELOPMENT CO. Houston TX (E. Doyle)
SHELL OIL CO. HOUSTON, TX (MARSHALL), Houston TX (R. de Castongrene)
SWEDEN VBB (Library), Stockholm

TIDEWATER CONSTR. CO Norfolk VA (Fowler)
TRW SYSTEMS CLEVELAND, OH (ENG. LIB.), REDONDO BEACH, CA (DAI)
UNITED KINGDOM D. New, G. Maunsell & Partners, London, Shaw & Hatton (F. Hansen), London, Taylor, Woodrow Constr (014P), Southall, Middlesex, Taylor, Woodrow Constr (Stubbs), Southall, Middiesex, Univ. of Bristol (R. Morgan), Bristol
UNITED TECHNOLOGIES Windsor Locks CT (Hamilton Std Div., Library)
WESTINGHOUSE ELECTRIC CORP. Annapolis MD (Oceanic Div Lib, Bryan)
WM CLAPP LABS - BATTELLE DUXBURY, MA (LIBRARY), DUXBURY, MA (RICHARDS)
GREG PAGE EUGENE, OR